

การวิเคราะห์ทางทฤษฎีของเซลล์เชื้อเพลิงชนิดออกไซด์แข็งที่เกิดการรีฟอร์มมิงของก๊าซมีเทนภายใน



นางสาวณัฏฐิพร พัชรวร โชติ

วิทยานิพนธ์นี้เป็นส่วนหนึ่งของการศึกษาตามหลักสูตรปริญญาวิศวกรรมศาสตรดุษฎีบัณฑิต

สาขาวิชาวิศวกรรมเคมี ภาควิชาวิศวกรรมเคมี

คณะวิศวกรรมศาสตร์ จุฬาลงกรณ์มหาวิทยาลัย

ปีการศึกษา 2552

ลิขสิทธิ์ของจุฬาลงกรณ์มหาวิทยาลัย

THEORETICAL ANALYSIS OF SOLID OXIDE FUEL CELL WITH
INTERNAL METHANE REFORMING



Miss Yaneeporn Patcharavorachot

A Dissertation Submitted in Partial Fulfillment of the Requirements
for the Degree of Doctor of Engineering Program in Chemical Engineering

Department of Chemical Engineering

Faculty of Engineering

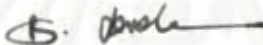
Chulalongkorn University

Academic Year 2009

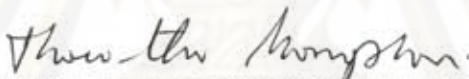
Copyright of Chulalongkorn University

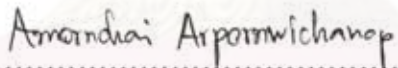
Thesis Title THEORETICAL ANALYSIS OF SOLID OXIDE FUEL CELL
WITH INTERNAL METHANE REFORMING
By Miss Yaneeporn Patcharavorachot
Field of Study Chemical Engineering
Thesis Advisor Assistant Professor Amornchai Arpornwichanop, D.Eng.

Accepted by the Faculty of Engineering, Chulalongkorn University in Partial
Fulfillment of the Requirements for the Doctoral Degree


..... Dean of the Faculty of Engineering
(Associate Professor Boonsom Lerdhirunwong, Dr.Ing.)

THESIS COMMITTEE


..... Chairman
(Associate Professor Tharathon Mongkhonsi, Ph.D.)


..... Thesis Advisor
(Assistant Professor Amornchai Arpornwichanop, D.Eng.)


..... Examiner
(Assistant Professor Soorathep Kheawhom, Ph.D.)


..... External Examiner
(Assistant Professor Wanwilai Kraipech Evans, Ph.D.)


..... External Examiner
(Assistant Professor Worapon Kiatkittipong, D.Eng.)

ญาณีพร พัทธวร โสคติ : การวิเคราะห์ทางทฤษฎีของเซลล์เชื้อเพลิงชนิดออกไซด์แข็งที่เกิดการรีฟอร์มมิงของก๊าซมีเทนภายใน (THEORETICAL ANALYSIS OF SOLID OXIDE FUEL CELL WITH INTERNAL METHANE REFORMING) อ. ที่ปรึกษาวิทยานิพนธ์หลัก : ผศ.ดร. อมรชัย อภรณ์วิชา นพ, 164 หน้า.

งานวิจัยนี้นำเสนอการวิเคราะห์สมรรถนะของเซลล์เชื้อเพลิงชนิดออกไซด์แข็งแบบระบบที่เกิดการรีฟอร์มมิงของก๊าซมีเทนภายในเซลล์เชื้อเพลิงโดยตรงซึ่งดำเนินงานในช่วงอุณหภูมิปานกลาง เซลล์เชื้อเพลิงที่ศึกษาจะใช้อิเล็กโทรไลต์ทั้งแบบที่มีความสามารถในการนำออกซิเจนไอออนและนำโปรตอน แบบจำลองทางไฟฟ้าเคมีซึ่งพิจารณาศักย์ไฟฟ้าสูญเสียทั้ง 3 ชนิด (ได้แก่ ศักย์ไฟฟ้าสูญเสียที่เกิดจากความต้านทานไฟฟ้า จากปฏิกิริยาไฟฟ้าเคมี และจากความแตกต่างของความเข้มข้นของสาร) ที่นำมาใช้ในงานวิจัยนี้ได้ถูกเปรียบเทียบความถูกต้องกับผลการทดลองที่ได้จากงานวิจัยที่ผ่านมา สมรรถนะทางไฟฟ้าของเซลล์เชื้อเพลิงถูกวิเคราะห์โดยการพิจารณาบทบาทของโครงสร้างรองรับเซลล์และผลของพารามิเตอร์ที่เกี่ยวข้องกับการออกแบบ ผลการจำลองแสดงให้เห็นว่าการออกแบบเซลล์เชื้อเพลิงโดยใช้ขั้วแอโนดเป็นโครงสร้างรองรับจะให้สมรรถนะที่ดีที่สุด นอกจากนี้ยังพบว่าการลดความหนาของชั้นอิเล็กโทรไลต์และการเพิ่มขนาดรูพรุนและความพรุนของขั้วอิเล็กโทรดสามารถเพิ่มสมรรถนะของเซลล์เชื้อเพลิงทั้งสองประเภท ส่วนการลดความหนาของขั้วแคโทดและแอโนดจะไม่มีผลต่อสมรรถนะของเซลล์เชื้อเพลิงแบบนำออกซิเจนไอออนและนำโปรตอนตามลำดับ

สมรรถนะของเซลล์เชื้อเพลิงชนิดออกไซด์แข็งที่ใช้ขั้วแอโนดเป็นโครงสร้างทั้งสองประเภทโดยดำเนินการภายใต้สภาวะการรีฟอร์มมิงของก๊าซมีเทนภายในและอุณหภูมิคงที่ที่ถูกวิเคราะห์โดยอาศัยแบบจำลอง 1 มิติที่สภาวะคงตัวร่วมกับแบบจำลองทางไฟฟ้าเคมี จากการศึกษาพบว่าการเพิ่มอุณหภูมิ ความดัน และอัตราส่วนเชิงโมเลกุลระหว่างน้ำ คาร์บอนสามารถเพิ่มประสิทธิภาพของเซลล์เชื้อเพลิงทั้งสองแบบได้ เมื่อพิจารณาที่อุณหภูมิ 1073 เคลวิน และความดันบรรยากาศ พบว่าสมรรถนะของเซลล์เชื้อเพลิงแบบที่มีการนำโปรตอนมีค่าน้อยกว่าแบบที่มีการนำออกซิเจนไอออนมากเพราะอิเล็กโทรไลต์มีค่าการนำโปรตอนน้อยส่งผลให้เกิดค่าศักย์ไฟฟ้าสูญเสียเนื่องจากความต้านทานไฟฟ้ามาก ในกรณีของเซลล์เชื้อเพลิงแบบนำโปรตอนพบว่าการเพิ่มปริมาณน้ำในก๊าซออกซิเจนทำให้สมรรถนะของเซลล์เชื้อเพลิงลดลงและยังพบว่ามีก๊าซคาร์บอนมอนอกไซด์เกิดขึ้นในช่องกรไหลเชื้อเพลิงของเซลล์เชื้อเพลิงชนิดนี้ในปริมาณสูง

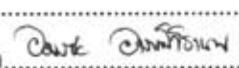
เพื่อหลีกเลี่ยงปัญหาของเซลล์เชื้อเพลิงชนิดออกไซด์แข็งแบบที่นำโปรตอนที่เกี่ยวข้องกับสมรรถนะการทำงานที่ต่ำและการเกิดก๊าซคาร์บอนมอนอกไซด์ในปริมาณสูง งานวิจัยนี้จึงได้นำเสนอระบบร่วมของเซลล์เชื้อเพลิงที่ประกอบด้วยเซลล์เชื้อเพลิงชนิดออกไซด์แข็งแบบที่นำออกซิเจนไอออนและนำโปรตอน โดยสมรรถนะของระบบเซลล์เชื้อเพลิงถูกวิเคราะห์โดยใช้แบบจำลองที่ได้มาจากสมการอนุกรมมวลและแบบจำลองไฟฟ้าเคมี จากการศึกษาพบว่าสมรรถนะของระบบร่วมของเซลล์เชื้อเพลิงจะให้ประสิทธิภาพที่สูงกว่าเมื่อเปรียบเทียบกับการใช้เซลล์เชื้อเพลิงแบบเดี่ยว และยังพบว่าการเพิ่มอุณหภูมิ ความดัน ระดับของการเกิดปฏิกิริยารีฟอร์มมิง และการลดความเร็วของการป้อนเชื้อเพลิงและค่าศักย์ไฟฟ้าในการดำเนินงานสามารถเพิ่มประสิทธิภาพของระบบเซลล์เชื้อเพลิงดังกล่าวได้

ภาควิชา.....วิศวกรรมเคมี....

สาขาวิชา.....วิศวกรรมเคมี....

ปีการศึกษา...2552.....

ลายมือชื่อนิติศ..........

ลายมือชื่อ อ.ที่ปรึกษาวิทยานิพนธ์หลัก..........

4870276221 : MAJOR CHEMICAL ENGINEERING

KEYWORDS : SOLID OXIDE FUEL CELL / THEORETICAL ANALYSIS / INTERNAL REFORMING / METHANE

YANEEPORN PATCHARAVORACHOT : THEORETICAL ANALYSIS OF SOLID OXIDE FUEL CELL WITH INTERNAL METHANE REFORMING.

ADVISOR : ASSISTANT PROFESSOR AMORNCHAI ARPORNWICHANOP, D.Eng., 164 pp.

This research presents a performance analysis of a planar solid oxide fuel cell (SOFC) fed by methane with direct internal reforming under an intermediate temperature operation. The electrolyte material used in SOFC was focused on an oxygen ion-conducting (SOFC-O²⁻) and a proton-conducting electrolyte (SOFC-H⁺). A detailed electrochemical model that takes into account all voltage losses (i.e., ohmic, activation and concentration losses) used in this study was validated with experimental data reported in literature. The characteristic performance of SOFC was analyzed by considering the role of support structure and the effect of design parameters. The simulation results showed that an anode-supported design of both the SOFCs gives the best performance. Further, it was found that decreasing electrolyte thickness and increasing electrode pore size and porosity can improve the performance of SOFC-O²⁻ and SOFC-H⁺. A decrease in cathode thickness has less effect on the performance of SOFC-O²⁻ whereas a decrease in anode thickness is less sensitive to the performance of SOFC-H⁺.

The performance of the anode supported SOFC-O²⁻ and SOFC-H⁺ under the direct internal reforming operation of methane and isothermal condition was analyzed based on a one-dimensional steady-state fuel cell model coupled with a detailed electrochemical model taking into account all various voltage losses. It was found that increases in operating temperature, pressure and steam to carbon ratio can enhance the efficiency of both the SOFCs. Under the operating temperature of 1073 K and pressure of 1 atm, the performance of SOFC-H⁺ was considerably lower than SOFC-O²⁻ because a low protonic conductivity of electrolyte leads to much higher ohmic loss in the SOFC-H⁺. In case of SOFC-H⁺, the effect of water content in oxidant was considered and found that the SOFC-H⁺ performance decreases with an increase in water content in oxidant. Further, high CO content at a fuel channel was observed and this may hinder the SOFC-H⁺ performance by reducing catalyst activity.

To avoid the problems associated with low actual performance and the presence of high CO content at the fuel channel of SOFC-H⁺, a SOFC combined system consisting of SOFC-O²⁻ and SOFC-H⁺ was proposed in this research. The performance of the SOFC system was primarily evaluated by using the SOFC model based on the conservation of mass and a detailed electrochemical model. The results showed that the performance of the SOFC-O²⁻-SOFC-H⁺ combined system provides a higher efficiency compared with the use of a single SOFC. Further, it was indicated that increasing the operating temperature, pressure, degree of pre-reforming as well as decreasing the inlet fuel velocity and cell voltage can improve the efficiency of the SOFC system.

Department : Chemical Engineering

Student's Signature 

Field of Study : Chemical Engineering

Advisor's Signature Amornchai Arpornwichanop

Academic Year : 2009

ACKNOWLEDGEMENTS

I would first like to express my gratitude to my thesis advisor, Assistant Professor Amornchai Arpornwichanop, for his inspiration and encouragement. He has guided me in both research and non-research areas. It has been a great opportunity and experience for me to work with him.

I am deeply grateful to the other member of my thesis committee, Associate Professor Tharathon Mongkhonsi, Assistant Professor Soorathep Kheawhom, Assistant Professor Worapon Kiatkittipong and Assistant Professor Wanwilai Kraipech Evans, for their time and useful comments on this thesis.

I would like to acknowledge Chulalongkorn University (The 90th Anniversary of Chulalongkorn University Fund, Ratchadaphiseksomphot Endowment Fund) and The Thailand Research Fund for financial support on this research and the graduate school of Chulalongkorn University for giving me partial fund to attend an international conference. I would also like to thank Thailand's Commission on Higher Education under the program "Strategic Scholarships for Frontier Research Network" for granting fund to do a short-term research at UK during my doctoral degree study.

My appreciation is also expressed to Professor Nigel Brandon who provides me the opportunity to join his fuel cell group, for his guidance during my research work at Department of Earth Science & Engineering, Imperial College, London, UK. Special thanks to my friends in the fuel cell group for their assistance while I lived in London. They shared their knowledge and experience in fuel cell area.

I would also thank all of the members of the Control and Systems Engineering Research Laboratory in the Department of Chemical Engineering, Chulalongkorn University for their friendship.

Finally, I would like to thank my beloved parents for their love and encouragement. Also special thanks to Mr. Nakarin Jirapathanathip, who always beside me when I was exhausted. Without their support, my research would not have finished.

CONTENTS

	PAGE
ABSTRACT IN THAI.....	iv
ABSTRACT IN ENGLISH	v
ACKNOWLEDGEMENTS.....	vi
CONTENTS.....	vii
LIST OF TABLES	xii
LIST OF FIGURES	xiv
LIST OF ABBREVIATIONS.....	xviii
CHAPTER	
I INTRODUCTION	1
1.1 Introduction.....	1
1.2 Research objective	5
1.3 Scope of research	5
1.4 Dissertation overview	6
II LITERATURE REVIEWS	7
2.1 Modeling of SOFC.....	7
2.1.1 Electrochemical model.....	9
2.1.2 Transportation model.....	11
2.2 SOFC with supported structure.....	15
2.3 SOFC with different electrolyte types	15
2.4 SOFC hybrid system	18
2.4.1 SOFC with gas turbine system.....	19
2.4.2 SOFC with other fuel cells system.....	20
III THEORY	22
3.1 Fuel cell.....	22
3.1.1 Cell Components.....	22
3.1.2 Types of fuel cell	23
3.1.3 Advantages of fuel cell	25

CHAPTER	PAGE
3.2 Solid oxide fuel cell	26
3.2.1 SOFC features	26
3.2.2 SOFC operation	26
3.2.3 SOFC characteristics	28
3.2.4 SOFC material	29
3.2.5 SOFC design	32
3.2.5.1 Sealless tubular design	31
3.2.5.2 Planar design	32
3.2.6 SOFC configuration	33
3.2.7 SOFC: An intermediate-temperature operation	34
3.2.8 Types of fuel and oxidant	35
3.2.9 Internal reforming SOFC	36
3.2.9.1 Indirect internal reforming SOFC (IIR-SOFC)	39
3.2.9.2 Direct internal reforming SOFC (DIR-SOFC)	40
IV MATHEMATICAL MODEL OF SOFC	41
4.1 Model configuration	41
4.2 Model assumption	42
4.3 Model equations	46
4.3.1 Mass balance equation	47
4.3.2 Electrochemical model	48
4.3.3.1 Reversible open-circuit voltage	49
4.3.3.2 Actual fuel cell voltage	50
4.4 Numerical solution	56
4.4.1 Electrochemical model	56
4.4.2 Steady-state fuel cell model	58
4.5 SOFC performance	60
4.5.1 Power generation	60
4.5.2 Fuel cell efficiency	60
4.5.3 Fuel utilization	61
4.6 Model validation	61
4.6.1 Model validation of SOFC-O ²⁻	61

CHAPTER	PAGE
4.6.2 Model validation of SOFC-H ⁺	62
V SOLID OXIDE FUEL CELL BASED ON OXYGEN ION-CONDUCTING ELECTROLYTE	64
5.1 Introduction.....	64
5.2 Electrochemical study	65
5.2.1 Results and discussions.....	66
5.2.1.1 Role of support structures.....	69
5.2.1.2 Effect of electrolyte thickness	72
5.2.1.3 Effect of anode thickness.....	72
5.2.1.4 Effect of cathode thickness.....	75
5.2.1.5 Effect of electrode porosity	75
5.2.1.6 Effect of electrode pore size	75
5.2.2 Conclusions	78
5.3 Anode-supported SOFC performance.....	78
5.3.1 Results and discussions.....	80
5.3.1.1 Effect of operating temperature.....	85
5.3.1.2 Effect of operating pressure.....	85
5.3.1.3 Effect of degree of pre-reforming of methane.....	88
5.3.1.4 Effect of steam to carbon ratio	88
5.3.1.5 Effect of inlet fuel velocity.....	92
5.3.2 Conclusions	92
VI SOLID OXIDE FUEL CELL BASED ON PROTON-CONDUCTING ELECTROLYTE	93
6.1 Introduction.....	93
6.2 Electrochemical study	95
6.2.1 Results and discussions.....	95
6.2.1.1 Role of support structures.....	98
6.2.1.2 Effect of electrolyte thickness	102
6.2.1.3 Effect of cathode thickness.....	102
6.2.1.4 Effect of electrode porosity	105

CHAPTER	PAGE
6.2.1.5 Effect of electrode pore size	105
6.2.2 Conclusions	108
6.3 Anode-supported SOFC-H ⁺ performance	108
6.3.1 Results and discussions	110
6.3.1.1 Effect of steam to carbon ratio	115
6.3.1.2 Effect of operating temperature	116
6.3.1.3 Effect of operating pressure	116
6.3.1.4 Effect of water content	121
6.3.2 Conclusions	121
VII A HYBRID SYSTEM OF SOLID OXIDE FUEL CELLS WITH DIFFERENT ELECTROLYTES	123
7.1 Introduction	123
7.2 Single SOFC-O ²⁻ and SOFC-H ⁺ model	125
7.2.1 SOFC configuration	125
7.2.2 SOFC operation	126
7.2.3 SOFC model	126
7.3 SOFC-O ²⁻ -SOFC-H ⁺ system model	130
7.4 Results and discussion	131
7.4.1 Performance of a single SOFC-O ²⁻ and SOFC-H ⁺	131
7.4.2 Performance of a SOFC-O ²⁻ -SOFC-H ⁺ system	136
7.4.1.1 Effect of operating temperature	136
7.4.1.2 Effect of operating pressure	138
7.4.1.3 Effect of degree of pre-reforming	138
7.4.1.4 Effect of inlet fuel velocity	138
7.4.1.5 Effect of cell voltage	140
7.5 Conclusions	141
VIII CONCLUSION AND RECOMMENDATIONS	142
8.1 Conclusions	142
8.1.1 Solid oxide fuel cell based on oxygen ion-conducting electrolyte	143

CHAPTER	PAGE
8.1.2 Solid oxide fuel cell based on proton-conducting electrolyte	143
8.1.3 Performance comparisons between SOFC-O ²⁻ and SOFC-H ⁺	144
8.1.4 A hybrid system of solid oxide fuel cells with different electrolytes.....	145
8.2 Recommendations.....	146
REFERENCES	147
APPENDICES	158
APPENDIX A.....	159
APPENDIX B	162
VITA.....	164

LIST OF TABLES

TABLE	PAGE
3.1	Types of fuel cell..... 24
3.2	Requirement for ceramic SOFC component (Mihn and Takahashi, 1995) 30
3.3	Characteristics of SOFC Stack design (Minh and Takahashi, 1995)..... 32
3.4	Comparison of three primary fuel reforming reactions (Hayre et al., 2006) 37
3.5	Advantages and disadvantages of three primary H ₂ production processes (Hayre et al., 2006) 38
4.1	The materials used as the electrodes and electrolyte for SOFC-O ²⁻ and SOFC-H ⁺ 42
4.2	Pre-exponential factor and activation energy for computing the exchange-current density 53
4.3	The conductivities of cell component used in the calculations of the internal resistance (Ferguson et al., 1996) 53
5.1	Electrochemical model of SOFC used in the present study 67
5.2	Model geometries and material property parameters 68
5.3	Operating conditions for SOFC at the standard case 68
5.4	Model input parameters and operating conditions 80
6.1	Electrochemical model of SOFC-H ⁺ 96
6.2	Values of input parameters used in the present study 97
6.3	Model parameters used in the performance analysis of SOFC-H ⁺ 111
7.1	Reactions considered in the SOFC-O ²⁻ and SOFC-H ⁺ model 127
7.2	Steady-state solid oxide fuel cell model: Mass balance 127
7.3	Electrochemical model in SOFC-O ²⁻ and SOFC-H ⁺ 128
7.4	The values of electrode exchange current densities ($i_{0,electrode}$) for computing the activation overpotential 129
7.5	Operation conditions used in the performance analysis of SOFC-O ²⁻ -SOFC-H ⁺ system 132
7.6	Performance results of single-SOFC-O ²⁻ and SOFC-H ⁺ and SOFC hybrid system 135

TABLE	PAGE
A.1 Collision integral constants	160
A.2 Lennard–Jones potential	161



ศูนย์วิทยทรัพยากร
จุฬาลงกรณ์มหาวิทยาลัย

LIST OF FIGURES

FIGURES	PAGE
3.1 Basic components of a fuel cell and its operation.....	23
3.2 Basic principle of the SOFC operation based on an oxygen conducting electrolyte.....	27
3.3 Basic principle of the SOFC operation based on a proton conducting electrolyte.....	27
3.4 Ideal and actual fuel cell voltage/current characteristics	29
3.5 Sealless tubular SOFC design.....	33
3.6 Planar SOFC design	33
3.7 SOFC single cell configurations (a) electrolyte-supported, (b) anode-supported, and (c) cathode-supported	34
3.8 Schematic of an external reforming SOFC.....	36
3.9 Schematic of an indirect internal reforming SOFC	39
3.10 Schematic of a direct internal reforming SOFC.....	40
4.1 Configuration of a co-flow planar solid oxide fuel cell.....	42
4.2 The schematic of a co-flow planar solid oxide fuel cell: (a) solid oxide fuel cell based on an oxygen ion-conducting electrolyte, (b) solid oxide fuel cell based on a proton-conducting electrolyte.	45
4.3 Ideal and actual fuel cell voltage/current characteristic (Hirschenhofer et al., 1998)	51
4.4 Flow diagram of numerical solution for determining electrochemical performance of SOFC.	57
4.5 Flow diagram of numerical solution for determining steady-state SOFC performance.	59
4.6 Comparison between model predictions and experimental results (Zhao and Virkar, 2005).	63
4.7 Comparison of cell characteristics of SOFC-H ⁺ obtained from model prediction and experimental data (Iwahara, 1988).....	63
5.1 Performance of an anode-supported planar SOFC at different current densities.....	69

FIGURES	PAGE
5.2 Comparison of SOFC with different support structures: (a) cell performance and (b) average overpotentials	71
5.3 Effect of electrolyte thickness at different current densities on: (a) cell voltage and power density and (b) ohmic loss.....	73
5.4 Effect of anode thickness at different current densities on: (a) cell voltage and power density and (b) concentration overpotential.....	74
5.5 Effect of electrode porosity at different current densities on: (a) power density, and (b) concentration overpotential.....	76
5.6 Effect of electrode pore size at different current densities on: (a) power density, and (b) concentration overpotential.....	77
5.7 Performance characteristics of an anode-supported SOFC at different cell voltages	81
5.8 (a) Mole fraction profiles of gas compositions at fuel channel, (b) Mole fraction profiles of gas compositions at air channel, (c) distribution of current density, and (d) distribution of individual voltage losses.....	83-84
5.9 Effect of operating temperature on: (a) fuel cell efficiency and power density and (b) activation, ohmic and anode concentration overpotentials	86
5.10 Effect of operating pressure on: (a) fuel cell efficiency and power density and (b) anode concentration overpotentials.	87
5.11 Effect of degree of pre-reforming of methane: (a) fuel cell efficiency and power density and (b) anode concentration overpotentials.....	89
5.12 Effect of steam to carbon ratio on: (a) fuel cell efficiency and power density and (b) anode concentration overpotentials.....	90
5.13 Effect of inlet fuel velocity on: (a) fuel cell efficiency and power density and (b) anode concentration overpotentials.	91
6.1 The electrical characteristics of anode-supported SOFC-H ⁺ at different current densities under isothermal condition: (a) open-circuit voltage, cell voltage and power density and (b) individual overpotentials in the cell.....	99
6.2 Comparison of SOFC-H ⁺ with different support structures: (a) power density, (b) ohmic loss, and (c) concentration overpotential.	100-101

FIGURES	PAGE
6.3 Effect of electrolyte thickness at different current densities on: (a) power density, and (b) ohmic loss.	103
6.4 Effect of cathode thickness at different current densities on (a) power density, and (b) concentration overpotential.....	104
6.5 Effect of electrode pore size at different current densities on: (a) power density, and (b) concentration overpotential.....	106
6.6 Effect of electrode porosity at different current densities on: (a) power density, and (b) concentration overpotential.....	107
6.7 Performance characteristics of an SOFC-H ⁺ at different cell voltages and fuel velocities.....	112
6.8 (a) Profiles of gas compositions at fuel channel, (b) Profiles of gas compositions at air channel, (c) distribution of current density, and (d) distribution of individual voltage losses	113-115
6.9 Effect of steam/carbon ratio on: (a) molar flow rate of CO and fuel utilization, and (b) cell efficiency and power density	117
6.10 Effect of operating temperature on: (a) molar flow rate of CO and fuel utilization and (b) cell efficiency and power density	118
6.11 Effect of operating pressure on: (a) molar flow rate of CO and fuel utilization and (b) cell efficiency and power density	119
6.12 Effect of water content on: (a) molar flow rate of CO and fuel utilization and (b) cell efficiency and power density	120
7.1 Schematic of the SOFC-O ²⁻ -SOFC-H ⁺ system.....	125
7.2 Distributions of all voltage losses in: (a) SOFC-O ²⁻ , and (b) SOFC-H ⁺	134
7.3 Comparison the results of all voltage losses in SOFC-O ²⁻ and SOFC-H ⁺	135
7.4 Effect of operating temperature on the efficiency of the SOFC-O ²⁻ , SOFC-H ⁺ , and SOFC hybrid system.....	137
7.5 Effect of operating pressure on the efficiency of the SOFC-O ²⁻ , SOFC-H ⁺ , and SOFC hybrid system.....	137
7.6 Effect of degree of pre-reforming on the efficiency of the SOFC-O ²⁻ , SOFC-H ⁺ , and SOFC hybrid system.....	139
7.7 Effect of inlet fuel velocity on the efficiency of the SOFC-O ²⁻ , SOFC-H ⁺ , and SOFC hybrid system	139

FIGURES

PAGE

- 7.8 Effect of changing the cell voltage in the SOFC-O²⁻, SOFC-H⁺, and SOFC hybrid system on the efficiency of the SOFC hybrid system 140



ศูนย์วิทยทรัพยากร
จุฬาลงกรณ์มหาวิทยาลัย

LIST OF ABBREVIATIONS

A	Fuel cell area [m^2]
ASR	Area specific resistance [$\Omega \text{ m}^2$]
C_i	Molar concentration of component i [mol m^{-3}]
$D_{\text{an,eff}}$	Effective gas diffusion coefficient in the anode side [$\text{m}^2 \text{ s}^{-1}$]
$D_{\text{ca,eff}}$	Effective gas diffusion coefficient in the cathode side [$\text{m}^2 \text{ s}^{-1}$]
E_a	Activation energy [kJ mol^{-1}]
E^{OCV}	Open-circuit voltage [OCV] [V]
E^0	OCV for standard temperature and pressure and pure reactants for the H_2 oxidation reaction [V]
F	Faraday's constant [C mol^{-1}]
F_{air}	Molar flow rate of air [mol s^{-1}]
F_{fuel}	Molar flow rate of the fuel [mol s^{-1}]
h_a	Air channel height [m]
h_f	Fuel channel height [m]
i_{ave}, i	Average and local current density [A m^{-2}]
$i_{0,\text{electrode}}$	Exchange current density [A m^{-2}]
K_{eq}	Equilibrium constant for water gas shift reaction
k_0	Pre-exponential constant for reforming reaction [$\text{mol s}^{-1} \text{ m}^{-2} \text{ bar}^{-1}$]
k_{WGSR}	Pre-exponential factor for water gas shift reaction [$\text{mol s}^{-1} \text{ m}^{-3} \text{ Pa}^{-2}$]
L	Cell length [m]

LHV	Lower heating value [kJ mol^{-1}]
n	Number of electrons participating in the electrochemical reaction
P	Pressure [kPa]
p_i	Partial pressure of component i [kPa]
P_{SOFC}	Power density [W m^{-2}]
R_{ohm}	Ohmic resistance [$\Omega \text{ m}^2$]
\mathfrak{R}	Gas constant [$\text{kJ mol}^{-1} \text{ K}^{-1}$]
R_j	Rate of reaction j [$\text{mol m}^{-2} \text{ s}^{-1}$]
S/C	Steam to carbon ratio
T	Temperature [K]
U_{fuel}	Fuel utilization
u_a	Air velocity [m s^{-1}]
u_f	Fuel velocity [m s^{-1}]
V	Operating cell voltage [V]
W	Cell width [m]
y_i	Mole fraction of component i

Greek symbols

α	Transfer coefficient
ε	Porosity of electrode
$\varepsilon_{\text{SOFC}}$	Fuel cell efficiency [%]

η_{act}	Activation overpotential [V]
η_{con}	Concentration overpotential [V]
η_{ohm}	Ohmic overpotential [V]
σ_{an}	Conductivity of anode [$\Omega^{-1} \text{ m}^{-1}$]
σ_{ca}	Conductivity of cathode [$\Omega^{-1} \text{ m}^{-1}$]
σ_{ele}	Conductivity of electrolyte [$\Omega^{-1} \text{ m}^{-1}$]
τ_{an}	Anode thickness [m]
τ_{ca}	Cathode thickness [m]
τ_{ele}	Electrolyte thickness [m]
ν_{ij}	Stoichiometric coefficient of component i in reaction j

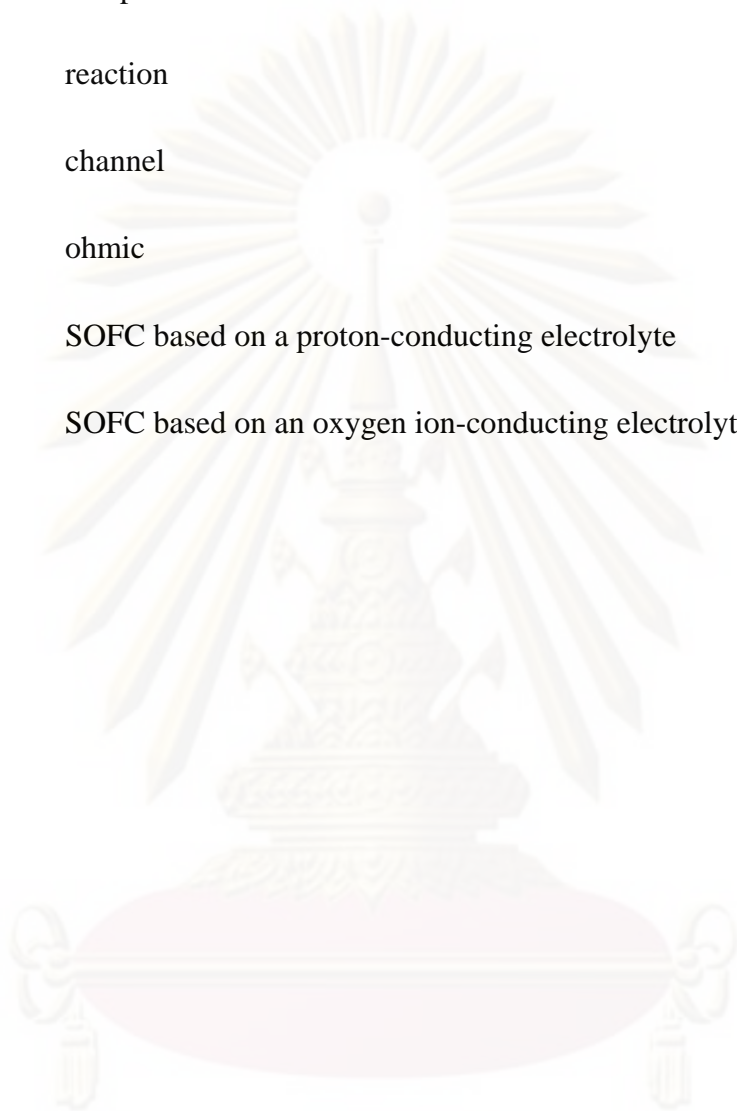
Superscripts

I	Electrode electrolyte interface
in	Feed inlet condition

Subscripts

a	air channel
act	activation
an	anode
ca	cathode
conc	concentration

<i>ele</i>	electrolyte
<i>f</i>	fuel channel
<i>i</i>	component
<i>j</i>	reaction
<i>k</i>	channel
ohm	ohmic
SOFC-H	SOFC based on a proton-conducting electrolyte
SOFC-O	SOFC based on an oxygen ion-conducting electrolyte



ศูนย์วิจัยทรัพยากร
จุฬาลงกรณ์มหาวิทยาลัย

CHAPTER I

INTRODUCTION

1.1 Introduction

Increasing global energy consumption had led to critical environmental problems including global warming and climate change. Since a conventional combustion-based process for power generation has low efficiency and releases greenhouse gas that is a major cause of global warming, the development of a new technology with high efficiency and environmental friendliness is of great interest. Fuel cells have emerged as an electrochemical device that generates electricity efficiently since they can directly convert chemical energy contained in gaseous fuel into electricity through an electrochemical process. In addition, fuel cells produce electricity without combustion process as an intermediate step and releases only steam; the emission of NO_x , SO_x and other ground level pollutants leading to air pollution is either negligible or undetectable for their system (Singhal, 2002; Larminie and Dicks, 2003).

Among the various types of fuel cell, the solid oxide fuel cell (SOFC) is received considerable interest due to having the highest efficiency compared with other types of fuel cell. The high-temperature operation of SOFCs (1023-1273 K) offers several advantages that include a high electrochemical-reaction rate, the flexibility of using various fuel types, and a tolerant to impurities. Moreover, the high temperature of waste gases could be used as a heat source for cogeneration applications and bottoming cycles or be integrated with a gas turbine to further increase the overall efficiency of the power system (Petruzzi et al., 2003; Xue et al., 2005; Hussian et al., 2006). Another important feature of SOFC is its all-solid-state construction with ceramic materials; there is no liquid electrolyte with its attendant material corrosion and water management problems (Dincer, 2002).

For SOFCs, not only pure hydrogen but also any hydrocarbon fuels such as natural gas, methanol, ethanol, and gasoline, can be used as a fuel. In general, hydrocarbon fuels are needed to be reformed into hydrogen-rich gas via an external reformer before being fed into an SOFC stack. However, the reforming of hydrocarbon fuels can be internally carried out within SOFC, which is called an internal reforming SOFC (IR-SOFC), as the operating temperature of SOFC is in the range of that used in reforming reactions (between 1023 and 1173 K) (Clarke et al., 1997). This can eliminate the requirement of the external reformer, resulting in improved overall efficiency and reduced operating cost (Fellows, 1998; Aguiar et al., 2002). Under an internal reforming operation, the reforming section is close to the electrochemical section; therefore, the heat released from the electrochemical reaction can supply the reforming reaction. Commonly, the internal reforming operation can be divided into two main approaches, depending on the position of a reformer section and a fuel cell anode: indirect (IIR) and direct (DIR) internal reforming. In the former, fuel gas is fed into the reforming section which is separated but adjacent to the fuel cell anode side whereas in the latter, it is directly introduced to the fuel cell and directly reformed on the anode material. Recently, a DIR-SOFC has attracted much interest because hydrogen produced from the reforming reaction is continuously consumed during the oxidation of hydrogen for generating electricity and thus, the conversion of the equilibrium-limited reforming reaction is enhanced (Aguiar et al., 2004).

In general, an SOFC can have either a planar or tubular configuration. The planar design has recently received much attention since it is simpler to fabricate and more flexible in terms of cell geometry (i.e., circular or prismatic) and gas manifolding (i.e., co-, counter- and cross-flow direction) (Minh and Takahashi, 1995). In addition, due to the fact that its short current path results in low internal electrical resistances, a planar SOFC provides higher power density, compared with a tubular design (Yakabe et al., 2001; Costamagna et al., 2004). Unfortunately, the planar SOFC has some technical challenges because the high operating temperature results in the internal stresses in cell components, mismatch in thermal expansion coefficient among cells and requirement in the high temperature gas seal to prevent gas leak (Yakabe et al., 2001; Leah et al., 2005; Hussian et al., 2006). Furthermore, the high operating temperature causes problems in high material costs, slow start-up and

shorter life cell (Leng et al., 2004; Liu et al., 2006). To reduce these problems, an intermediate temperature solid oxide fuel cells (IT-SOFC) operated between 873 and 1023 K has been proposed for the possibility of using a wider range of materials and the promise of low-cost fabrication.

When an SOFC is operated and the current is drawn from the fuel cell, the cell voltage falls due to three overpotential losses. They are (1) ohmic overpotential, (2) activation overpotentials, and (3) concentration overpotentials. An efficient operation of SOFC requires that all of these losses are as small as possible. However, one of the problems associated with the low temperature operation (IT-SOFC) is an increase in ohmic loss of the cell (Liu et al., 2006). Since the temperature reduction causes a relevant reduction of the ionic conductivity of the electrolyte. The higher ohmic loss under the low temperature operation could be reduced by: (1) applying thinner conventional electrolyte material of yttria-stabilized zirconia (YSZ) and/or (2) replacing YSZ by alternative electrolytes (Xin et al., 2006).

Most of researches have focused on an anode-supported SOFC, in which the anode is the thickest component and support structure, thus reducing the electrolyte thickness to several microns (typically between 8 to 20 μm). Considering the characteristics of the anode-supported SOFC, it has been reported that activation and concentration overpotentials can often outweigh the benefit of reduced ohmic loss due to smaller electrolyte thickness so that the specific resistance of the anode-supported SOFC at an intermediate temperature may be larger than that of the high-temperature SOFC (Virkar et al., 2000; Chan et al., 2001; Shi et al., 2006). Thus, a number of researchers have focused on the improvement of the electrode and electrolyte, aiming at obtaining a higher and more stable electrochemical performance under the lower operating temperature. Further, it is well known that the characteristics of SOFCs are strongly affected not only by operating conditions such as temperature and pressure, and partial pressures of fuel and oxidant but also by design parameters such as the thickness of electrode and electrolyte and the porosity of electrode. Therefore, the performance analysis of fuel cells should take these parameters into account as it will lead to an optimum design and operation of SOFCs.

Apart from a conventional SOFC based on an oxygen-ion conducting electrolyte (SOFC- O^{2-}), SOFC can use a proton conductor as electrolyte in the

operation (SOFC-H⁺). The main advantage of SOFC-H⁺ is that a higher H₂ partial pressure can be achieved as H₂O is produced at the cathode side, resulting in an improved open-circuit voltage and enhanced efficiency of the SOFC systems (Epifanio et al., 2008). More complete hydrogen utilization of SOFC-H⁺ makes further the SOFC system possible to be simple and compact by eliminating the need of the afterburner (Zamfirescu and Dincer, 2009). In addition, the SOFC-H⁺ exhibits high proton conductivity at intermediate temperature operations (300-700°C) which can achieve an acceptable start-up time and may be possible to use in vehicular application (Epifanio et al., 2008; Zamfirescu and Dincer, 2009). In the past years, many researchers have directed to the synthesis and characterization of proton-conducting materials for SOFC-H⁺ (Iwahara, 1996; Coore, 2003; Fukada et al., 2006; Potter and Baker, 2006; Pekridis et al., 2007; Suksamai and Metcalfe, 2007; Epifanio et al., 2008). There are currently limited works concentrating on the modeling and analysis of the SOFC-H⁺. Further, most studies investigated the theoretical performance of the SOFC-H⁺ without considering the presence of actual losses in a real operation of fuel cells (Demin and Tsiakaras, 2001; Jamsak et al., 2006; Zamfirescu and Dincer, 2009). Therefore, a detailed electrochemical model, taking into account all voltage losses in real fuel cell operation (i.e., activation, ohmic, and concentration losses), to predict accurately the characteristic performance of SOFC-H⁺ is particularly required for analysis, design, and improvement of SOFC-H⁺ (Chan et al., 2001; Hernandez-Pacheco et al., 2004; Ni et al., 2007).

For the SOFC-H⁺ operating with direct internal reforming (DIR) of methane, H₂O, which is required for the reforming reaction at the anode side, is lower and is insufficient to convert hydrocarbon fuel into H₂-rich gas and thus, the CO content in the fuel stream is higher. The presence of high CO content in the anode side may deteriorate the SOFC-H⁺ performance by reducing catalyst activity. Therefore, the development of an SOFC-H⁺ system with high efficiency is of great interest. Due to the internal reforming operation of SOFC-O²⁻, it can produce both electrical power and exhaust gas containing unreformed fuel and other gaseous substances. When the exhaust gas stream is directly supplied to the SOFC-H⁺, the remaining CO can further react with H₂O via water gas shift reaction to produce more H₂ without the requirement of external reformers or shift reactors to treat CO, and then H₂ undergoes the electrochemical reaction. As a result, the electrical power of an SOFC hybrid

system can be more produced. Since the study on a combined SOFC system with different electrolytes (SOFC-O²⁻ and SOFC-H⁺) has not been reported, the performance of the SOFC-O²⁻-SOFC-H⁺ system should be investigated to clarify the possibility of combining two SOFC stacks in this research.

1.2 Research Objective

The aim of this research is to analyze the performance of a planar solid oxide fuel cell fed by methane with direct internal reforming under an intermediate temperature operation.

1.3 Scope of research

In this study, the performance of SOFC based on different types of electrolyte, i.e., SOFC-O²⁻ and SOFC-H⁺ is analyzed by using an electrochemical model which takes into account the voltage losses, i.e., ohmic, activation and concentration losses. The validation of the model used in the study is performed by comparing the model prediction with experimental data in literatures (Iwahara, 1988; Zhao and Virkar, 2005). The electrical characteristics of SOFC in terms of operating voltage, power density and efficiency are studied by considering the role of support structure (anode-, cathode- and electrolyte-supported SOFC) and the effect of design parameters (i.e., cell component thickness, electrode porosity and electrode pore size). When the optimal configuration of SOFC is preliminarily determined, the performance of SOFC-O²⁻ and SOFC-H⁺ operated with direct internal reforming of methane under steady state condition is analyzed. A steady-state model of SOFC based on mass balance and electrochemical model is employed to analyze the cell characteristics (i.e., gas composition and current density profiles) and performances (i.e., operating voltage, power density and efficiency) over a wide range of operating conditions (i.e., temperature, pressure and fuel composition). In addition, the performance of a hybrid system of SOFC-O²⁻ and SOFC-H⁺ is evaluated. Further, the SOFC hybrid system performance is investigated with respect to important operating conditions, such as temperature, pressure, degree of pre-reforming, inlet fuel velocity, and cell voltage.

1.4 Dissertation Overview

This dissertation is organized as follows. Chapter II reviews the literature related to the development of SOFC model that includes an electrochemical model and mass and energy balances, the use of two different electrolytes in SOFC, and the integration of SOFCs with other devices.

Chapter III introduces the basic theory of a fuel cell and SOFCs. A general principle of SOFCs including their features, operations, types of electrolyte, materials, and design is described.

Chapter IV explains a mathematical model of SOFCs based on both an oxygen ion conducting (SOFC-O²⁻) and proton conducting (SOFC-H⁺). The model configuration, model assumption and model equations are described. The validation of the SOFC model used in this study is described.

Chapter V presents the study on a planar SOFC-O²⁻ performance by considering the role of support structures, i.e., anode, cathode, and electrolyte supports with respect to the design parameters (cell component thickness and electrode microstructure). When a suitable support structures of SOFC-O²⁻ is determined, a steady-state performance of SOFC-O²⁻ is further investigated.

Chapter VI involves the performance analysis of a planar SOFC-H⁺. The effect of support structures, i.e., electrode (anode and cathode) and electrolyte supports and design parameters on fuel cell power density and voltage losses is discussed.

Chapter VII discusses the performance evaluation of a hybrid system of solid oxide fuel cells with different electrolytes (SOFC-O²⁻ and SOFC-H⁺). The effect of important operating conditions such as temperature, pressure, degree of pre-reforming, inlet fuel velocity, and cell voltage on the performance of the fuel cell system is given.

Chapter VIII gives the conclusion of this dissertation and the recommendation for future work.

CHAPTER II

LITERATURE REVIEWS

This chapter presents a literature review on solid oxide fuel cells (SOFCs). In Section 2.1, the development of mathematical model for simulation of SOFC is given. Section 2.2 describes an overview of SOFC fabricated with different supported structures. The literature reviews on SOFC based on a proton-conducting electrolyte are summarized in Section 2.3. Finally, Section 2.4 presents previous studies related to an SOFC system and its performance.

2.1 Modeling of SOFC

There have been many publications focusing on the development of a mathematical model of a solid oxide fuel cell (SOFC). The electricity generation of SOFC involves the transport of gaseous components and electrochemical reactions. In general, the model of SOFC is used to describe the electrical characteristics and behavior of SOFC in various aspects.

Considering an electrochemical model, there are many expressions proposed for describing different overpotentials occurred in SOFC: activation, ohmic and concentration overpotentials. For the voltage loss due to activation overpotential, three models are generally considered, i.e., Butler-Volmer equation, Tafel equation and semi-correlation. However, the comparison of these activation overpotential models was found that Butler-Volmer equation gives the most accurate overpotential (Hernandez-Pacheco et al., 2004). Exchange current density is a crucially important factor for determining the activation overpotential. It was assumed to be constant in a number of studies (Chan et al., 2001, Li and Chyu, 2003; Burt et al., 2004). Some authors (Zhu and Kee, 2003; Camparani and Iora, 2004; Costamagna et al., 2004; Hernandez-Pacheco et al., 2004; Qi et al., 2005) proposed the expression dependent on temperature, activation energy and partial pressure of reactants and products for computing a exchange current density. However, semi-empirical correlations based

on experimental data are usually used for explaining the exchange current density (Aguiar et al., 2004), which depends on only temperature and activation energy.

For ohmic resistance related to ohmic overpotential, it is considered to be constant in a number of papers (Nagata et al., 2001; Haynes, 2002; Burt et al., 2004; Xue et al., 2005). Since the ohmic resistance is sensitive to temperature, a number of researches (Ferguson et al., 1996; Aguiar et al., 2004; Ni et al., 2007) considered that the electrical resistivity depends on temperature. Aguiar et al. (2004) and Ni et al. (2007) proposed only the temperature dependent expression for resistivity of the electrolyte while Ferguson et al. (1996) presented that the electrical resistivities of both electrodes and electrolyte are considered to be temperature dependent.

Concentration overpotential due to the diffusion effect of gaseous species inside porous anode and cathode has been considered in a number of studies. The diffusion through the porous media is either modeled by writing detailed mass transfer equations (Nagata et al., 2001; Aguiar et al., 2004; Morel et al., 2005; Qi et al., 2005) or by considering concentration overpotential expressed in terms of a limiting current (Burt et al., 2004). In general, the mass transport through porous electrode can be described by Fick's model, the dusty gas model or the Stefan-Maxwell model. The Stefan-Maxwell model is usually discarded due to its exclusion in Knudsen diffusion. If Knudsen diffusion is dominant, the dusty gas model predictions are more accurate than those from Fick's model. Suwanwarangkul et al. (2003) reported that the dusty gas model is the most suitable model for the H_2 - H_2O and CO - CO_2 systems and recommended for multicomponent system of H_2 - H_2O - CO - CO_2 . They also claimed that the dusty gas model is only required for conditions of high operating current density, low reactant concentration and small pore size where high accuracy of model prediction is required. Although the dusty gas model is superior to Fick's model in its capability to predict the fluxes inside porous media, Fick's model is more frequently used and simpler to implement than the dusty gas model because the explicit analytical expressions can be easily derived for fluxes. In SOFC modeling, many studies have been investigated the gas transport inside porous electrode by using Fick's model (Chan et al., 2001; Aguiar et al., 2004; Ni et al., 2007).

Indeed, the electrochemical model can be only used for predicting the performance of SOFC at predetermined condition. This model was applied in many

studies to eliminate the ambiguity of a suitable model used in calculating the real performance of SOFC under different design and operating conditions. The characteristic performance of SOFC based on the electrochemical model is presented in Section 2.1.1. However, in order to describe the intricate interdependency between the gas transport, temperature effect and electrochemical processes, the electrochemical model should be integrated with the system model (i.e., mass and energy balances). The combined system and electrochemical models are developed for investigating various types of SOFC system. Such models can be for various types of state (steady or dynamic), dimension (one, two or three dimensional), design (tubular, planar or integrated planar), electrolyte (an oxygen ion conducting and proton conducting electrolyte), support structure (electrolyte and electrode-supported), flow configurations (cross-, co-, or counter-flow). Section 2.1.2 presents an overview of SOFC simulations based on a full system model. It is noted that the review of SOFC presented in this section was focused on the SOFC based on an oxygen ion-conducting electrolyte.

2.1.1 Electrochemical model

Chan et al. (2001) presented a complete model of a SOFC with humidified H₂ as fuel. They used the Butler-volmer equation to describe the activation overpotential instead of using Tafel equation. The exchange current densities of anode and cathode were equal to 5300 and 2000 A m⁻², respectively. For the concentration overpotential, both ordinary and Knudsen diffusions were considered to cater for different porous electrode designs. Their work showed the sensitivity of the cell voltage drop on changes in the thickness of respective cell components. They reported that an anode-supported fuel cell is the best design when operated at 800°C.

Zhu and Kee (2003) developed a general mathematical model of SOFC system operating on methane as fuel. The SOFC model was employed to analyze the effects of various resistances on an anode-supported SOFC performance under intermediate temperature ($T = 750^{\circ}\text{C}$). The activation overpotentials were described in terms of the Butler-Volmer equation. Concentration overpotentials in the porous electrode structures were based on a dusty-gas model. Ohmic losses depended on ion resistance in the electrolyte.

Aguiar et al. (2004) investigated the electrical characteristics of a planar anode-supported SOFC in terms of cell voltage and power density at different current density. They used semi-empirical correlations, which is a function of operating temperature and activation energy, for calculating the exchange current densities. The conductivity of electrolyte was the temperature dependent while that of the electrodes was kept constant. The electrochemical performance of the fuel cell was analyzed for several temperatures and fuel utilisations.

Hernandez-Pacheco et al. (2004) presented a macro-level model of an anode-supported SOFC. The Butler–Volmer equation, the dusty gas model, and Ohm’s law were used to determine the polarization terms. However, the exchange current densities of electrodes were constant value as proposed in Chan et al. (2001). The fuel cell characteristic curves were calculated under intermediate temperatures (600–800°C) with different fuels (hydrogen, methane, and carbon monoxide as pure fuels).

Hernandez-Pacheco et al. (2005) studied the performance of a conventional anode-supported SOFC operated at different temperatures and fuel utilizations. The activation polarization was determined by the use of the Butler-Volmer equation. The exchange current density was expressed in terms of the activation energy, temperature and partial pressures of gaseous reactants. The dusty-gas model was used for determining the mass fluxes through the porous electrodes. Ohmic polarization was determined by using Ohm’s law in which the total cell resistance was calculated in terms of the resistivity and an equivalent area corresponding to the thickness of the electrodes or electrolyte.

Ni et al. (2007) developed an electrochemical model of SOFC to study the current-voltage characteristics. The Butler-Volmer equation, Fick’s model and Ohm’s law were used to determine the activation, concentration and ohmic overpotentials, respectively. One important feature of this model was that the effects of the structural/operational parameters on the concentration and activation overpotentials were taken into consideration in terms of effective diffusion coefficients and exchange current density, respectively. The simulated results showed good agreement with experimental data. Parametric analyses were performed to investigate the structural/operational parameter effects on the individual overpotentials, overall current-voltage characteristics and energy efficiency.

2.1.2 Transport model

For fuel cell operation, a hydrocarbon fuel is necessary to convert into a hydrogen-rich gas, which is required for the electrochemical reaction on the anode side. One option for converting the fuel feed is to use an external reformer as a fuel processor. Another interesting approach is to reform the fuel feed internally within fuel cells since SOFC is operated at high temperatures (Aguair et al., 2004) which is compatible with the endothermic steam reforming reactions. The SOFC with internal reforming can be operated in two modes: indirect internal reforming (IIR) and direct internal reforming (DIR). As mentioned in Chapter I that a DIR-SOFC is useful more than an IIR-SOFC in terms of that part of the steam required for the reforming reaction can be obtained from the electrochemical reaction and the equilibrium of the reforming reaction may be further shifted to the product side due to the continuing consumption of hydrogen. Many researchers have focused on this system (Achenbach, 1994; Furguson et al., 1996; Demin and Tsiakaras, 2001; Aguiar et al., 2004; Assabumrungrat et al., 2004; Assabumrungrat et al., 2005; Pfafferodt et al., 2005; Jamsak et al., 2006; Jamsak et al., 2007). Besides a number of researchers studied the simulation of SOFC with internal reforming of fuel, the effects of operating condition, flow direction and design parameters on the SOFC performance are also investigated. Details on previous studies concerning about the simulation of SOFC with internal reforming of fuel are explained below.

Achenbach (1994) presented a mathematical model for the simulation of a planar SOFC. Three-dimensional and time-dependent model was used to study the SOFC with internal reforming of methane fuel. Gas recycling and heat transfer by conduction, convection and radiation were considered. The model allowed the determination of temperature, flow and current distributions at various gas flow direction, i.e., co-, counter- and cross-flows. The simulation results showed that the highest cell efficiency was obtained for the counter-flow, the most uniform current density distribution for the co-flow and the largest temperature gradients for the cross-flow. However, this study does not consider the effect of cell overpotentials, stack design, and operating conditions.

Furguson et al. (1996) developed a three-dimensional numerical simulation for the SOFC with the internal reforming of natural gas fuel. Various SOFC geometries

(i.e., tubular, planar and cylindrical) and different flow direction (i.e., cross-, counter- and co-flow designs) for a planar SOFC geometry were considered. The influence of rib width on overall efficiency, the influence of electrode thickness on efficiency, and the comparisons of losses between the tubular and the planar geometry are also studied. They found that the planar design was more efficient than tubular one because of lower ohmic resistances and counter-flow planar design was the most efficient. However, this model can be further improved by incorporating heat radiation between fuel and air channels.

Nagata et al. (2001) presented a one-dimensional steady-state model coupled with electrochemical and internal reforming reactions for the tubular SOFC to compute the temperature and substance distribution along the flow direction. A tubular internal reformer with adjusted catalyst density was inserted into the tubular stack to avoid the inhomogeneous temperature distribution caused by the strong endothermic reforming reaction at the entrance of the internal reformer, resulting in a increase in the power generation efficiency and the exhaust gas temperature. Effects of fuel recirculation, fuel inlet temperature, air recirculation and air inlet temperature on the cell performance were studied. In this work, each control volume used to describe the behavior of the tubular fuel cell was considered to behave as a well-mixed reactor similar to the idea of Debenedetti and Vayenas (1983). In addition, the model geometry did not represent the actual cell geometry within a stack and the heat transfer coefficient was calculated based on fully developed laminar flow at a constant temperature.

Yakabe et al. (2001) concentrated on the estimation of thermal stress in the cell component using a three-dimensional mathematical model for a planar SOFC. A single-unit model with double channels of co- and counter-flow configurations was used to calculate the concentrations of chemical species, the potential distribution, the local and average current density, and temperature distribution inside the cell. They reported that the internal reforming would generate large tensile stresses in the electrolyte and the co-flow configuration was better in terms of reducing the stress produced by the drop in temperature at the entrance of the cell, due to the endothermic reforming reaction.

Aguiar et al. (2002) developed a steady-state model IIR-SOFC with an indirect internal reforming of methane for both co- and counter-flow configurations to study the mismatch between the thermal load associated with the rate of steam reforming at typical SOFC temperatures and the local amount of heat available from the fuel cell reactions. Results showed the local cooling effect, undesirable for ceramic fuel cells, close to the reformer entrance. The system behavior toward changes in catalyst activity, fuel inlet temperature, current density, and operating pressure was studied.

Aguiar et al. (2004) presented a dynamic anode-supported planar SOFC model with internal reforming of methane fuel that allows for both co-flow and counter-flow operation. This model consisted of mass and energy balances and an electrochemical model. The electrochemical performance of the fuel cell was analyzed for several temperatures and fuel utilizations by considering the voltage and power density versus current density curves. The steady-state performance of the cell and the impact of changes in fuel and air inlet temperatures, fuel utilization, average current density, and flow configuration were studied. They concluded that the SOFC operation under counter-flow showed the steep temperature gradients and uneven current density distributions.

Hernandez-Pacheco et al. (2005) developed the SOFC model for determining the current–temperature profiles. The model was integrated by a detailed electrochemical module and a material-energy module. The integrated model was used to analyze the performance of the cell with respect to different operating conditions. In addition, the model was used to analyze the response of the fuel cell under different compositions of fuel gas obtained from a downdraft gasifier. The results showed that high hydrogen concentration yields high performance while high steam to fuel ratio can suppress coke formation.

Pfafferodt et al. (2005) presented a one-dimensional steady state model of an SOFC to be used in an Auxiliary Power Unit (APU). The fuel cell was fed by a pre-reformed gas from an external autothermic reformer. The model predicts concentrations and temperatures and uses an equivalent circuit approach to describe the current–voltage characteristics of the cell. They concluded that the co-flow configuration was preferred because of the high temperatures within the active cell

area for the counter-flow configuration. The operational range was determined in terms of temperature and amount of cathode air used.

Sangtongkitcharoen et al. (2005) analyzed carbon formation boundary for SOFCs fueled by methane with different operating modes of SOFCs (ER, IIR and DIR). The carbon formation boundary was determined by finding the value of inlet steam/methane ($\text{H}_2\text{O}/\text{CH}_4$) ratio. For SOFC- O^{2-} , ER-SOFC and IIR-SOFC showed the same values of $\text{H}_2\text{O}/\text{CH}_4$ ratio required at the carbon formation boundary, independence of the extent of electrochemical reaction of hydrogen. In contrast, DIR-SOFC can be operated at lower values of the $\text{H}_2\text{O}/\text{CH}_4$ ratio compared to the other modes of SOFC operation.

Inui et al. (2006) investigated the influence of the mixing ratio of hydrogen and carbon monoxide in the fuel on the performance of the SOFC through numerical simulations for a single cell plate of the co-flow type planar cell. It was clear that the cell performance is almost the same and excellent, independence of the mixing ratio of hydrogen and carbon monoxide under the nominal operating condition. The influence of inlet gas temperature and additional amount of water vapor and carbon dioxide was also investigated. It was found that the electromotive force of the hydrogen rich fuel gas is a little higher than that of the carbon monoxide rich fuel gas and the internal voltage drop in the cell decreases as the fraction of carbon monoxide becomes high.

As mentioned in this section, a number of publications related to SOFC models have appeared most frequently in the recent years. The literature reviews show that so far the studies of SOFC have focused almost exclusively on H_2 and natural gas or methane operation. This motivates the development of an SOFC model that takes into account the internal reforming of fuel gas such as natural gas and methane.

2.2 SOFC with supported structures

For the planar-type SOFC concentrated in this research, there are two basic configurations for the development of SOFC: an electrolyte- and an electrode-supported structure. In the past years, numerous experimental researches studying on

the performance of the electrolyte-supported SOFC in the temperature range of 800-1000 °C were performed (Huang et al., 1997; Ishihara et al., 1998; Maric et al., 1999; Hibino et al., 2000; Suzuki et al., 2004; Joo et al., 2009). From the experimental data extracted from literatures, it was found that a single electrolyte-supported SOFC was fabricated by using the electrolyte thickness of 500 μm . However, when the SOFC is operated at lower operating temperatures, a number of researches have proposed the fabrication of the SOFC with an anode-supported and a cathode-supported structure due to a high ohmic loss occurred in the SOFC stack (Leng et al., 2004; Kim et al., 2005; Zhao and Virkar, 2005; Liu et al., 2006; Xin et al., 2006; Chen et al., 2007; Lin et al., 2008; Yamaguchi et al., 2008). For the planar-type SOFCs, most of researches have focused on the anode-supported SOFC; for example, Zhao and Virkar (2005) investigated the individual polarization occurred in an anode-supported SOFC. SOFC with yttria-stabilized zirconia (YSZ) electrolyte, Ni-YSZ anode support and strontium doped lanthanum manganate (LSM)-YSZ cathode interlayer were fabricated. The effect of various parameters such as the thicknesses of electrolyte, anode support and cathode interlayer, and anode support porosity, on cell performance was evaluated. The electrochemical performance of SOFC was measured with humidified hydrogen as fuel (97% H_2) and air as oxidant (21% O_2) at the temperature varied from 600 to 800°C. The results of cell tests showed that the anode support thickness = 0.5 mm, anode support porosity = 57%, electrolyte thickness = 8 μm and cathode interlayer = 20 μm provides the optimized parameters. The maximum power density obtained are 1.8, 0.8 and 0.4 Wcm^{-2} at 800, 700 and 600°C, respectively.

2.3 SOFC with different electrolyte types

As mentioned in Chapter I, there are two types of electrolytes (i.e., oxygen ion and proton conducting electrolytes) for applying to SOFCs. Previous investigations as presented in the above section are mainly focused on SOFCs with an oxygen ion conducting electrolyte (SOFC- O^{2-}). Since 1982, Iwahara and his coworkers have been trying to fabricate a high temperature fuel cell using SrCeO_3 -based ceramic as a solid electrolyte and porous platinum as an electrode material worked stably at 800-1000°C. They found the conduction of proton in the electrolyte due to the presence of hydrogen or water vapor at the cathode side. However, the power output was

practically unsatisfying due to rather large ohmic resistance. They suggested that the fuel cell should be used as thin film to reduce ohmic loss.

As solid oxides with proton conduction have been discovered and developed (Iwahara et al., 1982; Zhu and Mellander, 1994; Iwahara, 1996, Coore, 2003; Meng et al., 2007), a number of the researches related to the use of such a proton-conducting solid oxides for SOFC (SOFC-H⁺) have been reported (Demin and Tsiakaras, 2001; Assabumrungrat et al., 2004; Taherparvar et al., 2003; Fukada et al., 2006; Potter and Baker, 2006; Pekridis et al., 2007; Suksamai et al., 2007). However, most studies have directed to the synthesis and characterization of proton-conducting materials. There are very few studies on mathematical modeling of SOFC-H⁺ systems.

In 2001, Demin and Tsiakaras analyzed the efficiency of an SOFC-H⁺ fed with hydrogen. The influence of various parameters such as hydrogen purity, air humidity, hydrogen and oxygen utilization as well as working temperature on fuel cell efficiency was investigated. They reported that SOFC-H⁺ provides higher efficiency than SOFC-O²⁻ for a system fed with hydrogen. Later in 2004, Demin et al. demonstrated a possibility of the utilization of CO-containing fuel in the SOFC-H⁺. When methane was used as fuel in this system, the average EMF of the SOFC-H⁺ is higher than that of the SOFC-O²⁻ under the same conditions and, hence, the maximum efficiency of the SOFC-H⁺ system is about 15% higher than of the SOFC. It is noted that in their researches (Demin and Tsiakaras, 2001; Demin et al., 2002), the fuel cell efficiency was analyzed by using the thermodynamic model.

Assabumrungrat and his coworker (2004, 2005) presented a detailed thermodynamic analysis which is carried out to provide useful information for the operation of solid oxide fuel cells with direct internal reforming (DIR). Equilibrium calculations were performed to find the ranges of inlet steam/ethanol (H₂O/EtOH) ratio to avoid carbon formation. Comparison between two types of fuel cell electrolytes indicated that the SOFC-H⁺ fed by ethanol, methanol and methane is impractical due to the tendency for carbon formation. With a higher extent of the electrochemical reaction of hydrogen, a higher value of the H₂O/EtOH ratio is required for the operation of SOFC-H⁺ without the formation of carbon.

Jamsak et al. (2006) presented the theoretical performance of ethanol-fuelled solid oxide fuel cells (SOFCs) with oxygen ion conducting and proton conducting electrolytes. In order to compare the theoretical performances of SOFCs with different electrolytes, the benefit of reduced inlet steam requirement for the SOFC with oxygen ion conducting electrolyte is taken into account. It was demonstrated from the theoretical calculations assuming no polarization losses that the use of the proton conducting electrolytes for SOFC is more attractive than the oxygen ion conducting electrolytes. However, it was observed that many previous studies on SOFC-H⁺ was carried out based on theoretical calculations. If the effect of all voltage losses are included in the calculation, the performance of SOFC-H⁺ should be lower than that of SOFC-O²⁻.

Jamsak et al. (2007) continually investigated the performance of ethanol-fuelled solid oxide fuel cells with different SOFC electrolytes. Although, their previous work reported that the SOFC-H⁺ shows superior theoretical performance over the SOFC-O²⁻, it was shown in this study that the actual performance of the SOFC-O²⁻ (Ni-YSZ|YSZ|YSZ-LSM) becomes significantly better than that of SOFC-H⁺ (Pt|SCY|Pt) if all cell resistances are taken into account. The maximum power density of the SOFC-O²⁻ is about 34 times higher than that of the SOFC-H⁺. Due to the superior theoretical performance of the SOFC-H⁺, it is not necessary to reduce the SOFC-H⁺ total resistance to the same values as the one for SOFC-O²⁻. They also introduced that the reduction of only the electrolyte resistance is not sufficient to improve the SOFC-H⁺ performance and, therefore, the other resistances including activation and electrodes resistances need to be reduced simultaneously.

Ni et al. (2008) developed an electrochemical model to study the methane-fed SOFC using a proton conducting electrolyte (SOFC-H⁺) and an oxygen ion conducting electrolyte (SOFC-O²⁻). All voltage losses, i.e. activation overpotential, ohmic overpotential and concentration overpotential, were considered in the model. Detailed comparisons between SOFC-H⁺ and SOFC-O²⁻ were made to better understand the working mechanisms of SOFC-H⁺ and SOFC-O²⁻ and to identify key sources of voltage loss for further improvement. It is noted that the dusty gas model was selected to study the multicomponent mass transfer within the porous SOFC electrodes.

Although the investigation of SOFC-H⁺ in the aspect of modeling and detailed analysis of SOFC-H⁺ has been proposed, an electrochemical model to predict accurately the characteristic performance of SOFC-H⁺ is particularly required for analysis, design, and improvement of SOFC-H⁺. Furthermore, fuel and oxidant activities relating to the fuel and oxidant utilizations were not considered in previous studied. As a result, an actual performance of an SOFC-H⁺ taking into account the distribution of substance components and all voltage losses within fuel cell should be studied to reflect a real fuel cell operation.

2.4 SOFC hybrid system

In general, the SOFC system consists of three main parts: (1) a fuel processor to reform hydrocarbon fuels to hydrogen-rich gas, (2) an SOFC stack where the electric power is generated, and (3) a power conditioner for converting the DC power to utilizable AC power. For SOFC operated at the fuel utilization of 80-90%, the exhaust gas from the cell stack containing valuable residual fuel and a waste heat is produced simultaneously with the electrical power. As a result, the utilization of the high-quality heat and the remaining fuel existing SOFC can further improve the efficiency of the SOFC system. This brings the SOFC system to a combined process with other devices for additional electric power generation. Moreover, the utilization of the exhaust gases from SOFCs makes the completeness of fuel conversion in the SOFC stack which decreases the size and the cost of the SOFC stack (Granovskii et al., 2007). In general, the exhaust gas obtained from the SOFC is often used bottoming cycles such as a gas turbine (GT). It was reported that the hybrid SOFC system and gas turbine system (SOFC-GT system) can improve an overall electrical efficiency up to 70% (Dokiya, 2002; Palsson et al., 2000; Möller et al., 2004; Calise et al., 2006; Haseli et al., 2008). However, since the efficiency of fuel cell that its energy conversion efficiency remains almost constant even as the system output decreases, is generally higher than that of gas turbine, a number of researches have been concentrated on the integration of an SOFC and other fuel cells (Dicks et al., 2000; Yokoo and Take, 2004; Araki et al., 2006; Musa and Paepe, 2008). This section presents an overview of SOFC-GT system and the combination of SOFC system with other fuel cell.

2.4.1 SOFC with gas turbine system

Palsson et al. (2002) investigated a SOFC–GT system featuring external pre-reforming and anode gas recycling. The effluent from anode was partially recycled in order to supply steam and heat to the external reformer. The remained anode effluent was burnt with cathode effluent in the combustor. The hot gases were then delivered to the gas turbine for generating additional electrical power whereas the exhaust gas from the gas turbine was utilized for preheating the feeds. This work analyzed the influences of operating parameters such as pressure, air flow rate, fuel flow rate and air inlet temperature on the system performance. It was shown that the pressure ratio has a large impact on performance and that electrical efficiencies of more than 65% are possible at low pressure ratios.

Selimovic and Palsson (2002) analyzed a combination of networked SOFC with a gas turbine. The networked SOFC-GT systems consisted of two substacks in which the fuel feed was arranged in series whereas air was fed into the stack in series and parallel. When the reactant and air were fed to the SOFC stacks in series, a significant increase of system efficiency was observed. This is due to the improved cooling of the cell, leading to a more homogenous temperature profile and higher total fuel utilization in the stack. However, when air stream were fed in parallel, the system efficiency was drop by 1.5%.

Möller et al. (2004) examined an optimization of a hybrid system combining SOFC and GT with and without CO₂-capture using a genetic algorithm (GA) optimizer. With CO₂ capture, the system consisting of two SOFC stacks was added with a desulfurizer unit before pre-reformer. The reforming gas was equally split between the two stacks and fed to anode in parallel. On the air side, the stacks were connected in series. The rest of the fuel was burnt in the gas turbine combustor with supplementary fuel supply. In the SOFC-GT system with CO₂-capture, the fuel gas was cooled and dried in an exhaust gas condenser. From the results, it was found that a SOFC-GT system integrated with the CO₂-capture exhibited an electrical efficiency above 60%.

Calise et al. (2006) presented the simulation of full and partial load exergy analysis of a hybrid SOFC-GT power plant. At full-load operation, a maximum value

of 65.4% of electrical efficiency was achieved. Three different partial-load strategies were introduced, based on the fuel and air mass flow rates variations. The simulation of partial-load operation of the SOFC-GT hybrid plant showed that the best performance can be achieved in case of constant fuel to air ratio. However, a lower value of net electrical power (34% of nominal load) could be achieved by reducing fuel flow rate, at constant air flow rate.

Haseli et al. (2008) examined the performance of a high-temperature SOFC combined with a conventional recuperative gas turbine (SOFC-GT) plant. The simulation results showed that increasing the turbine inlet temperature resulted in the decreased thermal efficiency of the cycle, whereas it improved the net specific power output. Moreover, an increase in either the turbine inlet temperature or compression ratio leads to a higher rate of entropy generation within the plant. It was observed that the combustor and SOFC contribute predominantly to the total irreversibility of the system. The SOFC-GT plant and a traditional GT cycle, based on identical operating conditions, were also made. It was found that the SOFC-GT plant had about 27.8% higher efficiency than the traditional GT plant.

2.4.2 SOFC with other fuel cells system

Dicks et al. (2000) presented the system combining high- and low-temperature fuel cell types. A high-temperature solid oxide fuel cell may be used to produce electricity and carry out fuel reforming simultaneously. The exhaust stream from an SOFC can be processed by shift reactors and supplied to a low-temperature polymer electrolyte membrane. The simulation result showed that overall efficiency of the hybrid system (61%) is better than a Reformer-PEM system or an SOFC-only system (37-42%). The estimation of approximate capital and running cost showed significant benefits compared to the other two systems.

Yokoo and Take (2004) numerically evaluated the performance of the system combining an SOFC stack and a polymer electrolyte fuel cell (PEFC) stack. They reported that the electrical efficiency of the SOFC-PEFC system at 190 kW ac was 59% (LHV), which was equal to that of the SOFC-gas turbine combined system at 1014kW ac. The simulation results also presented that the electrical efficiency of the

SOFC–PEFC system increases with increasing oxygen utilization rate in the SOFC stack.

Araki et al. (2006) proposed the power generation system consisting of two-staged SOFCs with serial connection of low and high temperature SOFCs. This system was developed since low-temperature SOFCs, which run in the range of temperature around 600 °C or above, can give high power generation efficiency. The numerical results showed that the power generation efficiency of the two-staged SOFCs is 50.3% and the total efficiency of power generation with gas turbine is 56.1% under standard operating conditions.

Musa and Paepe (2008) evaluated a combined cycle of two-staged SOFC using numerical models. Two types of combined cycles are compared: (i) a combined cycle consisting of a two-staged combination of IT-SOFC and HT-SOFC and (ii) a two stages of IT-SOFC. In both the combined cycles, the anode gas flows of the first and second stage fuel cell stacks are connected in parallel while the cathode gas flow is connected serially. The simulation results showed that a single-staged HT/SOFC and IT/SOFC have the efficiency of 57.6% and 62.3%, respectively. A combined cycle of two-staged IT-SOFC can give 65.5% efficiency under standard operational conditions. Further, the effect of operating temperature, pressure and current density on the efficiency of a combined cycle were investigated.

CHAPTER III

THEORY

This chapter presents a basic theory of a fuel cell. A general principle of fuel cells including their components, types and advantages is explained in Section 3.1. Section 3.2 presents the description of a solid oxide fuel cell (SOFC) which is the type of fuel cell studied in this work.

3.1 Fuel Cell

A fuel cell is an electrochemical device that converts the chemical energy of a fuel gas and an oxidant gas directly to electrical energy without combustion as an intermediate step. Although, in general, the operational principles of a fuel cell are similar to those of a battery in terms of generating direct current (DC) electricity from electrochemical reactions, the fuel cell does not run down or require recharging; it employs gases (from an external source) as reactants, and can operate as long as both the fuel and the oxidant are supplied to electrodes.

3.1.1 Cell components

The basic structure of fuel cell consists of an electrolyte sandwiched between two electrodes (anode and cathode) where electrochemical reactions take place. In an operation of fuel cell, fuel (typically hydrogen) is fed to the anode where it is oxidized and electrons are released to the external (outer) circuit while oxidant (typically oxygen) is fed to the cathode where it is reduced and electrons are accepted from the external circuit. The electrons flow from the anode to the cathode through the external circuit produces direct-current (DC) electricity, exhaust gases and heat. Figure 3.1 demonstrates the basic component of fuel cell and its operation.

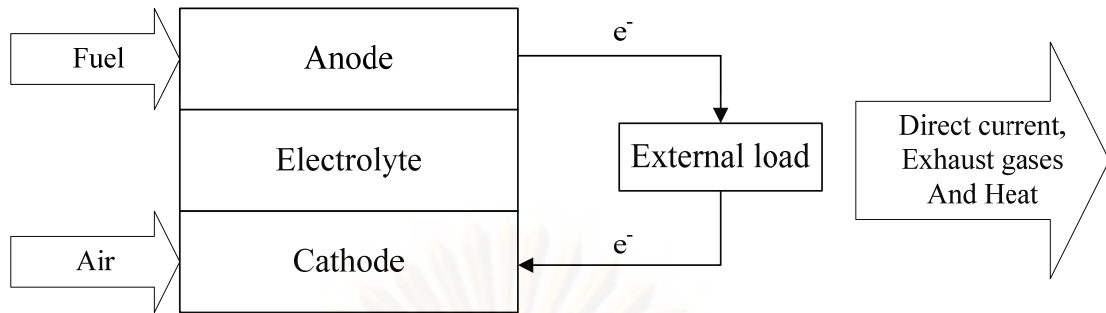


Figure 3.1 Basic components of a fuel cell and its operation.

3.1.2 Types of fuel cells

In general, fuel cells can be classified by the type of electrolyte materials used in the cells which are significantly related to operating temperature. Detailed information for each type of fuel cell is summarized in Table 3.1. As shown in Table 3.1, the fuel cells are listed following the sequence of an operating temperature, ranging from 80°C for a PEMFC to 1000°C for an SOFC. The operating temperature of fuel cells can dictate the type of electrolyte used in the cell. Aqueous electrolytes (H^+ or OH^- ions) are dominant ionic current carrier for the low temperature fuel cell (PEMFC, AFC and PAFC). At high temperatures, CO_3^{2-} and O^{2-} are utilized as the ionic current carrier for MCFC and SOFC, respectively.

The operating temperature also plays an important role in dictating the type of fuel that can be utilized in a fuel cell. The low temperature fuel cells (PEMFC, AFC and PAFC) are restricted to hydrogen as a fuel. For high temperature fuel cells (MCFC and SOFC), various hydrocarbon fuels, i.e., natural gas, methane, methanol and ethanol, can be applied as they can be reformed to hydrogen within the fuel cell itself.

Due to its different operating temperature and efficiency, a fuel cell can be utilized in numerous applications. PEMFC and AFC are operated at low operating temperatures, resulting in low electrical power. They are primarily used as a battery for a notebook, mobile or portable electronic equipment. In addition, PEMFC is also suitable for vehicle applications since low temperature operation allows quick start-up. PAFC, which has a higher operating temperature compared to PEMFC and AFC,

Table 3.1 Types of fuel cell

	Type of fuel cell				
	Polymer Electrolyte Membrane Fuel Cell (PEMFC)	Alkaline Fuel Cell (AFC)	Phosphoric Acid Fuel Cell (PAFC)	Molten Carbonate Fuel Cell (MCFC)	Solid Oxide Fuel Cell (SOFC)
Temperature (°C)	50-85	50-250	160-220	630-650	800-1000
Electrolyte	Ion exchange membrane	Alkaline	Phosphoric acid	Alkaline Carbonate mixtures	Stabilized zirconia (ZrO ₂)
Charge carrier	H ⁺	OH ⁻	H ⁺	CO ₃ ⁻	O ²⁻
Fuel	H ₂	H ₂	H ₂	Synthesis gas, CH ₄	Synthesis gas, CH ₄
Oxidant	O ₂	O ₂	O ₂	O ₂ + CO ₂	O ₂
Contaminant tolerance	<50 ppm No Sulfur	No CO, CO ₂ No Sulfur	< 1-2% CO <50 ppm Sulfur	< ppm Sulfur	< 10-100 ppm Sulfur
Corrosion	None	None	High	High	No
Size (MW)	0.25	Very small	11	2	1-2
Application	Transportation, small appliances	Small power in aerospace	Power generation, CHP	Power generation, CHP	Power generation, CHP
Efficiency (%)	<40	>60	40-45	50-60	50-60

is suitable for small stationary applications whereas MCFC and SOFC that are operated at higher operating temperatures are used in large stationary applications.

3.1.3 Advantages of fuel cells

Although fuel cells have some disadvantages in high production cost and limited operational lifetime, they offer a number of advantages including:

- **High efficiency:** Fuel cells can convert the chemical energy of fuel directly into electrical energy. Thus, the usual losses involved in the conversion of fuel to heat, to mechanical energy and then to electrical energy are avoided. This leads to a high fuel-to-electricity conversion efficiency (45 to 60%). The efficiency of a fuel cell is further improved when the byproduct heat is fully utilized in a cogeneration and bottom cycle.
- **Low emission:** The by-product of the main fuel cell reaction, when hydrogen is the fuel, is only pure water; therefore, the production of undesirable materials such as NO_x , SO_x and particulates is either negligible or undetectable for a fuel cell system. This means a fuel cell can be essentially 'zero emission' This is a major advantage when used in vehicles, as there is a requirement to reduce vehicle emission, and even eliminate them within cities.
- **Simplicity:** The essentials of a fuel cell are very simple, meaning no moving parts. This can lead to highly reliable and long-lasting systems.
- **Silence:** Fuel cells are very quiet, even those with extensive extra fuel processing equipment. This is very important in both portable power applications and local power generation in combined heat and power schemes.

3.2 Solid oxide fuel cell

3.2.1 SOFC features

Solid oxide fuel cell (SOFC) has all-solid-state construction, along with high operating temperatures. SOFC offers several advantages over the other types of fuel cell as follows:

- The electrode reactions are rapid; therefore, expensive noble metal catalysts are not needed.
- SOFC can be operated by hydrogen or suitable fuels including coal, biomass, gasoline, ethanol and natural gas. Due to the high operating temperatures, hydrocarbon fuels can be reformed internally within the fuel cell; it does not require external reformers.
- SOFC do not suffer from CO poisoning. Indeed, CO can be used directly as fuel in SOFC. The SOFC can tolerate relatively high impurity content in the fuel.
- SOFC produces useful high-temperature waste gas that can be used in cogeneration applications and bottoming cycles. The overall efficiency of the system can be significantly increased when this waste gas is fully utilized.
- Because the SOFC electrolyte is solid, the material corrosion and electrolyte management are not problems.

However, the high temperature operating condition also imposes some challenges which include the potential thermal fatigue failure of the cell material, sealing under high temperature, and the associated control mechanism/power required to maintain the operation.

3.2.2 SOFC operation

A SOFC single cell consists of two porous electrodes, the anode and cathode, which are separated by a dense solid ceramic electrolyte. Generally, there are two types of

ceramic electrolytes which are possible for SOFC operation; namely, an oxygen ion-conducting electrolyte and a proton-conducting electrolyte. Figure 3.2 and 3.3 show the reactions in an oxygen ion-conducting electrolyte and a proton-conducting electrolyte, respectively. The major difference between both types of electrolytes is the location of water produced. With an oxygen ion-conducting electrolyte, water is produced in the reaction mixture in the anode side. In the case of the proton-conducting electrolyte, water appears on the cathode side. Commonly, an oxygen ion-conducting electrolyte is employed in SOFC operation, due to its chemical stability and low resistance and therefore, high performance can be achieved.

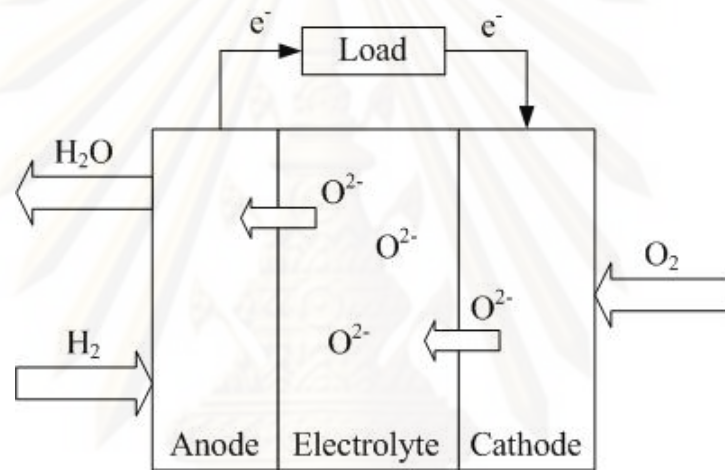


Figure 3.2 Basic principle of the SOFC operation based on an oxygen ion-conducting electrolyte.

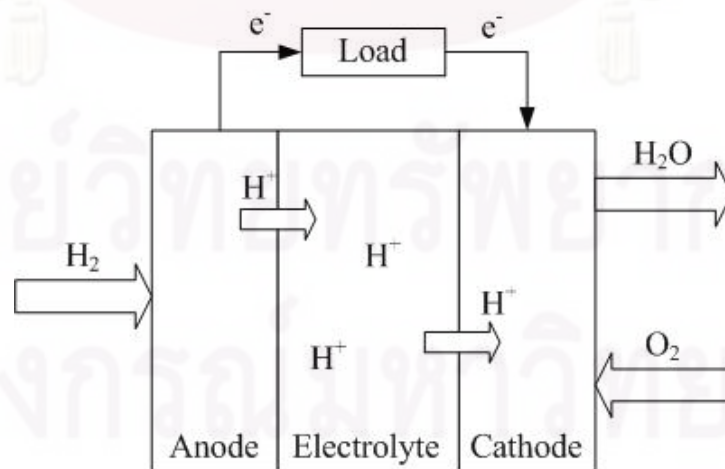
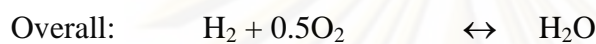
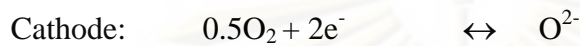


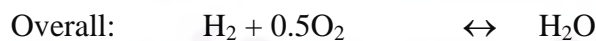
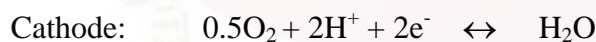
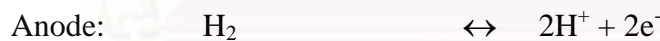
Figure 3.3 Basic principle of the SOFC operation based on a proton-conducting electrolyte.

For the SOFC based on an oxygen ion-conducting electrolyte (SOFC-O²⁻), the oxygen ions formed at the cathode migrate through the ion-conducting solid ceramic electrolyte to the anode/electrolyte interface where they react with the hydrogen contained in (and/or produced by) the fuel, producing water while liberating electrons that flow back to the cathode/electrolyte interface via an external circuit. The electrochemical reactions in the SOFC based on an oxygen conducting electrolyte are shown as follows:



As a result, the fuel gas is diluted by water vapor, and the cell performance deteriorates unless the fuel gas is circulated to remove vapor.

In case of the SOFC based on a proton-conducting electrolyte (SOFC-H⁺), hydrogen molecules in the fuel are separated into proton ions and electrons at the anode side. The electrons flow in the external circuit from anode to cathode while the proton ions move through the electrolyte to the interface where they react with oxygen molecules in the oxidant fed to the cathode side and here the water is produced. The electrochemical reactions in the SOFC based on a proton conducting electrolyte are shown as follows:



In this case it is unnecessary to recycle the fuel gas because water is not formed at the anode.

3.2.3 SOFC characteristics

The key performance measure of a fuel cell can be determined by characteristic curve or voltage-current curve, as shown in Figure 3.4. This curve presents the voltage output as a function of electrical current density drawn. Ideal voltage or theoretical

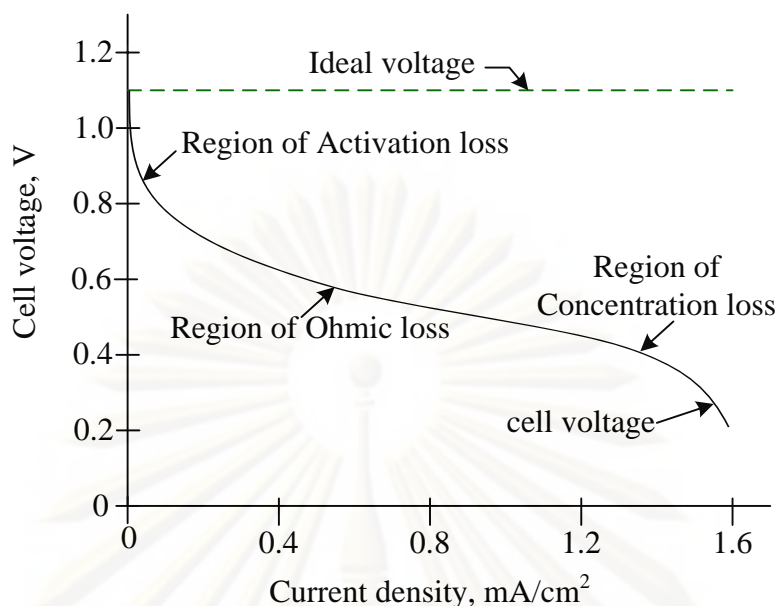


Figure 3.4 Ideal and actual fuel cell voltage/current characteristics.

voltage obtained at no load conditions is the maximum voltage that can be achieved by a fuel cell. The theoretical voltage can be calculated by the Nernst equation. However, as current passes through the cell, the voltage drops from the theoretical voltage due to internal losses. Therefore, actual voltage is always less than ideal voltage as shown in the Figure 3.4. Three main voltage losses are (1) activation loss, (2) ohmic loss and (3) concentration loss. These loss mechanisms are discussed in more detail in Section 4.3.2. The different loss mechanisms dominate at different levels of current density (i), as shown in Figure 3.4. The current density is defined as the current produced per unit geometrical area of a fuel cell.

3.2.4 SOFC Material

The components for ceramic SOFC must have similar coefficient of thermal expansion to avoid separation or cracking during fabrication and operation. Both the anode and cathode must be porous to allow gas transport to the reaction sites, whereas the electrolyte must be dense in order to separate the oxidant and fuel gases. Each component must have the proper stability (chemical, phase, morphological and dimensional) in oxidizing and/or reducing environments, chemical compatibility with other components, and proper conductivity. The requirements for each cell component are summarized in Table 3.2.

Table 3.2 Requirement for ceramic SOFC component (Mihn and Takahashi, 1995)

Component	Requirements		
	Conductivity	Stability	Compatibility
Electrolyte	High ionic conductivity Negligible electronic conductivity	Chemical, phase, morphological, and dimensional stability in fuel and oxidant environment	No damaging chemical interactions or interdiffusion with adjoining cell component
Cathode	High electronic conductivity	Chemical, phase, morphological, and dimensional stability in oxidant environment	No damaging chemical interactions or interdiffusion with adjoining cell component
Anode	High electronic conductivity	Chemical, phase, morphological, and dimensional stability in fuel environment	No damaging chemical interactions or interdiffusion with adjoining cell component

At present, the most common materials for the SOFC are oxide ion-conducting yttria-stabilized zirconia (YSZ) for the electrolyte, strontium-doped lanthanum manganite (LSM) for the cathode and nickel/YSZ for the anode. In addition, a number of proton-conducting oxides have been studied for use as SOFC electrolyte (Demin and Tsiakaras, 2001; Assabumrungrat et al., 2004; Taherparvar et al., 2003; Fukada et al., 2006; Potter and Baker, 2006; Pekridis et al., 2007; Suksamai et al., 2007). For example, Yb-doped SrCeO_3 ($\text{SrCe}_{0.95}\text{Yb}_{0.05}\text{O}_{3-\alpha}$ or SCYb) electrolyte is known as one of the classical proton conducting materials with a high proton transport number (Iwahara, 1996). For the use of the proton conductive electrolyte, the most common materials used for the electrodes are platinum (Pt). The porous platinum can be used for both cathode and anode because of its high catalytic activity and stability in oxidative and reductive atmosphere as well as it is a pure electronic conducting material (Sasaki et al., 2001; Feng et al., 2007).

3.2.5 SOFC design

Generally, the voltage from a single cell produces less than 1 V. A SOFC are not practically operated as single units, they are connected in electrical series to build voltage. A series of cells is referred to stack. At present, four common SOFC stack configurations have been proposed and fabricated: the sealless tubular, the segment-cell-in-series design, the monolithic design, and flat-plate design. The fabrication costs and ease of assembly vary among the designs. Table 3.3 compares the key characteristics of the four designs. However, tubular and planar design has been received great attention recently as discussed below.

3.2.5.1 Sealless tubular design

The sealless tubular design consists of the cell component configured as thin layers on a tubular support closed at one end (Figure 3.5). In this design, the porous support tube is overlaid with a porous cathode layer. A dense electrolyte layer covers the cathode except in a strip along the active cell length. The anode covers the entire electrolyte surface. For cell operation, oxidant is introduced to the cell through an injector tube, where it traverses and exits from the open annular between the support and oxidant injector tube. Fuel flows on the outside of the support tube. The advantage of the sealless

tubular design is that it has no gas seal, so that the problems with gastight seals for ceramics at high temperature are eliminated.

3.2.5.2 Planar design

The planar design consists of cell components configured as thin, planar plates (Figure 3.6). Common plate shapes are rectangular (square) or circular. Gas manifolding can be divided into 3 configurations, which are co-flow, counter-flow and cross-flow designs. The cell support can be either cathode-supported or anode-supported type. However, many researches have shown that the anode-supported design leads to better cell performance than the cathode-supported one (Yakabe et al., 2000; Chan et al., 2001). The advantage of planar design is more flexibility than the other in terms of cell geometry and gas manifolding. However, this cell presents a problem for building cell stacks because of difficulties with fabricating large flat thin and obtaining adequate gas seals. This design needs high temperature seals that prevent gas leakage and mining of fuel and oxidant.

Table 3.3 Characteristics of SOFC Stack design (Minh and Takahashi, 1995)

Feature	Cell Designs			
	Sealless Tubular	Segmented-Cell-in-Series	Monolithic	Flat-Plate
Structural support	Yes	Yes	No	No
Internal electrical resistance	High	High	Low	Medium
Gas sealing	No	Yes	No	Yes
Power density	Low	Low	High	Medium

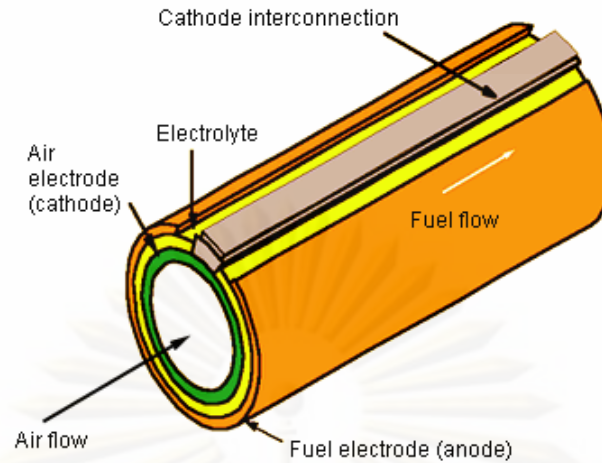


Figure 3.5 Sealless tubular SOFC design (<http://www.mech.gla.ac.uk>).

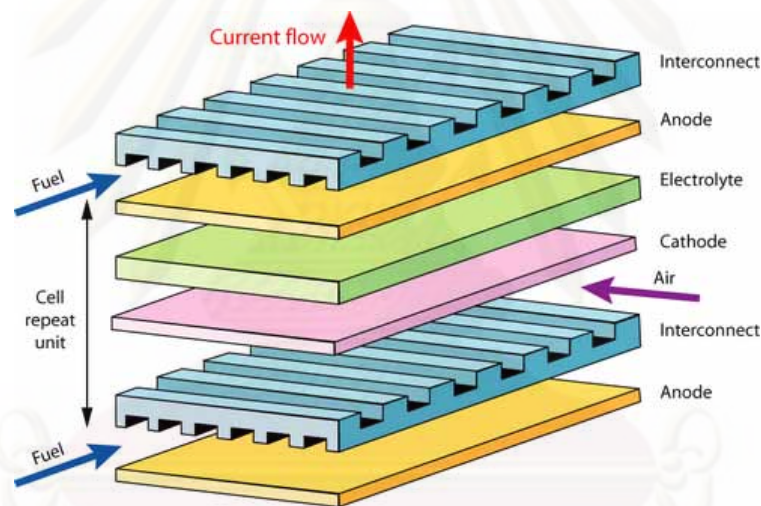


Figure 3.6 Planar SOFC design (<http://www.msm.cam.ac.uk/doitpoms/tlplib/fuel-cells/printall.php>).

3.2.6 SOFC configuration

Due to the difference in SOFC design, each shape results in distinct current paths and requires or incorporates different cell configurations. Currently, two basic configurations are proposed in the development of the SOFC; the electrolyte supported and the electrode-supported. The various cell configurations for the SOFC are schematically shown in Figure 3.7. In an electrolyte supported-SOFC, the electrolyte is the thickest component ($> 150 \mu\text{m}$) while the anode and cathode are very thin (about 50

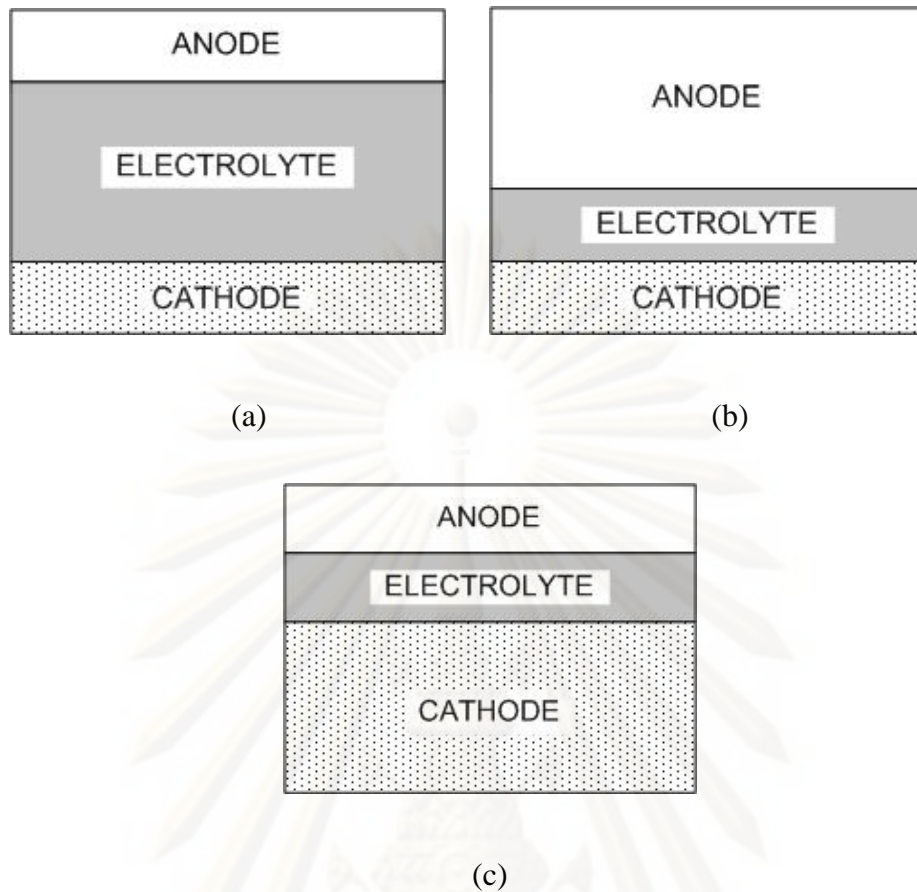


Figure 3.7 SOFC single cell configurations (a) electrolyte-supported, (b) anode-supported, and (c) cathode-supported.

μm), which results in high ohmic resistance. Thus, most current research efforts have been focused on the application of the electrolyte-supported SOFCs at a high operating temperature $\sim 1000^\circ\text{C}$. In an electrode-supported SOFC, one of the two electrodes, either the cathode or the anode, is the thickest component (around 2 mm) and support structure. This decreases the ohmic resistance and makes design better suited for operation at lower temperatures $\sim 800^\circ\text{C}$.

3.2.7 SOFC: An intermediate-temperature operation

Generally, a conventional high-temperature SOFC operation ($\sim 1000^\circ\text{C}$) causes problems in high material costs, slow start-up and shorter life cell. Decrease of the operating temperature of the SOFC to an intermediate-temperature SOFC operation (IT-SOFC) in the range of 600 to 800°C would have the following advantages:

- Offer the choice of low-cost metallic and construction materials. This makes both the stack and balance-of-plant cheaper and more robust.
- Offer the potential for more rapid start-up and shut-down procedures.
- Simplify the design and material requirements of the balance-of-plant.
- Significantly reduce the corrosion rates.

However, one of the problems associated with lowering operating temperature is an increase in ohmic loss of the cell. Two approaches commonly adopted to alleviate the problem of ohmic loss in a SOFC are: (1) using an electrode or a substrate to be the support structure, thus reducing the thickness of the electrolyte, and (2) sourcing alternative electrolyte materials with higher ionic conductivity than the conventional electrolyte material.

3.2.8 Type of fuel and oxidant

In general, hydrogen is currently the most common fuel, and oxygen the most common oxidant for use in SOFC. Hydrogen can be derived from many practical fuels such as natural gas, alcohol, or coal whereas oxygen is readily available from air.

Fuel

Although pure hydrogen is a superior cell fuel, but is a dangerous gas due to it is easily to fire so there is a problem on its storage and distribution. Hydrogen can be obtained from a number of hydrogen-containing fuels (e.g., natural gas) or from synthesis gases obtained by a gasification of carbon sources (e.g., coal). However, these hydrocarbon fuels must be converted into a hydrogen-rich gas via an external reformer, as shown in Figure 3.8. This process is known as fuel processing. In the fuel processing, three major types of fuel reforming process are normally used to produce a hydrogen-rich gas:

- Steam reforming (SR)
- Partial oxidation (POX) reforming
- Autothermal reforming (AR)

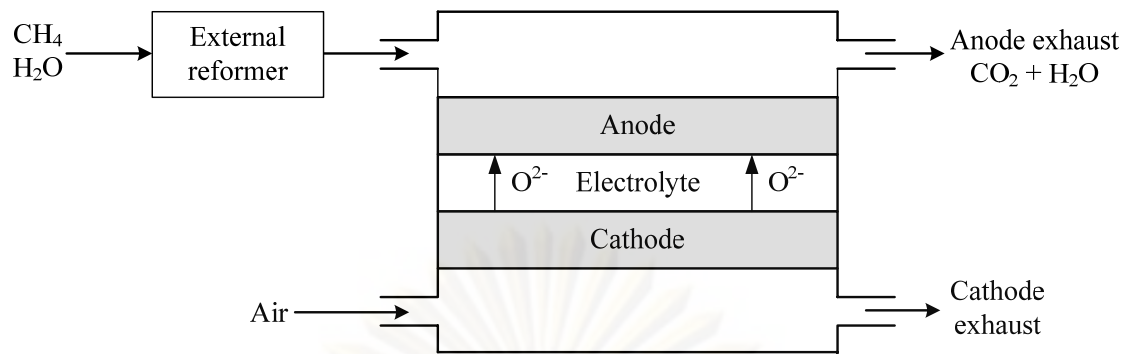


Figure 3.8 Schematic of an external reforming SOFC.

Each of the three main reforming processes produces a synthesis gas (syngas) with varying H_2 composition, require different steam-to-carbon ratios, and posses unique advantages and disadvantages. The major characteristics of these three reforming processes are described in Tables 3.4 and 3.5.

Oxidant

The performance of ceramic fuel cells is improved when pure oxygen is used as the oxidant; however, air is usually used because of its availability. The difference between cell voltage obtained with pure oxygen and that with air increases as the current density increases, suggesting that the diffusion polarization plays an important role during the reduction of oxygen in air. Because of the high operating temperature, a SOFC system needs an air supply blower, air preheater, and air recirculator.

3.2.9 Internal reforming SOFC

The steam reforming of hydrocarbons can be carried out in an external reformer (external reforming) or within the fuel cell (internal reforming). Developments of internal reforming fuel cells have generally adopted one of two approaches. These are usually referred to as a direct (DIR) and indirect (IIR) internal reforming as illustrated schematically in Figure 3.9 and 3.10, respectively. Application of internal reforming to SOFC operation offers several further advantages compared with external reforming operation:

Table 3.4 Comparison of three primary fuel reforming reactions (Hayre et al., 2006)

Type	Chemical Reaction	Temperature Range (°C)	Outlet Gas Composition (with Natural Gas Fuel)					Exothermic or Endothermic?
			H ₂	CO	CO ₂	N ₂	Others	
Steam reforming	$C_xH_y + xH_2O(g) \leftrightarrow xCO + (\frac{1}{2}y + x)H_2$ $\Rightarrow CO, CO_2, H_2, H_2O$	700-1000	76%	9%	15%	0%	Trace NH ₃ , CH ₄ , SO _x	Endothermic
Partial oxidation	$C_xH_y + \frac{1}{2}xO_2 \leftrightarrow xCO + \frac{1}{2}yH_2$	>1000	41%	19%	1%	39%	Some NH ₃ , CH ₄ , SO _x , HC	Exothermic
Autothermal reforming	$C_xH_y + zH_2O(g) + (x - \frac{1}{2}z)O_2$ $\leftrightarrow xCO + (z + \frac{1}{2}y)H_2$ $\Rightarrow CO, CO_2, H_2, H_2O$	600-900	47%	3%	15%	34%	Trace NH ₃ , CH ₄ , SO _x , HC	Neutral

Table 3.5 Advantages and disadvantages of three primary H₂ production processes (Hayre et al., 2006)

Type	Advantages	Disadvantages
Steam reforming	- Highest H ₂ yield	- Requires careful thermal management to provide heat for reaction especially for (a) start-up and (b) dynamic response - Only works on certain fuel
Partial oxidation	- Quick to start and respond because reaction is exothermic - Quick dynamic response - Less careful thermal management required - Works on many fuels	- Lowest H ₂ yield - Highest pollutant emissions (HCs, CO)
Autothermal reforming	- Simplification of thermal management by combining exothermic and endothermic reactions in same process - Compact due to reduction in heat generation - Quick to start	- Low H ₂ yield - Requires careful control-system design to balance exothermic and endothermic processes during load changes and start-up

- The heat released from the fuel cell reactions can supply the endothermic steam reforming reaction. In general, heat consumption by the steam reforming reaction is about half of the heat production rate in the stack under typical operating conditions.
- The capital investment and operating costs are reduced because a separate external reformer is not needed.
- The efficiency of the system is higher. This is mainly because internal reforming provides an elegant method of cooling the stack, reducing the need for excess cathode air. This in turn lowers the requirement for air compression and recirculation.

3.2.9.1 Indirect internal reforming SOFC (IIR-SOFC)

For an IIR-SOFC, the reforming reaction zone is separated but adjacent to the fuel cell anode as shown in Figure 3.9. The IIR operation benefits from close thermal contact between stack and reformer but suffers from the fact that heat is transferred well only from cells adjacent to the reformers and steam required for the reforming reaction must be raised separately. In addition, the conversion of methane to hydrogen is not promoted to the same extent as with direct internal reforming.

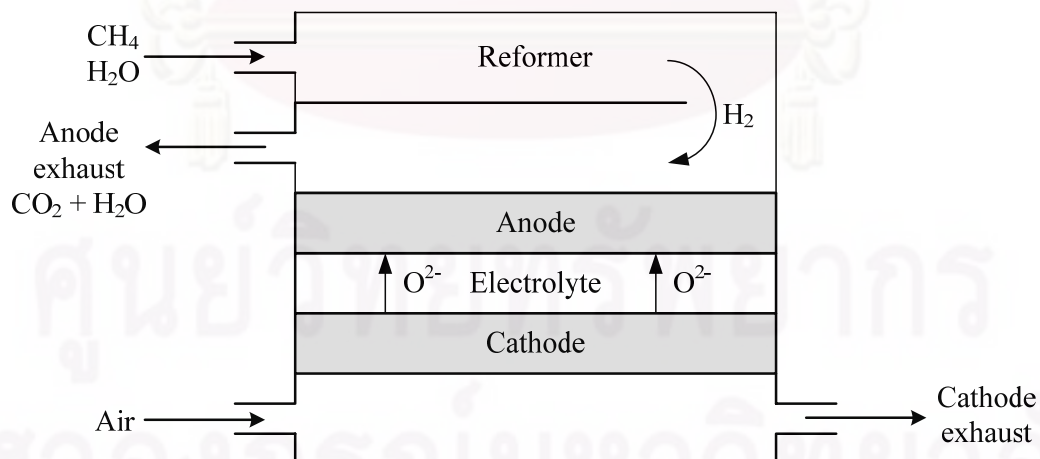


Figure 3.9 Schematic of an indirect internal reforming SOFC

3.2.9.2 Direct internal reforming SOFC (DIR-SOFC)

In a DIR-SOFC, the reforming reactions take place at the anode of fuel cell, as shown in Figure 3.10. The advantage of the DIR operation is that not only does it offer good heat transfer but also the chemical integration – product steam from the anode electrochemical reaction can be used for the reforming. In principle, the endothermic reaction can be used to control the temperature of the stack but the effect is not enough to completely offset the heat produced by the electrochemical reaction and therefore, the management of the temperature gradients is an issue.

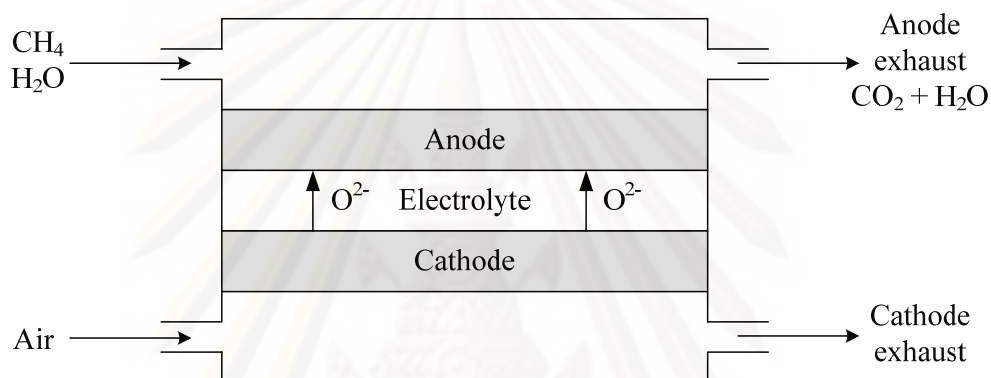


Figure 3.10 Schematic of a direct internal reforming SOFC

CHAPTER IV

MATHEMATICAL MODEL OF SOFC

A mathematical model is an essential tool in designing a fuel cell system since experimental studies on fuel cells are expensive, time-consuming and labor-intensive. The model can be used to understand the complex reactions and transport processes within fuel cells and to study the effects of operating conditions and design parameters on fuel cell performances. Modeling results can be further used to determine suitable design parameters and optimal operational conditions. Moreover, a theoretical study based on the reliable and accurate model that can predict the detailed processes of reaction and transport incorporated with experimental data take the advantage of reducing time and cost in fuel cell development.

This chapter presents a mathematical model of a solid oxide fuel cell (SOFC) based on oxygen ion-conducting (SOFC-O²⁻) and proton-conducting (SOFC-H⁺) electrolytes. This model is used to simulate SOFC and investigate its performance. Section 4.1 shows the configuration of SOFC used in this study. Details on the assumptions used and model equations are described in Section 4.2 and Section 4.3. Section 4.4 describes the numerical solutions for determining the characteristic curve or electrochemical performance and steady-state performance of SOFC. Further, Section 4.5 explains the key parameters used to evaluate the performance of SOFC-O²⁻ and SOFC-H⁺. The validation of the SOFC-O²⁻ and SOFC-H⁺ model used in this studied is given in Section 4.6.

4.1 Model Configuration

In this study, a single cell of a planar SOFC fed by fuel and air in a co-flow direction is considered. It consists of three compartments: the fuel and air channels and the solid part. A solid part consists of a dense ceramic electrolyte sandwiched between two porous electrodes, anode and cathode (often referred to as a Positive-electrode/Electrolyte/Negative-electrode (PEN) structure), as shown in Figure 4.1.

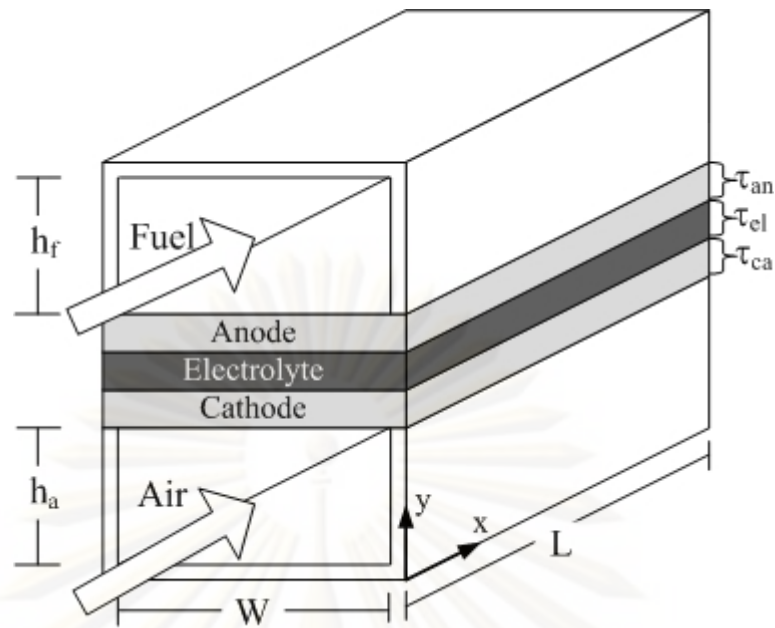


Figure 4.1 Configuration of a co-flow planar solid oxide fuel cell.

The x -direction is selected to be in parallel to the gas channels and the y - and z -directions are selected to be the cell height and cell width directions, respectively. Therefore, the fuel and oxidant gases flow along the x -direction.

The difference between SOFC- O^{2-} and SOFC- H^+ is the materials used as the electrodes and electrolyte. For SOFC- O^{2-} , the most common materials used are oxide ion conducting yttria-stabilized zirconia (YSZ) for the electrolyte, strontium-doped lanthanum manganite (LSM) for the cathode, and nickel/YSZ for the anode. In case of SOFC- H^+ , the materials of electrodes and electrolyte are made from platinum and Yb^{3+} -doped ceramic strontium cerate strontium ($SrCe_{0.95}Yb_{0.05}O_{3-\alpha}$, SCYb), respectively. Table 4.1 summarizes the materials used as the electrodes and electrolyte for SOFC- O^{2-} and SOFC- H^+ .

Table 4.1 Materials used as electrodes and electrolyte for SOFC- O^{2-} and SOFC- H^+

SOFC Type	Anode	Electrolyte	Cathode
SOFC- O^{2-}	Ni-YSZ	YSZ	LaSrMnO ₃
SOFC- H^+	Pt	SCYb	Pt

4.2 Model Assumption

In this study, the synthesis gas derived from a gas mixture of steam and methane at a ratio of 2 after 10% pre-reforming in an external reformer is considered as fuel whereas air is used as an oxidant. The effluent of a pre-reformer which consists of hydrogen, water, unreformed methane, carbon monoxide and carbon dioxide is fed to the fuel channel. Considering SOFC with direct internal reforming (DIR) operation, the remaining methane from the external reformer proceeds the steam reforming reaction within SOFC anode (Equation (4.1)):



This reaction is relatively slow and strongly endothermic. It is assumed that this reaction occurs at a finite rate. The rate expression of the steam reforming reaction (R_{ref}) on Ni-YSZ anode is written as (Achenbach and Riensche (1994)):

$$R_{\text{ref}} = k_0 p_{\text{CH}_4} \exp\left(-\frac{E_a}{\mathcal{R}T}\right) \quad (4.2)$$

where k_0 and E_a is a pre-exponential constant and an activation energy and equal to $4274 \text{ mol s}^{-1} \text{ m}^{-2} \text{ bar}^{-1}$ and 82 kJ mol^{-1} , respectively. It should be noted that in general, both the high temperature operation and the continuous hydrogen consumption in the electrochemical reaction can enhance the equilibrium-limited steam reforming of CH_4 . Therefore, since the kinetic of irreversible reforming reaction proposed by Achenbach and Riensche (1994) was used in this study as shown in Equation (4.2), only the operating temperature and the partial pressure of CH_4 have an effect on the reforming reaction.

Further, carbon monoxide, a byproduct of the reforming reaction, is reacted with residual water via a water gas shift reaction on Ni-YSZ anode to produce carbon dioxide and hydrogen as in:



The water gas-shift reaction is exothermic reaction and always assumed to occur under chemical equilibrium conditions. The rate expression of water gas shift reaction (R_{WGS}) developed from Herberman and Young (2004) is written as

$$R_{\text{WGS}} = k_{\text{WGS}} \times \tau_{\text{an}} \times \left(p_{\text{CO}} p_{\text{H}_2\text{O}} - \frac{p_{\text{CO}_2} p_{\text{H}_2}}{K_{\text{eq}}} \right) \quad (4.4)$$

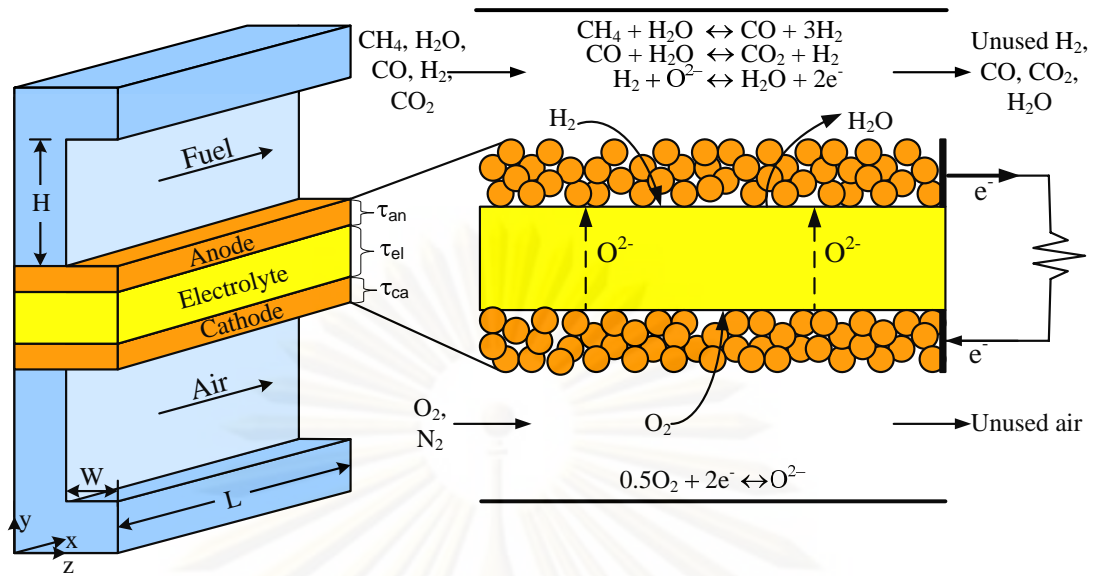
$$k_{\text{WGS}} = 0.0171 \exp\left(-\frac{103191}{\mathcal{R}T}\right) \quad (4.5)$$

$$K_{\text{eq}} = \exp\left(-0.2935Z^3 + 0.6351Z^2 + 4.1788Z + 0.3169\right), \quad Z = \frac{1000}{T(K)} - 1 \quad (4.6)$$

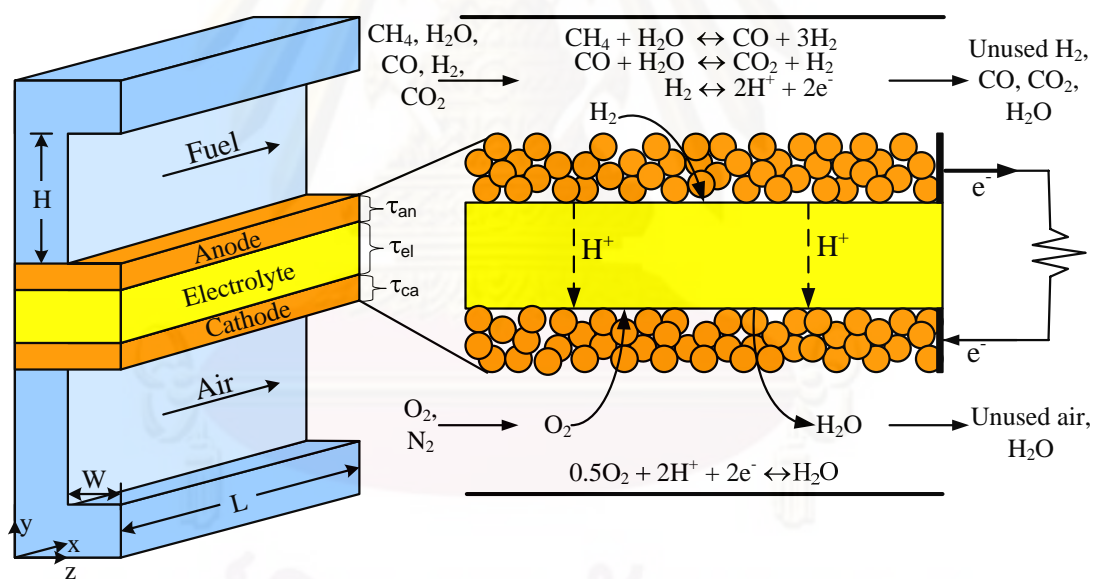
where k_{WGS} is the pre-exponential factor ($\text{mol m}^{-3} \text{Pa}^{-2} \text{s}^{-1}$) and K_{eq} is the equilibrium constant for water gas shift reaction.

In this study, it was assumed that the electrochemical conversion rate of carbon monoxide is negligible compared to that of hydrogen. Hydrogen produced from the reforming and water gas shift reactions at the anode undergoes an oxidation reaction, and releases electrons to the external circuit. Air containing oxygen is simultaneously fed to the air channel, accepts electrons from the external circuit, and undergoes a reduction reaction. The electron flow via the external circuit from the anode to the cathode produces direct-current electricity.

Since the difference between the SOFC- O^{2-} and SOFC- H^+ is the location of water vapor produced and thus, the electrochemical reaction occurred in the SOFC operation is also different, as demonstrated in Figure 4.2. For SOFC- O^{2-} , hydrogen produced from the reforming and water gas shift reactions is oxidized by oxygen ions at the anode|electrolyte interface, and produces water vapor and electron (Equation (4.7a)). Oxygen fed at the air channel, accepts electrons from the external circuit, and forms the oxygen ions at the cathode|electrolyte interface (Equation (4.7b)). In case of SOFC- H^+ , hydrogen is oxidized into protons and electrons at the anode|electrolyte interface (Equation (4.8a)). While the protons migrate through the electrolyte to the interface, oxygen reacts with protons and produces the water at this side (Equation (4.8b)). The electrochemical reaction occurred in the SOFC- O^{2-} and SOFC- H^+ can be summarized as:



(a)



(b)

Figure 4.2 The schematic of a co-flow planar solid oxide fuel cell: (a) solid oxide fuel cell based on an oxygen ion-conducting electrolyte (SOFC- O^{2-}), (b) solid oxide fuel cell based on a proton-conducting electrolyte (SOFC- H^+).

SOFC-O²⁻**SOFC-H⁺**

Faraday's law relates the flux of reactants and products to the electric current arising from electrochemical reactions. According to this law, the local amount of H₂ and O₂ consumed and H₂O produced through the electrochemical reaction (Equation (4.7) and Equation (4.8)) is related to the local electric current density, i , produced by fuel cell. The rate expression of electrochemical reaction (R_{ele}) can be given by:

$$R_{\text{ele}} = \frac{i}{2F} \quad (4.9)$$

4.3 Model Equations

A mathematical model of SOFC consists of mass balances around the fuel and air channels and an electrochemical model equation that relates the fuel and air composition and temperature to the cell voltage, current density, and other related-cell variables. The following assumptions are considered for developing the model of a planar SOFC with direct-internal reforming:

- Steady state operation is considered.
- One-dimensional variation of parameters in x -direction is considered.
- All gaseous components behave as an ideal gas.

- Methane presented in the fuel channel can only be reformed to generate H_2 and other gaseous components.
- Hydrogen is only electrochemically oxidized.
- Gas flows in the fuel and air channels are convective thereby the axial dispersion effect can be neglected.
- Pressure drop is negligible.
- Operating temperature is uniform over the model geometry.
- Cell voltage is constant along the cell coordinate.

4.3.1 Mass balance equation

Considering SOFC with DIR operation, three reactions considered inside the SOFC stack are steam reforming, water gas shift and electrochemical reactions. The fuel fed to the fuel channel consists of CH_4 , H_2O , CO , H_2 , and CO_2 for both SOFC- O^{2-} and SOFC- H^+ while in the air channel, the chemical species are considered as O_2 and N_2 for SOFC- O^{2-} and H_2O , O_2 and N_2 for SOFC- H^+ , respectively. The differential equations describing the change of component concentrations in fuel and air channels along the axial direction can be written as follows:

- Fuel channel

$$\frac{dC_{CH_4}}{dx} = \frac{1}{u_f h_f} (-R_{ref}) \quad (4.10)$$

$$\frac{dC_{H_2O(an)}}{dx} = \frac{1}{u_f h_f} (-R_{ref} - R_{WGS} + R_{ele}) \quad (\text{for SOFC-}O^{2-}) \quad (4.11)$$

$$\frac{dC_{H_2O(an)}}{dx} = \frac{1}{u_f h_f} (-R_{ref} - R_{WGS}) \quad (\text{for SOFC-}H^+) \quad (4.12)$$

$$\frac{dC_{\text{CO}}}{dx} = \frac{1}{u_f h_f} (R_{\text{ref}} - R_{\text{WGS}}) \quad (4.13)$$

$$\frac{dC_{\text{H}_2}}{dx} = \frac{1}{u_f h_f} (3R_{\text{ref}} + R_{\text{WGS}} - R_{\text{ele}}) \quad (4.14)$$

$$\frac{dC_{\text{CO}_2}}{dx} = \frac{1}{u_f h_f} (R_{\text{WGS}}) \quad (4.15)$$

$$C_{i,f} \Big|_{x=0} = C_{i,f}^0 \quad (4.16)$$

- Air channel:

$$\frac{dC_{\text{O}_2}}{dx} = \frac{1}{u_a h_a} (-0.5R_{\text{ele}}) \quad (4.17)$$

$$\frac{dC_{\text{N}_2}}{dx} = 0 \quad (4.18)$$

$$\frac{dC_{\text{H}_2\text{O}(\text{ca})}}{dx} = \frac{1}{u_a h_a} (R_{\text{ele}}) \quad (\text{for SOFC-H}^+) \quad (4.19)$$

$$C_{i,a} \Big|_{x=0} = C_{i,a}^0 \quad (4.20)$$

where “an” and “ca” stand for anode and cathode sides, respectively. $C_{i,f}$ and $C_{i,a}$ represent the molar concentration of component i in fuel and air channels, respectively.

4.3.2 Electrochemical Model

The operation of an SOFC involves the reduction of oxidant and the oxidation of fuel at the cathode and the anode, respectively. The difference between the thermodynamic potentials of the electrode reactions determines the reversible cell

voltage or open-circuit potential, E^{OCV} . However, an operating cell voltage, V , equals to the voltage falls due to internal resistances and overpotential losses.

4.3.2.1. Reversible open-circuit voltage

The reversible open-circuit voltage (E^{OCV}) is the maximum voltage that can be achieved by a fuel cell. For the SOFC system, it can be calculated by the following equation:

$$E^{\text{OCV}} = \frac{-\Delta\bar{g}_f}{nF} \quad (4.21)$$

where n is a number of electrons passing around the circuit per mole of fuel. F is the Faraday's constant which always equals to 96485.34 C/mol and $\Delta\bar{g}_f$ is Gibbs free energy.

Considering basic reactions for the hydrogen/oxygen fuel cell, it is shown that two electrons pass around the external circuit for each water molecule produced and each molecule of hydrogen used. Therefore, Equation (4.21) becomes:

$$E^{\text{OCV}} = \frac{-\Delta\bar{g}_f}{2F} \quad (4.22)$$

The activities of the reactants and products modify the Gibbs free energy change of a reaction. Using thermodynamic arguments, it can show that in the electrochemical chemical reaction:

$$\Delta\bar{g}_f = \Delta\bar{g}_f^0 - RT \ln \left(\frac{a_{\text{H}_2} a_{\text{O}_2}^{1/2}}{a_{\text{H}_2\text{O}}} \right) \quad (4.23)$$

Since SOFCs are usually operated at high temperatures (about 1000 °C), we can assume that all gaseous reactants and products behave as an ideal gas, and so

$$a_{\text{H}_2} = \frac{P_{\text{H}_2}}{P^0}, \quad a_{\text{O}_2} = \frac{P_{\text{O}_2}}{P^0}, \quad a_{\text{H}_2\text{O}} = \frac{P_{\text{H}_2\text{O}}}{P^0}$$

If all the pressures are given in bar, then $P^0 = 1$ and Equation (4.23) will become

$$\Delta \bar{g}_f = \Delta \bar{g}_f^0 - RT \ln \left(\frac{p_{\text{H}_2} p_{\text{O}_2}^{1/2}}{p_{\text{H}_2\text{O}}} \right) \quad (4.24)$$

Substituting the above equation into Equation (4.22):

$$E^{\text{OCV}} = -\frac{\Delta \bar{g}_f^0}{2F} + \frac{RT}{2F} \ln \left(\frac{p_{\text{H}_2} p_{\text{O}_2}^{1/2}}{p_{\text{H}_2\text{O}}} \right)$$

$$E^{\text{OCV}} = E^0 + \frac{RT}{2F} \ln \left(\frac{p_{\text{H}_2} p_{\text{O}_2}^{1/2}}{p_{\text{H}_2\text{O}}} \right) \quad (4.25)$$

Equation (4.25) is called the Nernst equation. E^0 is the open-circuit voltage at standard pressure and is a function of the operating temperature as can be given by the following expression (Ni et al., 2007):

$$E^0 = 1.253 - 2.4516 \times 10^{-4} T \quad (4.26)$$

Due to the difference in the location of water produced in the SOFC-O²⁻ and SOFC-H⁺, the partial pressure of water shown in Equation (4.25) are dissimilar as follows:

$$\text{SOFC-O}^{2-}: \quad E_{\text{SOFC-O}}^{\text{OCV}} = E^0 + \frac{\mathcal{R}T}{2F} \ln \left(\frac{p_{\text{H}_2(\text{an})} p_{\text{O}_2(\text{ca})}^{0.5}}{p_{\text{H}_2\text{O}(\text{an})}} \right) \quad (4.27)$$

$$\text{SOFC-H}^{+}: \quad E_{\text{SOFC-H}}^{\text{OCV}} = E^0 + \frac{\mathcal{R}T}{2F} \ln \left(\frac{p_{\text{H}_2(\text{an})} p_{\text{O}_2(\text{ca})}^{0.5}}{p_{\text{H}_2\text{O}(\text{ca})}} \right) \quad (4.28)$$

4.3.2.2 Actual fuel cell voltage

However, in a real operation, when a current is drawn from a fuel cell, an actual fuel cell voltage or an operating voltage (V) is always less than the open-circuit voltage, as shown in Equation (4.29). This is due to internal resistance and overpotential losses associated with the electrochemical reactions at the electrode|electrolyte interface. There are three loss mechanisms that result in the loss of useful cell voltage at a given operating cell voltage. These include (i) activation

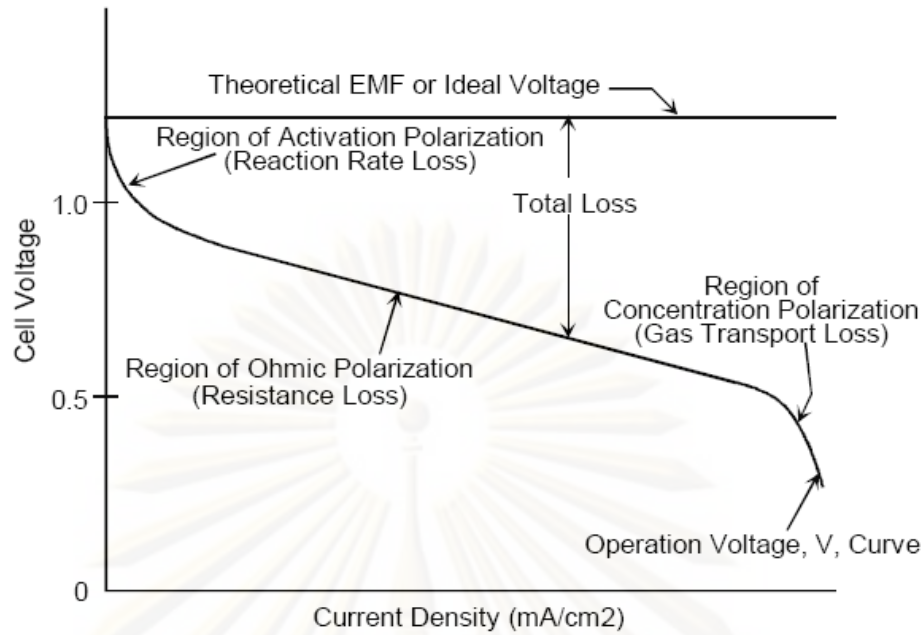


Figure 4.3 Ideal and actual fuel cell voltage/current characteristic (Hirschenhofer et al., 1998).

overpotential (η_{act}), (ii) ohmic overpotential (η_{ohm}), and (iii) concentration overpotential (η_{conc}).

$$V = E^{OCV} - (\eta_{act} + \eta_{ohm} + \eta_{conc}) \quad (4.29)$$

The different loss mechanisms dominate at different levels of current density (i), as shown in Figure 4.3. The current density is defined as the current produced per unit geometrical area of a fuel cell.

- Activation overpotential (η_{act}) is the loss associated with the electrochemical reactions at the electrode surfaces; that is, hydrogen oxidation and oxygen reduction reactions at the anode and cathode, respectively. Activation overpotential is often represented by the nonlinear Butler-Volmer equation as follows:

$$i = i_{0,electrode} \left[\exp\left(\frac{\alpha nF}{\mathfrak{R}T} \eta_{act,electrode}\right) - \exp\left(-\frac{(1-\alpha)nF}{\mathfrak{R}T} \eta_{act,electrode}\right) \right] \quad (4.30)$$

$$\text{electrode} \in \{\text{anode, cathode}\}$$

where α is the transfer coefficient, n is the number of electrons transferred in the single elementary rate-limiting reaction and $i_{0,\text{electrode}}$ is the exchange current density. The exchange current density is the forward and reverse electrode reaction rate at the equilibrium potential. A high exchange current density implies that a high electrochemical reaction rate and good fuel cell performance can be expected. The transfer coefficient is considered to be the fraction of the change in overpotential that leads to a change in the reaction rate constant, and its value is usually set to 0.5 for a SOFC (Chan et al., 2000; Aguiar et al., 2004; Ni et al., 2007). When $\alpha = 0.5$, the activation overpotential (Equation (4.30)) can be expressed as follows:

$$i = 2i_0 \sinh\left(\frac{nF\eta_{\text{act}}}{2\mathfrak{R}T}\right) \quad (4.31)$$

Then,

$$\eta_{\text{act}} = \frac{2\mathfrak{R}T}{nF} \sinh^{-1}\left(\frac{i}{2i_0}\right) \quad (4.32)$$

In fact, the exchange current density is a crucially important parameter for determining the activation overpotential. It is influenced by different factors which are not clearly understood; accordingly, its value changes drastically from author to author. In some modeling work, the exchange current density was assumed to be constant (Chan et al., 2001, Li and Chyu, 2003; Burt et al., 2004) or depends on temperature, activation energy and partial pressure of reactants and products (Zhu and Kee, 2003; Comparani and Iora, 2004; Costamagna et al., 2004; Hernandez-Pacheco et al., 2004; Qi *et al.*, 2005; Ni et al., 2007). In this study, semi-empirical correlations based on experimental data are used for computing the exchange current density which depends on the operating temperature, as shown in Equation (4.33). Table 4.2 gives the values of the pre-exponential factor ($k_{\text{electrode}}$) and the activation energy of the anode and cathode ($E_{\text{electrode}}$) used for computing $i_{0,\text{electrode}}$ (Aguiar et al., 2004).

$$i_{0,\text{electrode}} = \frac{\mathfrak{R}T}{nF} k_{\text{electrode}} \exp\left(-\frac{E_{\text{electrode}}}{\mathfrak{R}T}\right) \quad (4.33)$$

Table 4.2 Pre-exponential factor and activation energy for computing the exchange-current density

k_{cathode}	$2.35 \times 10^{11} \Omega^{-1} \text{m}^{-2}$	E_{cathode}	137 kJ mol^{-1}
k_{anode}	$6.54 \times 10^{11} \Omega^{-1} \text{m}^{-2}$	E_{anode}	140 kJ mol^{-1}

• Ohmic overpotential (η_{ohm}) is losses due to the resistance to the electronic flow in the electrodes and the resistance to the ion flow in the electrolyte. Because the ionic flow in the electrolyte and the electronic flow in the electrodes obey Ohm's law, the ohmic losses can be expressed by the equation:

$$\eta_{\text{Ohm}} = iR_{\text{Ohm}} \quad (4.34)$$

where R_{ohm} is the area-specific internal resistance of the cell resistance, including the area-specific resistances in the electrodes and the electrolyte. Because the current produced by the SOFC must flow serially through all of the components, R_{ohm} is simply the sum of all the individual resistance contributions. Unfortunately, it is experimentally very difficult to determine internal resistance; however, it can be estimated from the effective distance between the components coupled with conductivity data. Here, R_{ohm} is calculated from the conductivity of the individual layers (assuming negligible contact resistances, cross-plane charge flow, and series connection of resistances) by the following equation:

$$R_{\text{Ohm}} = \frac{\tau_{\text{an}}}{\sigma_{\text{an}}} + \frac{\tau_{\text{ele}}}{\sigma_{\text{ele}}} + \frac{\tau_{\text{ca}}}{\sigma_{\text{ca}}} \quad (4.35)$$

Table 4.3 The conductivities of cell component used in the calculations of the internal resistance (Ferguson et al., 1996)

Parameter	Anode	Electrolyte	Cathode
Conductivity ($\Omega^{-1} \text{m}^{-1}$)	$\frac{4.2 \times 10^7}{T} \exp\left(-\frac{1200}{T}\right)$	$33.4 \times 10^3 \exp\left(-\frac{10300}{T}\right)$	$\frac{9.5 \times 10^7}{T} \exp\left(-\frac{1150}{T}\right)$

where τ_{an} , τ_{ele} and τ_{ca} stand for the thickness of the anode, electrolyte and cathode, σ_{an} and σ_{ca} for the electronic conductivity of the anode and cathode, and σ_{ele} for the ionic conductivity of the electrolyte, respectively.

It is well known that the ohmic overpotential is sensitive to temperature, the ionic conductivity of the electrolyte is temperature dependent (Furguson et al., 1996; Aguiar et al., 2004; Ni et al., 2007). While the electrical conductivities of the electrodes are differently proposed from author to author; for example, Furguson et al. (1996) presented that the electrical conductivities of both the electrodes and electrolyte are considered to be temperature dependent. Ni et al. (2007) claimed that the electrodes generally have much higher electrical conductivity than the electrolyte and thus, their effect on the overall ohmic overpotential can be neglected. Lists of the values of ionic and electrical conductivities of electrolyte and electrodes for SOFC- O^{2-} as proposed in previous literatures are shown in Table 4.3.

In case of SOFC- H^+ , the protonic conductivity of the electrolyte as a function of temperature is extracted from the experimental results of Potter and Baker (2006) as shown in Equation (4.36) whereas the electrical conductivity of platinum used as electrodes are not available in the open literature.

$$\sigma_{ele-H^+} = 225.92 \exp\left(-\frac{6300}{T}\right) \quad (4.36)$$

- Concentration overpotential (η_{conc}) is the loss associated with the transport of gaseous reactants through porous electrodes. It is caused by a large reduction in the concentration of fuel at the electrode-electrolyte interface. This loss is more pronounced when fuel or oxidant gases with low purity is fed to a fuel cell stack or the reactant inlet flux and the product outlet flux from an electrode are slower than that corresponding to the discharged current and the concentration profiles develop across the electrode.

The concentration overpotential can be determined from the difference in the open-circuit potential calculated based on the reactant and product concentrations at three-phase boundaries (TPB) or the electrode|electrolyte interfaces (I) and that based

on the bulk concentrations. The open-circuit potential at the electrode|electrolyte interfaces (I), $E^{\text{OCV,I}}$, is written as;

$$\text{SOFC-O}^{2-}: \quad E_{\text{SOFC-O}}^{\text{OCV,I}} = E^0 + \frac{\mathfrak{R}T}{2F} \ln \left(\frac{p_{\text{H}_2(\text{an})}^{\text{I}} \left(p_{\text{O}_2(\text{ca})}^{\text{I}} \right)^{0.5}}{p_{\text{H}_2\text{O}(\text{an})}^{\text{I}}} \right) \quad (4.37)$$

$$\text{SOFC-H}^+: \quad E_{\text{SOFC-H}}^{\text{OCV,I}} = E^0 + \frac{\mathfrak{R}T}{2F} \ln \left(\frac{p_{\text{H}_2(\text{an})}^{\text{I}} \left(p_{\text{O}_2(\text{ca})}^{\text{I}} \right)^{0.5}}{p_{\text{H}_2\text{O}(\text{ca})}^{\text{I}}} \right) \quad (4.38)$$

The difference between E^{OCV} and $E^{\text{OCV,I}}$ gives the departure from the theoretical voltage as

$$\text{SOFC-O}^{2-}: \quad \eta_{\text{conc,SOFC-O}} = \frac{\mathfrak{R}T}{2F} \ln \left(\frac{p_{\text{H}_2\text{O}(\text{an})}^{\text{I}} p_{\text{H}_2(\text{an})}}{p_{\text{H}_2\text{O}(\text{an})}^{\text{I}} p_{\text{H}_2(\text{an})}^{\text{I}}} \right) + \frac{\mathfrak{R}T}{4F} \ln \left(\frac{p_{\text{O}_2(\text{ca})}}{p_{\text{O}_2(\text{ca})}^{\text{I}}} \right) \quad (4.39)$$

$$\text{SOFC-H}^+: \quad \eta_{\text{conc,SOFC-H}} = \frac{\mathfrak{R}T}{2F} \ln \left(\frac{p_{\text{H}_2(\text{an})}}{p_{\text{H}_2(\text{an})}^{\text{I}}} \right) + \frac{\mathfrak{R}T}{2F} \ln \left(\left(\frac{p_{\text{O}_2(\text{ca})}}{p_{\text{O}_2(\text{ca})}^{\text{I}}} \right)^{0.5} \frac{p_{\text{H}_2\text{O}(\text{ca})}^{\text{I}}}{p_{\text{H}_2\text{O}(\text{ca})}} \right) \quad (4.40)$$

The first term on the right-hand side of Equations (4.39) and (4.40) refers to the anode concentration overpotential ($\eta_{\text{conc,anode}}$) and the second term refers to the cathode concentration overpotential ($\eta_{\text{conc,cathode}}$).

To calculate the concentration overpotential, the partial pressure of H_2 , H_2O and O_2 at the electrode|electrolyte interfaces needs to be known. In this study, it was assumed that the rate of mass transport through the porous electrodes can be described by the diffusion of gases in pores using Fick's law; the electrochemical reaction occurs at the electrode|electrolyte interfaces; the diffusion rate of reactants to the interfaces is equal to the rate of electrochemical reaction. The following expressions were obtained from (Chan et al., 2001; Suwanwarangkul et al., 2003; Hernandez-Pacheco et al., 2005b; Bird et al., 2006):

$$\text{SOFC-O}^{2-}: \quad p_{\text{H}_2(\text{an})}^{\text{I}} = p_{\text{H}_2(\text{an})} - \frac{\mathfrak{R}T\tau_{\text{an}}}{2FD_{\text{an,eff}}}i$$

$$p_{\text{H}_2\text{O}(\text{an})}^{\text{I}} = p_{\text{H}_2\text{O}(\text{an})} + \frac{\mathfrak{R}T\tau_{\text{an}}}{2FD_{\text{an,eff}}}i \quad (4.41)$$

$$p_{\text{O}_2(\text{ca})}^{\text{I}} = P - (P - p_{\text{O}_2(\text{ca})}) \exp\left(\frac{\mathfrak{R}T\tau_{\text{ca}}}{4FD_{\text{ca,eff}}P}i\right)$$

$$\text{SOFC-H}^+: \quad p_{\text{H}_2(\text{an})}^{\text{I}} = P - (P - p_{\text{H}_2(\text{an})}) \exp\left(\frac{\mathfrak{R}T\tau_{\text{an}}}{2FD_{\text{an,eff}}P}i\right)$$

$$p_{\text{O}_2(\text{ca})}^{\text{I}} = p_{\text{O}_2(\text{ca})} - \frac{\mathfrak{R}T\tau_{\text{ca}}}{2FD_{\text{ca,eff}}}i \quad (4.42)$$

$$p_{\text{H}_2\text{O}(\text{ca})}^{\text{I}} = p_{\text{H}_2\text{O}(\text{ca})} + \frac{\mathfrak{R}T\tau_{\text{ca}}}{4FD_{\text{ca,eff}}}i$$

where $D_{\text{an,eff}}$ and $D_{\text{ca,eff}}$ represent the effective diffusivity coefficient of gases at the anode and cathode sides that can be explained by ordinary and Knudsen diffusions (Chan et al., 2001; Bird et al., 2006). For SOFC-O²⁻, the effective gas diffusivity coefficient in the anode is calculated from the average effective diffusivity coefficient of H₂ and H₂O whereas that in the cathode is calculated from the effective diffusivity coefficient of O₂ and N₂. In case of SOFC-H⁺, the effective gas diffusivity coefficient in the anode is calculated from the effective diffusivity coefficient of H₂ whereas that in the cathode is calculated from the effective diffusivity coefficient of O₂ and H₂O averaged by its mole fraction. The detail in the calculation of the effective diffusivity coefficient is given in Appendix A.

4.4 Numerical solutions

4.4.1 Electrochemical model

A flow diagram of numerical solution for calculating electrochemical characteristics of SOFC is presented in Figure 4.4. The electrochemical model of SOFC is solved by determining the cell voltage (V) for a given current density (i). For

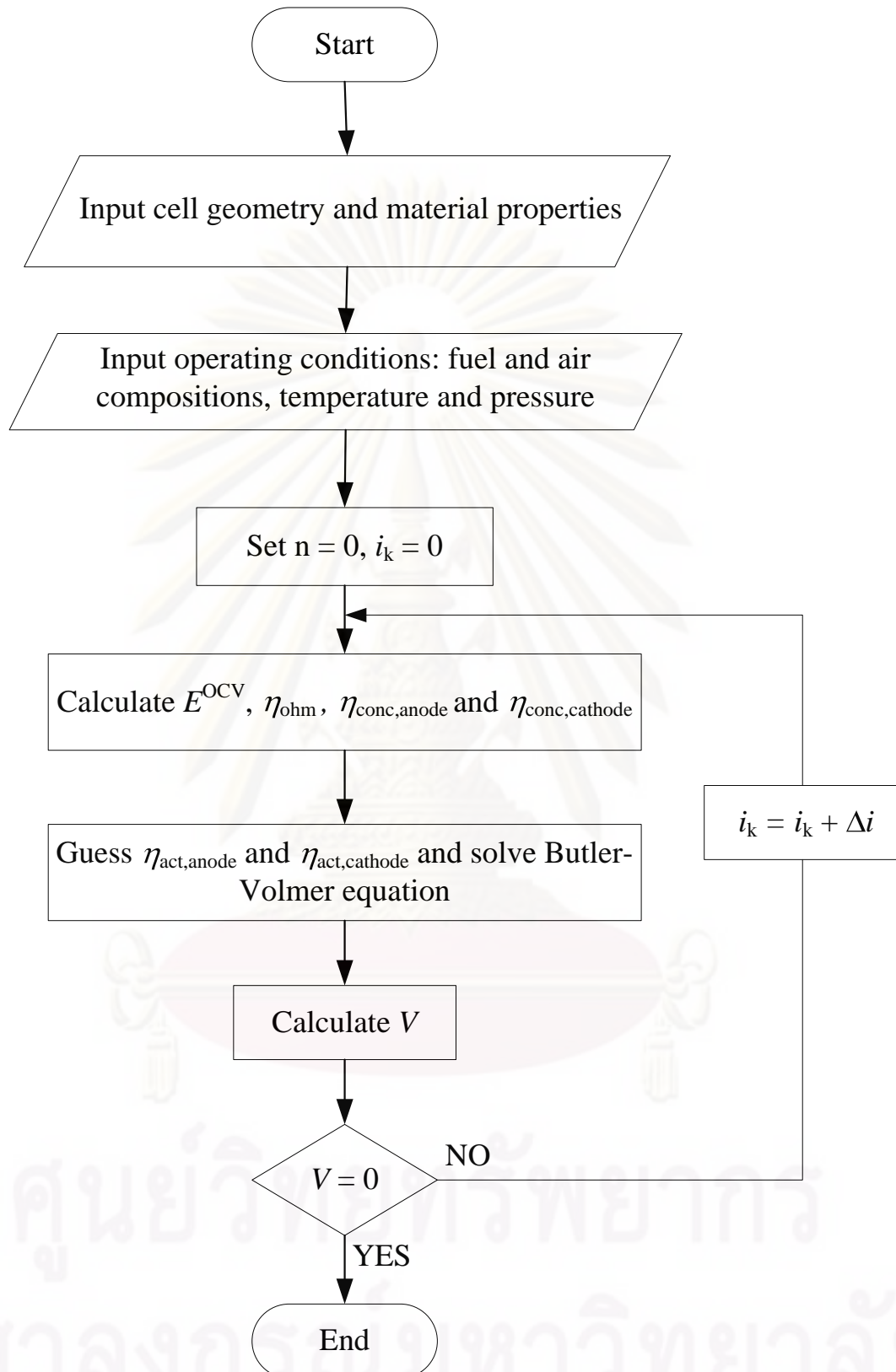


Figure 4.4 Flow diagram of numerical solution for determining electrochemical performance of SOFC.

the solution of electrochemical model, the cell geometry and material properties as well as operating conditions (i.e., fuel and air composition, temperature and pressure) must be specified. Based on the inlet gas composition, pressure and temperature, the open-circuit voltage (Equation (4.27) for SOFC-O²⁻ and Equation (4.28) for SOFC-H⁺) can be calculated. The ohmic overpotential (Equation (4.34)) and concentration overpotentials for anode and cathode (Equation (4.39) for SOFC-O²⁻ and Equation (4.40) for SOFC-H⁺) can be evaluated as an explicit function of current density. Since the activation overpotential is an implicit function of current density, the iterative procedure is required. With a specified exchange current density at the anode and cathode, the Butler-Volmer equation (Equation (4.30)) is solved to obtain the activation overpotentials for anode and cathode. From the open-circuit voltage and all the overpotentials, the cell voltage can be determined (Equation (4.29)). This procedure is assumed that the cell voltage is to be determined once a current density is specified. For the plot of characteristic curve or voltage-current curve, the procedure is repeated for the whole range of fuel cell operations until $V = 0$.

4.4.2 Steady-state fuel cell model

When the electrochemical model is integrated with mass balance equation, the SOFC model consists of a set of ordinary differential (Equations (4.10) to (4.20)) and algebraic equations (Equations (4.27) to (4.42)), which is solved by using Matlab. For the solution of the steady-state fuel cell model, in addition to all cell geometry, material property data, input model parameters (i.e., operating temperature and pressure) and inlet fuel and air composition, it must be specified the cell voltage. Figure 4.5 shows a flow diagram of numerical solution for determining the steady-state fuel cell performance. The mass balances can determine the gas composition distribution of each component in the gas channels. Due to the variation in gas compositions along the anode and cathode channels, the open-circuit voltage and consequently the local current density changes with the distance, which are determined by the electrochemical model. The average current density (i_{ave}) obtained is calculated by the integration of the current density distribution along the whole length of the cell channel. The steady-state performance in terms of power density, fuel cell efficiency and fuel utilization can be determined as described in Section 4.5.

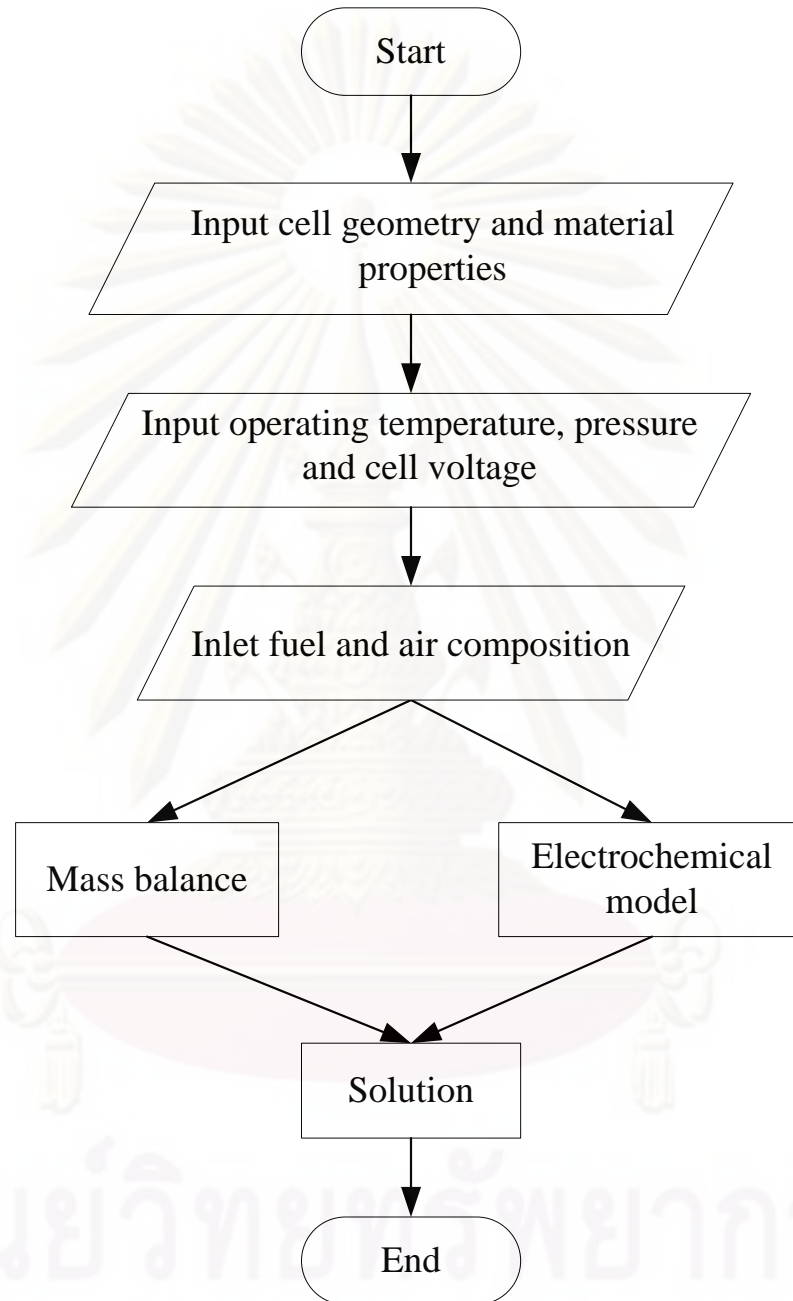


Figure 4.5 Flow diagram of numerical solution for determining steady-state SOFC performance.

4.5 SOFC performance

Generally, SOFC performance is assessed by power density and efficiency. In this study, when the cell voltage is specified, an average current density is calculated from the distribution of current density along the cell length. The cell voltage and average current density obtained are used to calculate the power density and the fuel cell efficiency. Besides the power density and efficiency, fuel utilization is key parameter to be used to evaluate the fuel cell performance.

4.5.1 Power generation

The power output of fuel cell is the product of the operating voltage and current density which can be given by:

$$P_{\text{SOFC}} = iV \quad (4.43)$$

where P_{SOFC} is the power density which is increased with increasing current density until a maximum power density reached. Afterward, the power density is reduced because the cell voltage is insufficient to maintain the power density.

4.5.2 Fuel cell efficiency

The efficiency of a fuel cell is defined as the fraction of the total chemical energy in the inlet fuel that is converted into electrical energy (power).

$$\varepsilon_{\text{SOFC}} = \frac{P_{\text{SOFC}}}{\Delta H_f} \times 100\% \quad (4.44)$$

where ΔH_f represents the enthalpy or thermal energy of fuel supplied to a fuel cell. In this work, CH_4 , CO and H_2 are considered as inlet fuel since CH_4 and CO can be reformed into H_2 which is electrochemically converted into electricity. Thus, ΔH_f is be determined as,

$$\Delta H_f = F_{\text{CH}_4}^{\text{in}} LHV_{\text{CH}_4} + F_{\text{CO}}^{\text{in}} LHV_{\text{CO}} + F_{\text{H}_2}^{\text{in}} LHV_{\text{H}_2} \quad (4.46)$$

where LHV_i and F_i^{in} represent the lower heating value and molar flow rate of component i (CH_4 , CO and H_2), respectively. The use of lower heating value is justified by water vapor being produced in the process. Because P_{SOFC} is defined in unit of Watt per area, Equation (4.46) can be written by:

$$\varepsilon_{\text{SOFC}} = \frac{P_{\text{SOFC}} LW}{F_{\text{CH}_4}^{\text{in}} LHV_{\text{CH}_4} + F_{\text{CO}}^{\text{in}} LHV_{\text{CO}} + F_{\text{H}_2}^{\text{in}} LHV_{\text{H}_2}} \times 100\% \quad (4.47)$$

4.5.3 Fuel utilization

The fuel utilization (U_{fuel}) is the fraction of the total fuel inlet used to produce electricity in the cell. As mentioned above, CH_4 , CO and H_2 are considered as inlet fuel and H_2 is electrochemically oxidized. It should be noted that moles of H_2 consumed due to electrochemical reactions are related to the current generation according to the Faraday's law (Aguiar et al., 2002b). Therefore, the fuel utilization can be expressed by:

$$U_{\text{fuel}} = \frac{iLW}{2F(4F_{\text{CH}_4}^{\text{in}} + F_{\text{H}_2}^{\text{in}} + F_{\text{CO}}^{\text{in}})} \quad (4.48)$$

4.6. Model Validation

4.6.1 Model Validation of SOFC- O^{2-}

To ensure that the electrochemical model of SOFC- O^{2-} (Equations (4.26)-(4.27), (4.29)-(4.30), (4.33)-(4.35), (4.39) and (4.41)) as proposed in the previous section can reliably predict the SOFC performance, the simulations were done to compare the modeling results with the experimental data reported in the literature (Zhao and Virkar, 2005). In their experiment, i - V characteristics of an anode-supported SOFC- O^{2-} were measured at temperatures of 873K, 973K and 1073 K and a pressure of 1 bar. The thickness of anode, cathode and electrolyte were 1000, 20 and 8 μm , respectively. The inlet fuel consists of 97% H_2 and 3% H_2O while the inlet oxidant consists of 21% O_2 . The comparison of the model prediction and experimental data in terms of cell voltage at different current densities and operating

temperatures is shown in Figure 4.6. It is observed that the model prediction agrees well with the experimental data.

4.6.2 Model Validation of SOFC-H⁺

As the SOFC-H⁺ is not as developed as the SOFC-O²⁻, the exchange current densities of electrodes are not presented in the open literature. Further, the use of the mass transport equation from Fick's model for computing the concentration overpotential may be ambiguous. Therefore, the electrochemical model of SOFC-H⁺ (Equations (4.26), (4.28)-(4.30), (4.34), (4.36), (4.40) and (4.42)) used in this study was validated with experimental data of Iwahara (1988). In the Iwahara's experiment, the materials used in SOFC-H⁺ for anode, electrolyte and cathode are Pt|SCY|Pt and their thicknesses were 50 μm , 500 μm , and 50 μm , respectively. The inlet fuel and oxidation used in the Iwahara's experiment were 10% H₂ (~3% H₂O) and dry air (<0.1% H₂O), respectively. Figure 4.7 shows a model prediction of the *i-V* characteristics of SOFC-H⁺ operated at three temperature levels (1073 K, 1173 K, and 1273 K) and a pressure of 1 atm in comparison with experimental data. It indicates that the calculated results from the proposed model are in good agreement with data in the literature when the exchange current densities of electrodes are set as equal to 800 A m⁻².

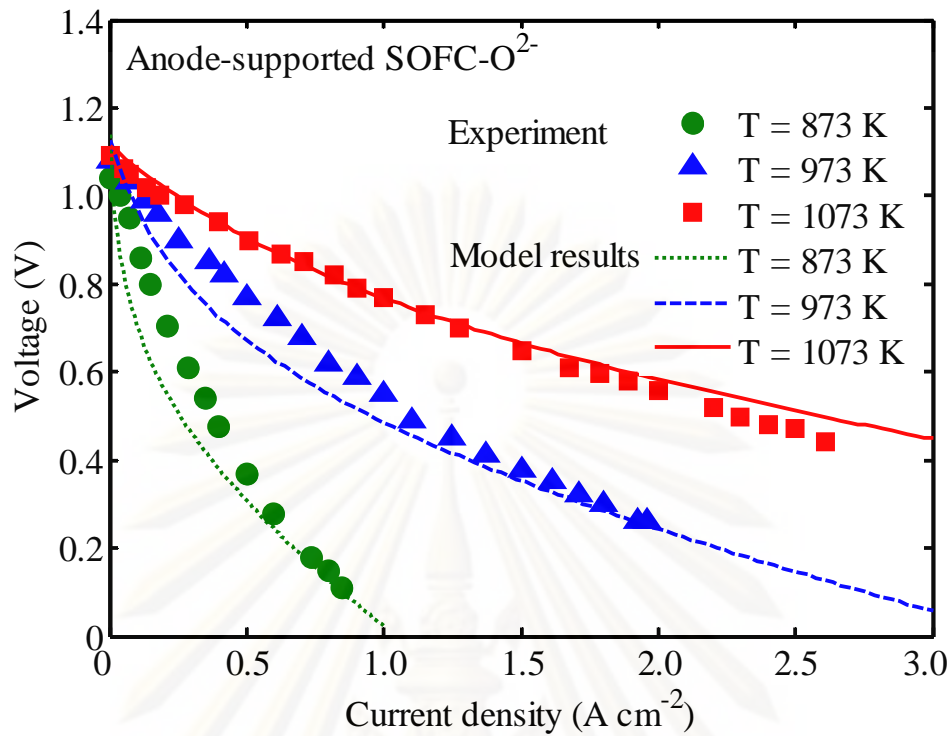


Figure 4.6 Comparison between model predictions and experimental results (Zhao and Virkar, 2005).

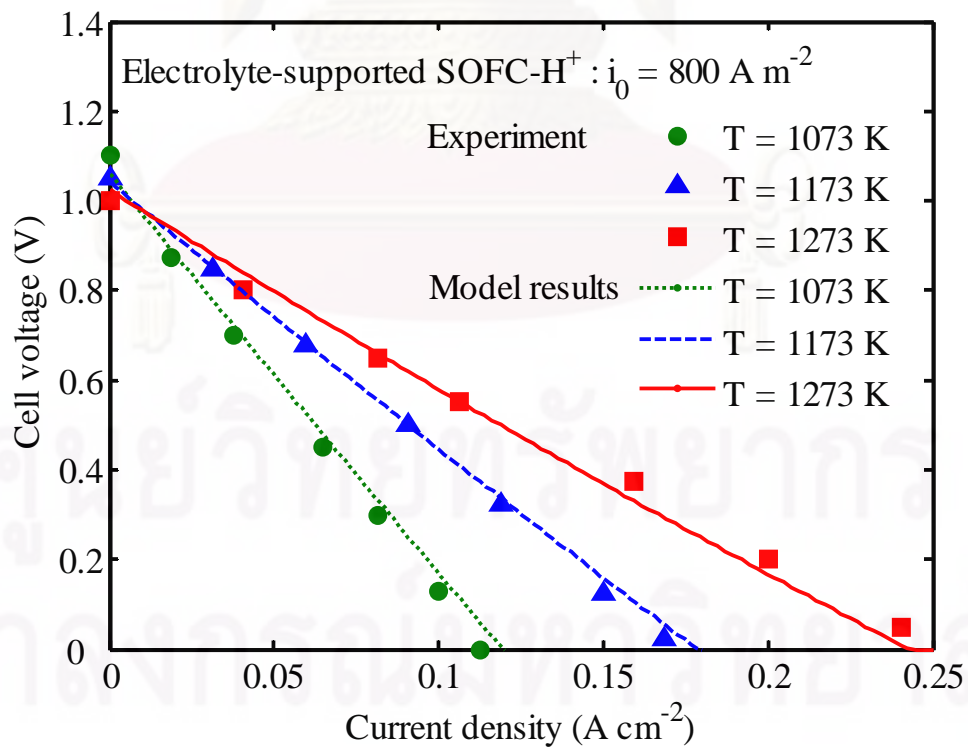


Figure 4.7 Comparison of cell characteristics of SOFC-H⁺ obtained from model prediction and experimental data (Iwahara, 1988).

CHAPTER V

SOLID OXIDE FUEL CELL BASED ON AN OXYGEN ION-CONDUCTING ELECTROLYTE

This chapter presents the performance analysis of a planar SOFC based on an oxygen ion-conducting electrolyte. First, the electrochemical model as explained in Chapter IV is used to analyze the electrical characteristics of SOFC with respect to support structure (i.e., anode-, cathode- and electrolyte-supported) and design parameters (i.e., cell component thicknesses and electrode microstructure). Then, a simulation of an optimal designed SOFC is performed under steady state and isothermal conditions. The operation of SOFC under direct internal reforming and intermediate temperature (873-1023 K) is considered. The fuel cell performances in terms of fuel cell efficiency, cell voltage and power density are analyzed taking into account the effect of key operating parameters such as temperature, pressure, degree of pre-reforming, steam to carbon ratio and inlet fuel velocity.

5.1 Introduction

As mentioned earlier, a planar-type SOFC has recently received much attention. Two basic approaches are proposed in the development of the planar SOFC. In an electrolyte-supported SOFC, the electrolyte is the thickest component ($> 150 \mu\text{m}$) while the anode and cathode are very thin (about $50 \mu\text{m}$) (Virkar et al., 2000; Kakaç et al., 2007), which results in high ohmic resistance. Thus, most current research efforts have been focused on the application of the electrolyte-supported SOFCs at a high operating temperature. In an electrode-supported SOFC, one of the two electrodes, either the cathode or the anode, is the thickest component (around 2 mm) and support structure (Virkar et al., 2000). This decreases the ohmic resistance and makes design better suited for operation at lower temperatures (873-1023 K); the system is referred to as an intermediate-temperature solid oxide fuel cell (IT-SOFC).

The development and performance improvement of the IT-SOFC have received much attention due to several potential benefits, e.g., the possibility of using a wider range of materials and the promise of low-cost fabrication.

Considering the characteristics of the electrode-supported SOFC, it has been reported that activation and perhaps concentration overpotentials can often outweigh the benefit of the reduced ohmic loss due to small electrolyte thickness so that the specific resistance of the electrode-supported SOFC at an intermediate temperature may be larger than that of the high-temperature SOFC. Further, it is well known that the characteristics of SOFCs are strongly affected not only by operating conditions such as temperature and pressure, and partial pressures of fuel and oxidant but also by design parameters such as the thickness of electrode and electrolyte and the porosity of electrode. Therefore, the performance analysis of fuel cells should take these parameters into account as it will lead to an optimum design and operation of SOFCs.

In this work, the role of the support structure and the influence of design parameters on the performance of a planar SOFC are investigated by considering its characteristics obtained from a detailed electrochemical model. When the optimal design of SOFC is determined, the performance analysis of a planar SOFC under steady state and isothermal conditions is presented. As mentioned earlier, high operating temperature of SOFC allows considerable flexibility in various types of fuels (i.e., methane, methanol and ethanol) due to the reforming capability of hydrocarbons. Therefore, in this work, methane is considered as fuel that is directly reformed within SOFC. The steady-state performance of SOFC in terms of fuel cell efficiency and power density is analyzed. The effects of key operating parameters such temperature, pressure, degree of pre-reforming, steam to carbon ratio and inlet fuel velocity are investigated.

5.2 Electrochemical study

This section presents the characteristic curves for cell voltage and power density as a function of current density. The electrochemical model taking into account operating and design parameters as presented in Chapter IV was used to analyze the characteristics performance of a planar SOFC with different support structures (i.e., anode-, cathode- and electrolytes-supported) and design parameters

(i.e., the thickness of cell components and electrode microstructure). Here, the non-linear Butler-Volmer equation is employed to describe the activation overpotential instead of using the simplified Tafel equation and the exchange-current density is dependent on the operating temperature. The ohmic loss is related to cell design parameters, i.e., the thickness of cell components, ionic and electronic conductivities that are changed by the operating temperature. Gas diffusion through the porous electrodes described by Fick's model is considered in the determination of the concentration overpotential. Table 5.1 summarizes the electrochemical model of SOFC used in this study.

5.2.1 Results and discussion

Table 5.2 shows the values of the cell geometry and material properties used in the study whereas the operating conditions are listed in Table 5.3 (Ferguson et al., 1996; Aguiar et al., 2004). The fuel composition given in Table 5.3 is based on a gas obtained from an external reformer fed by steam and methane at a ratio of 2. The methane steam reforming and water gas shift reaction are assumed to be at equilibrium. It is noted that an external reformer is usually installed before the SOFC system in order to produce hydrogen-rich feed and to reduce the possibility of carbon formation on the anode.

ศูนย์วิทยทรัพยากร

จุฬาลงกรณ์มหาวิทยาลัย

Table 5.1 Electrochemical model of SOFC used in the present study

Open-circuit voltage (E^{OCV}):

$$E^{\text{OCV}} = E^0 + \frac{\mathfrak{R}T}{2F} \ln \left(\frac{P_{\text{H}_2(\text{an})} P_{\text{O}_2(\text{ca})}^{0.5}}{P_{\text{H}_2\text{O}(\text{an})}} \right) \quad (5.1)$$

Operating voltage (V):

$$V = E^{\text{OCV}} - \eta_{\text{ohm}} - \eta_{\text{act}} - \eta_{\text{conc}} \quad (5.2)$$

Ohmic loss (η_{ohm}):

$$\eta_{\text{Ohm}} = iR_{\text{Ohm}} \quad \text{where} \quad R_{\text{Ohm}} = \frac{\tau_{\text{an}}}{\sigma_{\text{an}}} + \frac{\tau_{\text{ele}}}{\sigma_{\text{ele}}} + \frac{\tau_{\text{ca}}}{\sigma_{\text{ca}}} \quad (5.3)$$

Activation overpotential (η_{act}):

$$i = i_{0,\text{electrode}} \left[\exp \left(\frac{\alpha n F}{\mathfrak{R}T} \eta_{\text{act,electrode}} \right) - \exp \left(- \frac{(1-\alpha) n F}{\mathfrak{R}T} \eta_{\text{act,electrode}} \right) \right] \quad (5.4)$$

$$i_{0,\text{electrode}} = \frac{\mathfrak{R}T}{nF} k_{\text{electrode}} \exp \left(- \frac{E_{\text{electrode}}}{\mathfrak{R}T} \right) \quad (5.5)$$

Concentration overpotential (η_{conc}):

$$\eta_{\text{conc}} = \frac{\mathfrak{R}T}{2F} \ln \left(\frac{P_{\text{H}_2\text{O}(\text{an})}^I P_{\text{H}_2(\text{an})}}{P_{\text{H}_2\text{O}(\text{an})} P_{\text{H}_2(\text{an})}^I} \right) + \frac{\mathfrak{R}T}{4F} \ln \left(\frac{P_{\text{O}_2(\text{ca})}}{P_{\text{O}_2(\text{ca})}^I} \right) \quad (5.6)$$

where
$$P_{\text{H}_2(\text{an})}^I = P_{\text{H}_2(\text{an})} - \frac{\mathfrak{R}T \tau_{\text{an}}}{2FD_{\text{an,eff}}} i \quad (5.7)$$

$$P_{\text{H}_2\text{O}(\text{an})}^I = P_{\text{H}_2\text{O}(\text{an})} + \frac{\mathfrak{R}T \tau_{\text{an}}}{2FD_{\text{an,eff}}} i \quad (5.8)$$

$$P_{\text{O}_2(\text{ca})}^I = P - (P - P_{\text{O}_2(\text{ca})}) \exp \left(\frac{\mathfrak{R}T \tau_{\text{ca}}}{4FD_{\text{ca,eff}} P} i \right) \quad (5.9)$$

Table 5.2 Model geometries and material property parameters

Parameter	Anode	Electrolyte	Cathode
A-S structure ^a (μm)	500	40	40
C-S structure ^b (μm)	40	40	500
E-S structure ^c (μm)	40	500	40
Conductivity ($\Omega^{-1}\text{m}^{-1}$)	$\frac{4.2 \times 10^7}{T} \exp(-\frac{1200}{T})$	$33.4 \times 10^3 \exp(-\frac{10300}{T})$	$\frac{9.5 \times 10^7}{T} \exp(-\frac{1150}{T})$
Porosity	0.3	-	0.3
Pore radius (μm)	0.5	-	0.5
Tortuosity	6	-	6

^a A-S structure: Anode-supported SOFC

^b C-S structure: Cathode-supported SOFC

^c E-S structure: Electrolyte-supported SOFC

Table 5.3 Operating conditions for SOFC at the standard case

Parameter	Value
Operating temperature, T (K)	1073
Operating pressure, P (atm)	1
Fuel composition ^a	30% H ₂ , 42.3% H ₂ O, 19.7% CH ₄ , 3% CO and 5% CO ₂
Air composition	21% O ₂ , 79% N ₂

^aThe fuel composition is based on a fully reformed steam and methane mixture with S/C = 2

5.2.1.1 Role of support structures

The characteristics of an anode-supported SOFC under isothermal operation ($T = 1073 \text{ K}$) at different operating current densities (i) are presented in Figure 5.1. The cell voltage decreases with increase in operating current density due to the increased voltage losses from the irreversible SOFC cell resistance. The power density increases initially to a maximum value of 0.69 W cm^{-2} at a current density of 1.5 A cm^{-2} and then slightly decreases to zero at 3.17 A cm^{-2} . This indicates that the cell performance is not controlled by the concentration overpotential under these operating conditions. It should be noted that in this study, the fuel and oxidant are assumed to be undepleted. Since, however, the fuel and air compositions vary along the length of the cell under real operation, due to fuel and oxygen utilization by electrochemical reactions, the actual cell performance is lower than the predicted value as shown in Section 5.3.

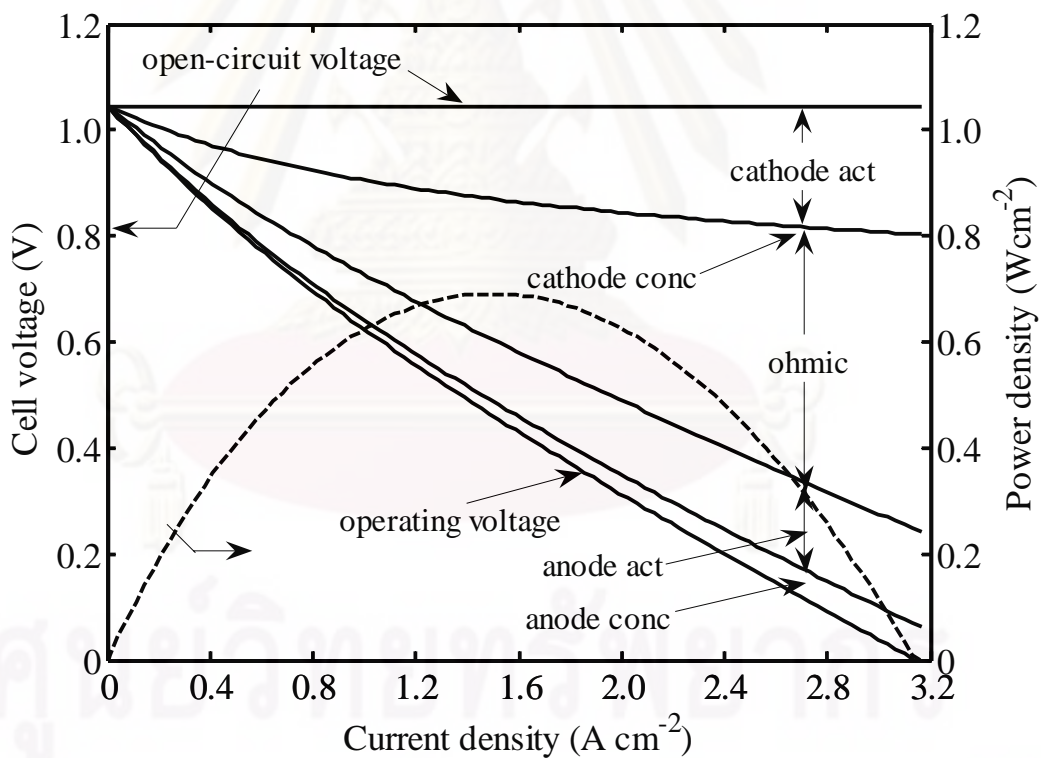


Figure 5.1 Performance of an anode-supported planar SOFC at different current densities (cathode act = cathode activation overpotential, cathode conc = cathode concentration overpotential, ohmic = ohmic overpotential, anode act = anode activation overpotential, anode conc = anode concentration overpotential).

As seen in Figure 5.1, the ohmic and cathode activation overpotentials represent a major loss in the cell, followed by anode activation overpotential. The activation overpotential at the cathode side is generally higher than that at the anode side due to the lower exchange current density. From this result, although the anode-supported SOFC is considered, the anode concentration overpotential is relatively small, compared with the other overpotentials.

A comparison of SOFC performance with different support structures (i.e., anode-, cathode- and electrolytes-supported) is given in Figure 5.2a. It is clearly shown that the performance of the electrode-supported SOFC is superior to that of the electrolyte-supported SOFC. The electrode-supported SOFC can operate at a higher power density and a wider range of current density, thus implying that a smaller cell area would be required to operate the SOFC system. In order to explain the influence of the support structure design on the cell performance, the relative magnitude of all the various losses in each type of SOFC is given in Figure 5.2b. The data show that the ohmic loss dominates the performance of the electrolyte-supported SOFC whereas activation and ohmic losses are the major loss in the electrode-supported counterpart. By comparing the various cell voltage losses, it is observed that the concentration overpotential is relatively small, even though the SOFC is supported by the electrode. Nevertheless, the concentration overpotential becomes more significant for the cathode-supported cell as a rapid drop of the cell voltage is observed at a current density of 2.8 A cm^{-2} . Under this operating condition, a large amount of oxidant is consumed at the cathode|electrolyte interface and therefore, the concentration overpotential is increasingly developed. From simulation results, it can be concluded that the anode-supported SOFC exhibits the better performance in comparison with the others; it can be operated at high current density and a greater power density is achieved. Further, Figure 5.2a shows that there is a possibility to improve the performance of the anode-supported SOFC as the limiting current density at the anode is still not reached. Therefore, in the next section, the effect of design parameter on the performance of an anode-supported SOFC performance is further investigated.

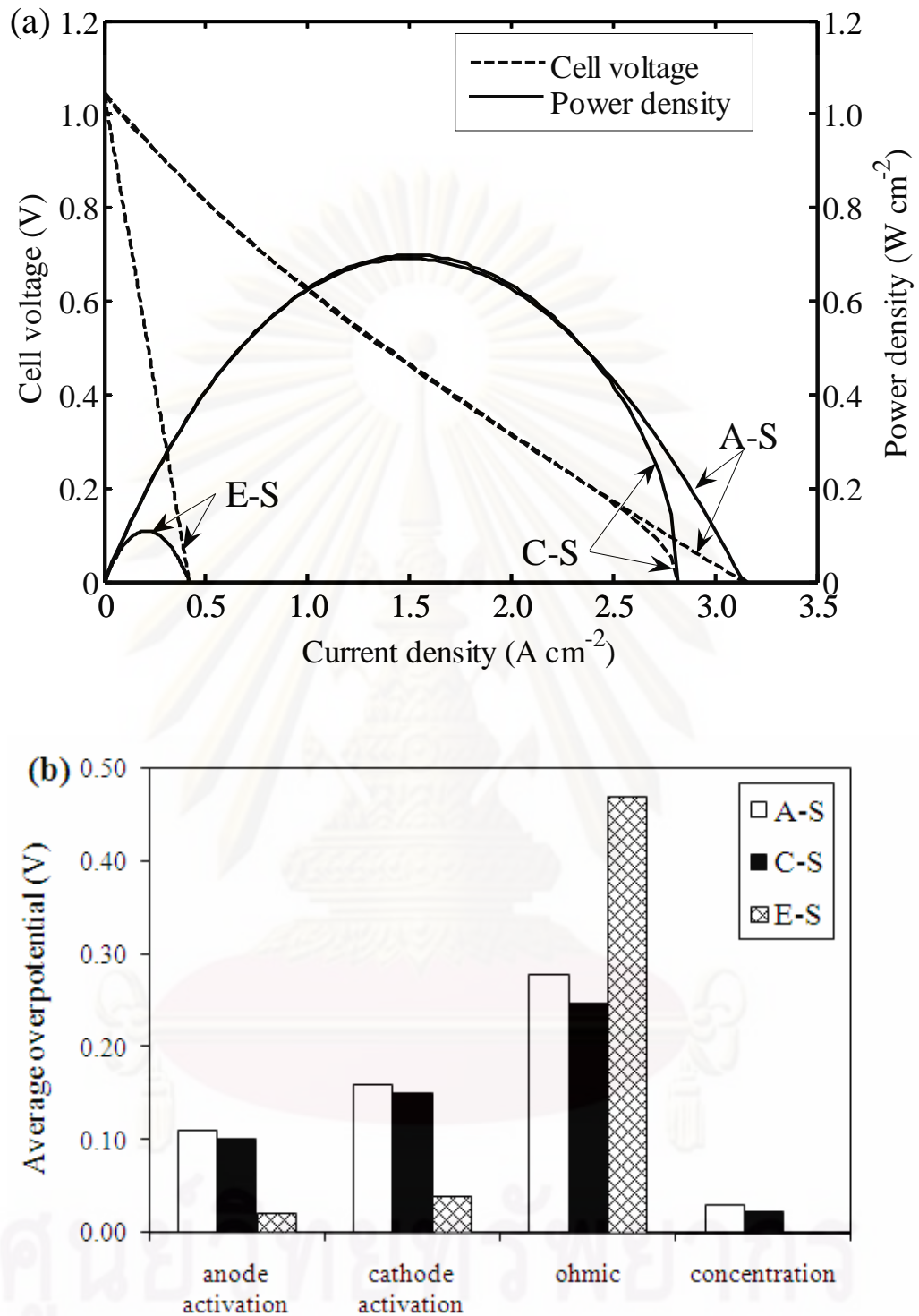


Figure 5.2 Comparison of SOFC with different support structures: (a) cell performance and (b) average overpotentials (A-S = Anode-supported, C-S = Cathode-supported, E-S = Electrolyte-supported).

5.2.1.2 Effect of electrolyte thickness

In this section, the impact of the electrolyte thickness on the performance of an anode-supported SOFC is analyzed. The electrolyte thickness varies from 10 to 40 μm while the anode and cathode thickness is fixed at 500 and 40 μm , as in the standard specification, respectively. The cell voltage and power density as a function of current density at different electrolyte thicknesses are given in Figure 5.3a. For each value of electrolyte thickness, there is an optimum current density and hence a maximum the power density; the current density corresponding to the maximum power density is moved to higher values with decrease in the electrolyte thickness. Thus, as expected, the cell performance increases when the electrolyte thickness decreases. This is because the decrease of the electrolyte thickness causes a significant decrease in the ohmic loss as shown in Figure 5.3b. By contrast, the anode concentration overpotential becomes a more significant loss when a thinner electrolyte is used. As can be seen in Figure 5.3a, the voltage of the anode-supported SOFC with an electrolyte thickness of 10 μm rapidly decreases at a current density of 4.75 A cm^{-2} due to a high anode concentration overpotential; a concave curvature is observed.

5.2.1.3 Effect of anode thickness

Figure 5.4a presents the characterization curve of an anode-supported SOFC at different anode thicknesses (500, 750, 1000 and 1250 μm). It is noted that the electrolyte and cathode thicknesses are fixed at 20 and 40 μm , respectively. The results show that the cell performance is significantly hindered when the anode thickness increases (Figure 5.4a). The latter causes a higher resistance to the gaseous species being transported in the porous anode and this results in an exponential increase in the concentration overpotential (Figure 5.4b). It can be further noticed that the concentration overpotential in an anode-supported SOFC with a larger anode thickness has a significant effect on cell performance; the maximum operating current density appears to approach the limiting current density of the anode.

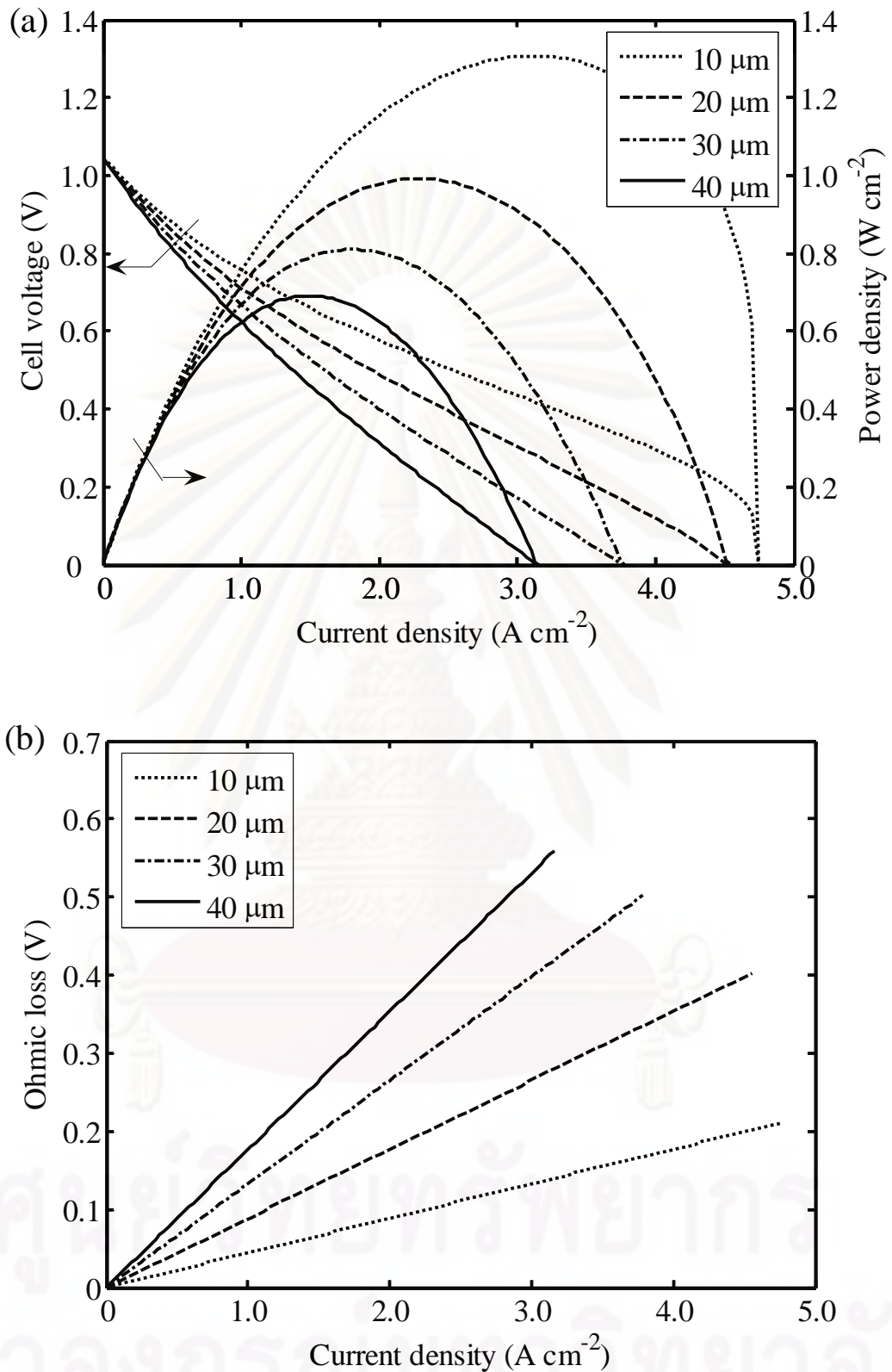


Figure 5.3 Effect of electrolyte thickness at different current densities on: (a) cell voltage and power density and (b) ohmic loss.

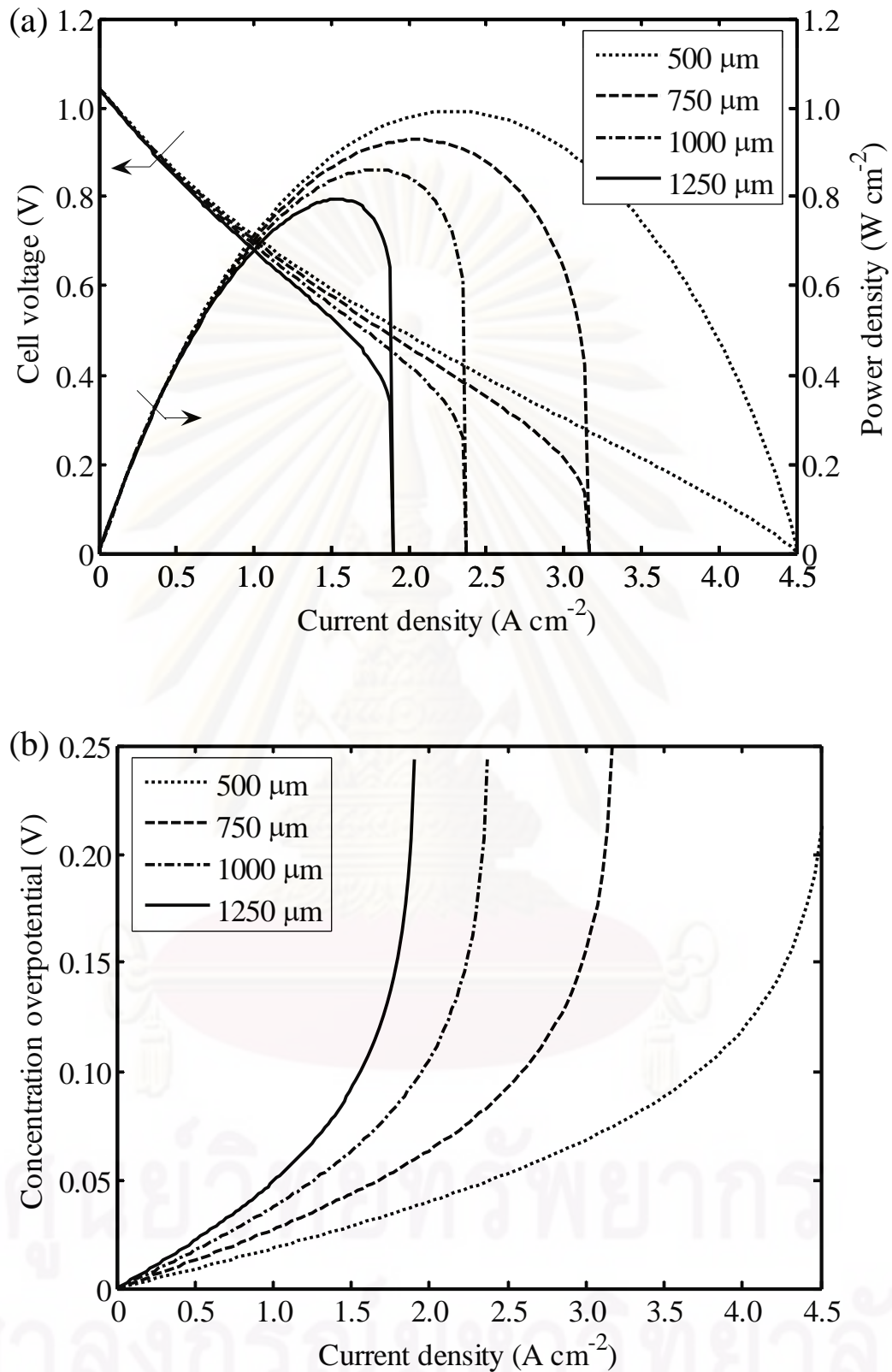


Figure 5.4 Effect of anode thickness at different current densities on: (a) cell voltage and power density and (b) concentration overpotential.

5.2.1.4 Effect of cathode thickness

The effect of cathode thickness (25, 50, 100 and 150 μm) on the performance of an anode-supported planar SOFC at different current densities has been investigated. The simulation results demonstrate that the thickness of the cathode has a less influence on the characteristics curve of the fuel cell; although, the concentration overpotential decreases slightly with reduction in cathode thickness (no figure). Considering the durability of an anode-supported SOFC, it should be fabricated with the cathode thickness of 50 μm (Aguiar et al., 2004; Hussain et al., 2006). It is noted that the anode, electrolyte and cathode thickness of 500, 20 and 50 μm are set as the standard cell geometry for a performance analysis of the anode-supported planar SOFC in subsequent sections.

5.2.1.5 Effect of electrode porosity

The effect of electrode porosity on the cell performance of an anode-supported planar SOFC at different current densities is presented in Figure 5.5a. The result shows that the characteristics performance of SOFC is improved with an increase in electrode porosity. Increasing electrode porosity leads to the enhanced gas diffusion in the porous electrodes and in turn, fuel and oxidant gases can easily diffuse to the electrode/electrolyte interface. This results in a significant decrease in the concentration overpotential (Figure 5.5b). As seen in Figure 5.5a, the cell performance of an anode-supported SOFC is rapidly dropped when the electrode porosity of 0.1 μm is used. This is because the high concentration overpotential in both the anode and cathode sides becomes more pronounced.

5.2.1.6 Effect of electrode pore size

Figure 5.6a presents the characterization curve of an anode-supported SOFC at different electrode pore size (0.1, 0.5 and 3 μm). Similar to the effect of electrode porosity, it is shown that the cell performance increases with increasing in electrode pore size. The gas transport process in the porous electrode is more facilitated when the electrode pore size increase. This brings to decreasing concentration overpotential as demonstrated in Figure 5.6b.

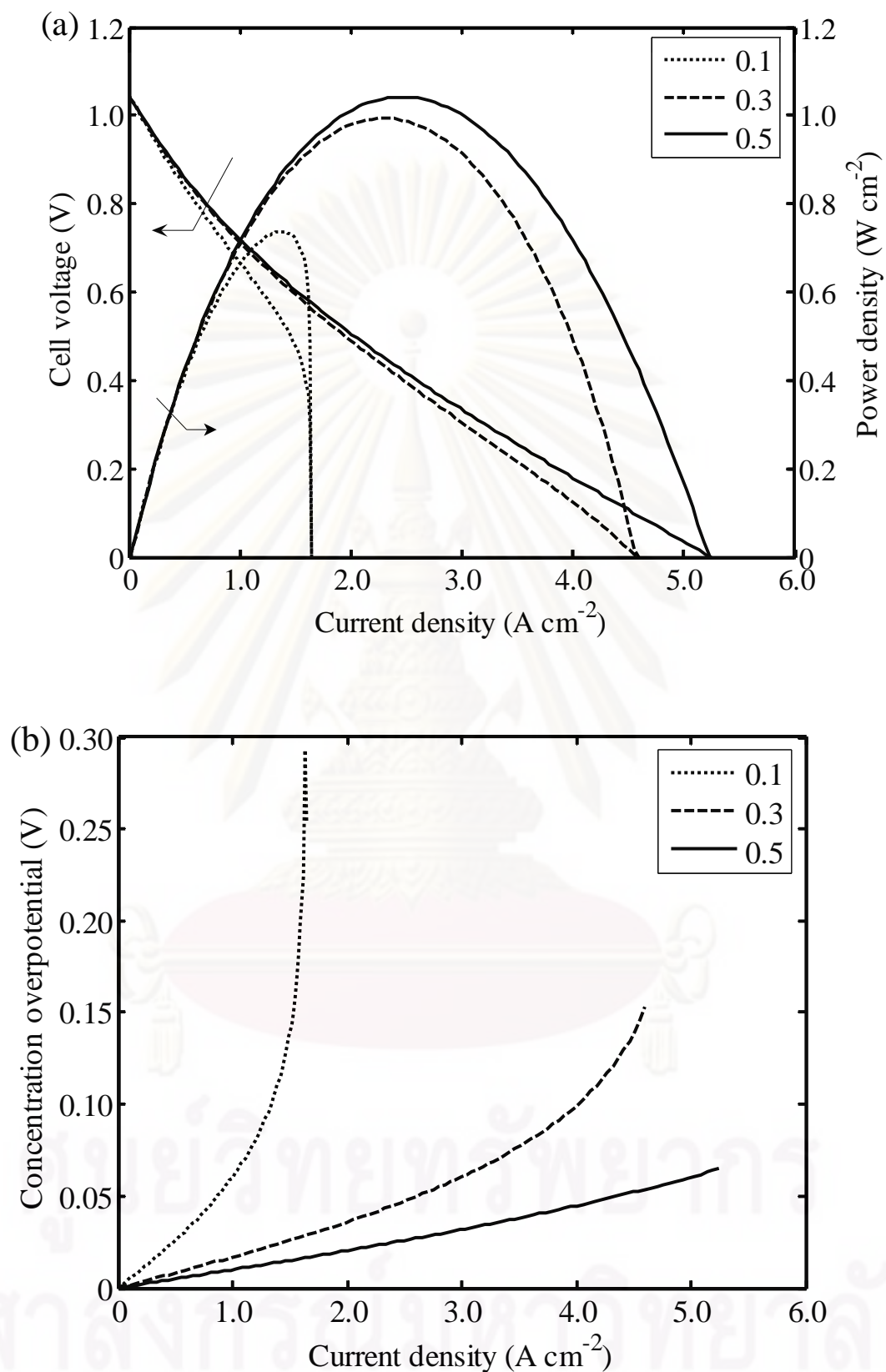


Figure 5.5 Effect of electrode porosity at different current densities on: (a) power density, and (b) concentration overpotential.

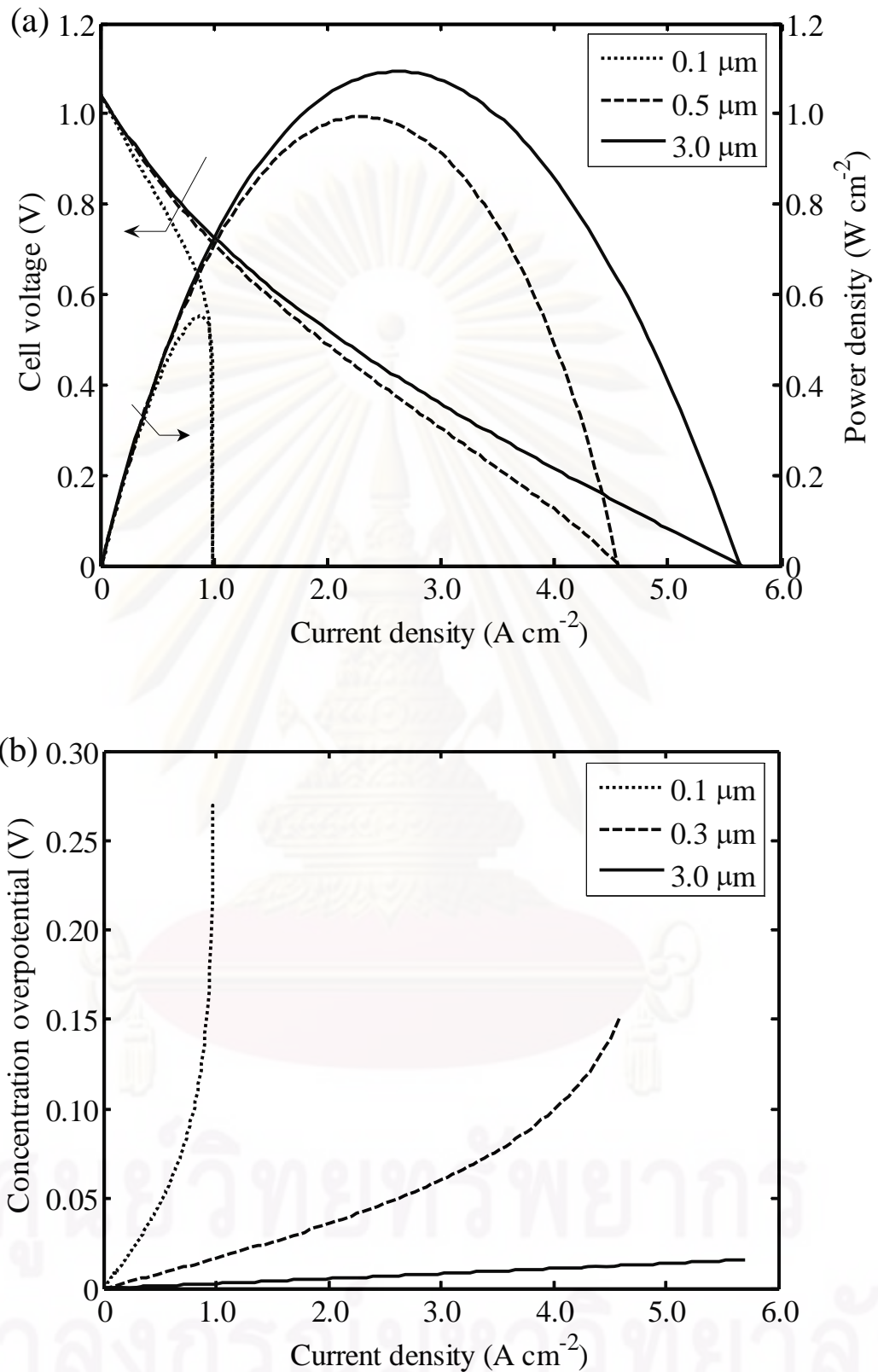


Figure 5.6 Effect of electrode pore size at different current densities on: (a) power density, and (b) concentration overpotential.

5.2.2 Conclusions

A numerical study of the performance of a SOFC with different support structures and design parameter was presented in this section. Under intermediate-temperature operation ($T = 1073$ K), it was found that an electrode-supported SOFC exhibits better electrical performance than an electrolyte-supported SOFC. Considering individual cell voltage loss, the results indicated that ohmic loss dominates the performance of the electrolyte-supported SOFC, whereas activation and ohmic losses constitute the major loss in an electrode-supported SOFC. Compared with the cathode-supported SOFC, the anode-supported SOFC delivers better performance in terms of a wider range of operating current density; the concentration overpotential becomes more significant for a cathode-supported cell as a rapid drop of the cell voltage is observed at high current density. Sensitivity analyses of the anode-supported SOFC were performed. The results demonstrated that decreasing the electrolyte and anode thickness can improve cell performance, whereas the cathode thickness has less effect on the cell characteristics curve. In addition, increase in electrode porosity and pore size enhances the cell performance of the anode-supported SOFC. It should be noted that although the anode-supported SOFC, which has thinner electrolyte and is suitable for low temperature operation, is used with the aim to decrease an ohmic loss, the loss is still relatively major in the fuel cell. In order to improve SOFC performance, an electrolyte with high ionic conductivity is required.

5.3 Anode-supported SOFC performance

As shown in Section 5.2, an anode-supported SOFC provides the best performance. In this section, the performance of an anode-supported SOFC fed by methane under a direct internal reforming operation and isothermal condition is investigated using a one-dimensional steady-state fuel cell model and a detailed electrochemical model taking into account all various voltage losses (i.e., activation, ohmic and concentration losses). The model is employed to determine the distribution of gas component, current density and various voltage losses along the length of fuel cell. Further, the impact of key operating parameters such as temperature, pressure, degree of pre-reforming, steam to carbon ratio and inlet fuel velocity is analyzed.

A mathematical model of a planar anode-supported SOFC with DIR operation was developed based on the following assumptions: (1) steady-state operation, (2) one-dimensional variation in gas flow direction, (3) uniform temperature and total pressure over the model geometry, (4) constant cell voltage along the cell coordinate and (5) constant fluid properties. By performing mass balances, the following equations are obtained

- Fuel channel ($i = \text{CH}_4, \text{H}_2\text{O}, \text{CO}, \text{H}_2,$ and CO_2):

$$\frac{dC_{i,f}}{dx} = \frac{1}{u_f} \sum_k v_{i,k} R_k \frac{1}{h_f} \quad (5.9)$$

$k \in$ steam reforming, water gas-shift and electrochemical reactions

- Air channel ($i = \text{O}_2$ and N_2):

$$\frac{dC_{i,a}}{dx} = \frac{1}{u_a} \sum_k v_{i,k} R_k \frac{1}{h_a} \quad (5.10)$$

$k \in$ electrochemical reaction

In order to evaluate the steady-state fuel cell performance, the model equations of SOFC consisting of mass balances (Equations (5.9)-(5.10)) and electrochemical relations (Equations (5.1)-(5.8)) are solved. The obtained potential and current density distribution are used to calculate the fuel utilization (U_{fuel}), power density (P_{SOFC}) and fuel efficiency ($\varepsilon_{\text{SOFC}}$) of fuel cells, which are expressed as follows:

$$U_{\text{fuel}} = \frac{i_{\text{ave}} LW}{2F(4y_{\text{CH}_4}^{\text{in}} + y_{\text{H}_2}^{\text{in}} + y_{\text{CO}}^{\text{in}})F_{\text{fuel}}} \quad (5.11)$$

$$P_{\text{SOFC}} = i_{\text{ave}} V \quad (5.12)$$

$$\varepsilon_{\text{SOFC}} = \frac{i_{\text{ave}} VLW}{(y_{\text{CH}_4}^{\text{in}} LHV_{\text{CH}_4} + y_{\text{H}_2}^{\text{in}} LHV_{\text{H}_2} + y_{\text{CO}}^{\text{in}} LHV_{\text{CO}})F_{\text{fuel}}} \times 100\% \quad (5.13)$$

5.3.1 Results and discussion

The values of model input: geometry and property data (properties of the materials and cell dimensions) and operating condition used in this study are listed in Table 5.4. The inlet fuel is considered as a gas mixture of CH₄, H₂O, CO, H₂, and CO₂. Its composition results from a mixture with a steam to carbon ratio equal to 2 after 10% pre-reforming, where the shift reaction is at equilibrium.

Table 5.4 Model input parameters and operating conditions

Parameters	Value
<i>Operating conditions</i>	
Operating temperature, T	1023 K
Operating pressure at anode, P_{an}	1.0 atm
Operating pressure at cathode, P_{ca}	1.0 atm
Inlet fuel velocity, u_f	1 m s ⁻¹
Inlet air velocity, u_a	18 m s ⁻¹
Air composition	21% O ₂ , 79% N ₂
Fuel composition ^a	28.1% CH ₄ , 56.7% H ₂ O, 0.5% CO, 12% H ₂ , and 2.7% CO ₂
<i>Dimensions of cell element</i>	
Cell length, L	0.4 m
Cell width, W	0.1 m
Fuel channel height, h_f	1 mm
Air channel height, h_a	1 mm
Anode thickness, τ_{an}	500 μ m
Cathode thickness, τ_{ca}	50 μ m
Electrolyte thickness, τ_{ele}	20 μ m

Before a simulation of a planar anode-supported SOFC with DIR is performed, its current-voltage characteristic is investigated to find a suitable condition in the operation. The performance characteristics of the SOFC under isothermal operation ($T = 1023$ K) are presented in Figure 5.7. Under a standard condition in Table 5.4, the cell voltage in the range of 0.65 to 1.0 V is specified and thus, the power density and fuel efficiency can be determined. As shown in this figure, it is found that an anode-supported SOFC can produce the maximum power density of 0.42 W cm^{-2} when the operating cell voltage is 0.65 V. Due to the obtainable of high fuel utilization (90%) at this condition, the cell voltage at 0.7 V is considered as it shows a good compromise on power density and fuel utilization.

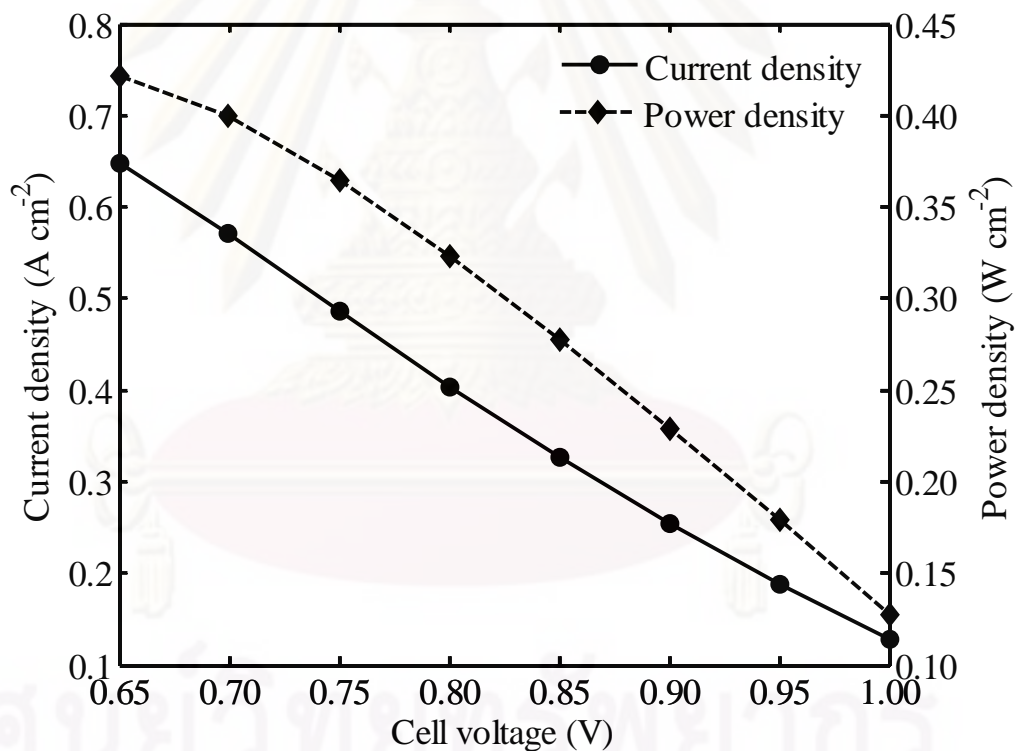
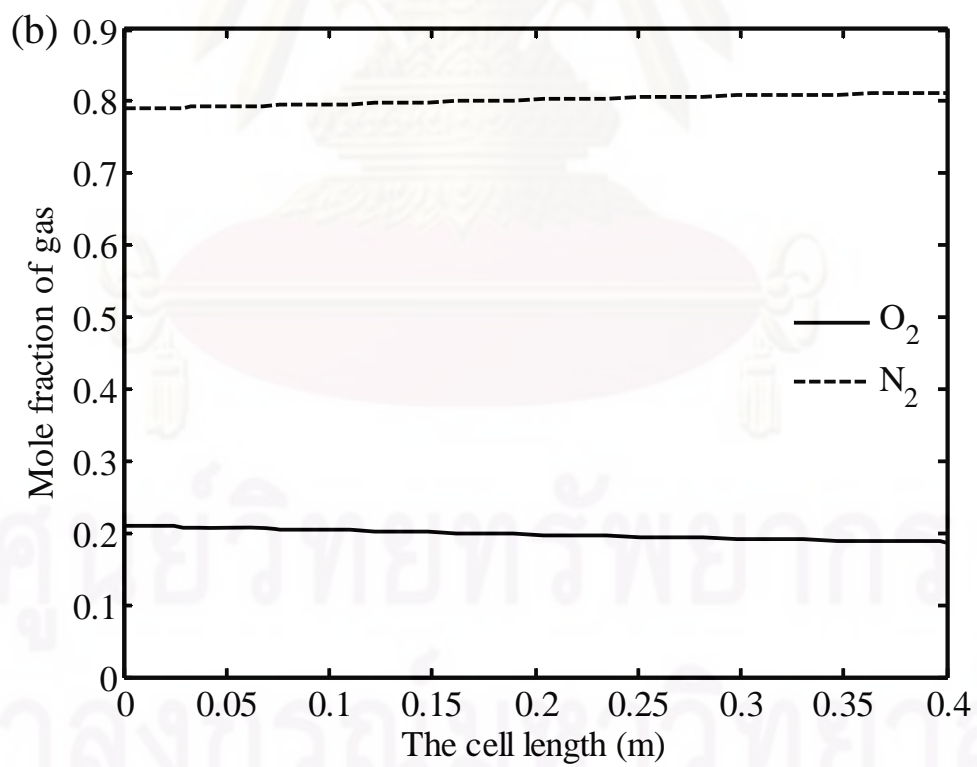
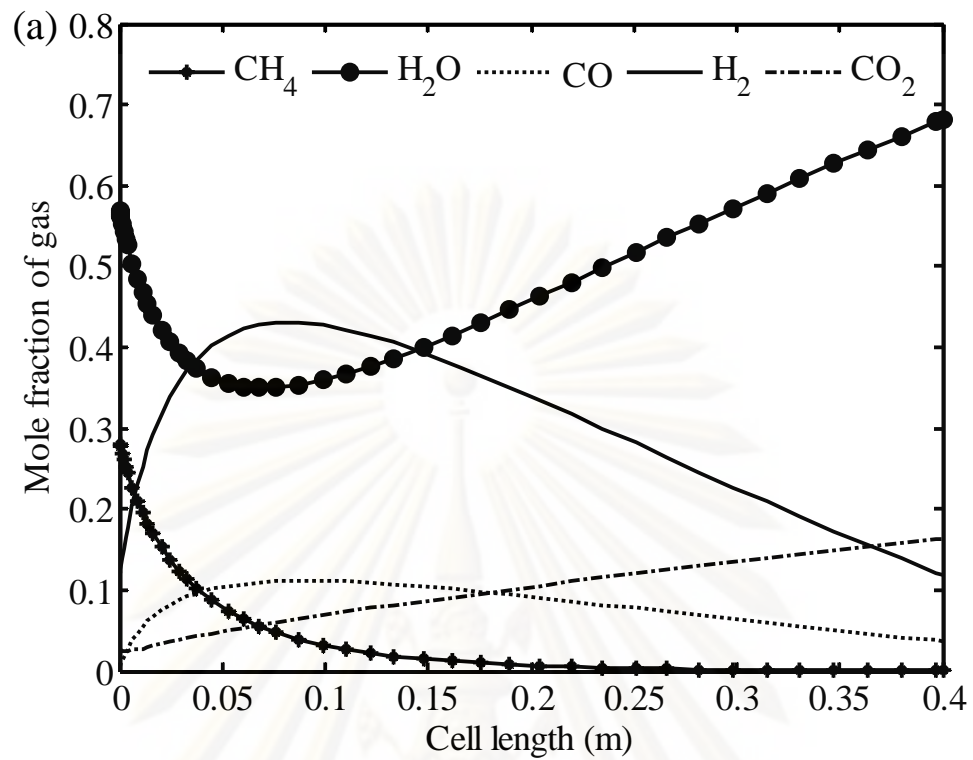


Figure 5.7 Performance characteristics of an anode-supported SOFC at different cell voltages.

When the cell voltage of 0.7 V is applied in the SOFC model, the distribution of gas composition in the fuel and air channels and all the electrochemical-related variables (open-circuit voltage, activation, ohmic, and concentration overpotential, and current density) as well as the fuel cell efficiency and power density are determined. Figures 5.8a and 5.8b present the mole fraction profiles of all components in fuel and air channels along the cell length. At the entrance of fuel channel, it can be seen that CH_4 and H_2O are rapidly consumed while H_2 and CO are more produced. This can be explained by high inlet CH_4 content and fast reaction rate of steam reforming. When most of CH_4 is completely consumed, the electrochemical reaction becomes faster reaction where the consumption of H_2 and the generation of H_2O are observed. At the exit of the fuel cell channel, the fuel stream molar compositions of 68.1% H_2O , 3.7% CO , 11.9% H_2 and 16.3% CO_2 are obtained whereas the oxidant stream consists of 18.7% O_2 and 81.3% N_2 .

For the isothermal condition, the key parameter affecting the electrochemical reaction rate is only the local H_2 concentration. Figure 5.8c shows the current density profiles along the cell length. It is found that the current density sharply increases at the inlet and continuously decreases toward the fuel cell outlet. The average current density is 0.57 A cm^{-2} . Figure 5.8d presents the voltage profile along the cell length as well as the individual contribution of all the various overpotentials. Since the open-circuit voltage is described by the Nernst equation which is a function of local H_2 concentration, the change of the open-circuit voltage is similar to that of H_2 concentration. From the figure, it is observed that the cathode activation overpotentials represent a major loss in the fuel cell, followed by the anode activation overpotentials. The ohmic overpotential becomes a minor loss in this system because much thinner electrolyte can be employed. The cathode activation overpotential is generally higher than that of the anode due to its lower exchange current density. In the contrast, the anode concentration overpotential is always much higher than that of the cathode due to the anode thickness used. It is noted that under the reference case, a power density of 0.40 Wcm^{-2} and fuel cell efficiency of 52% are predicted.



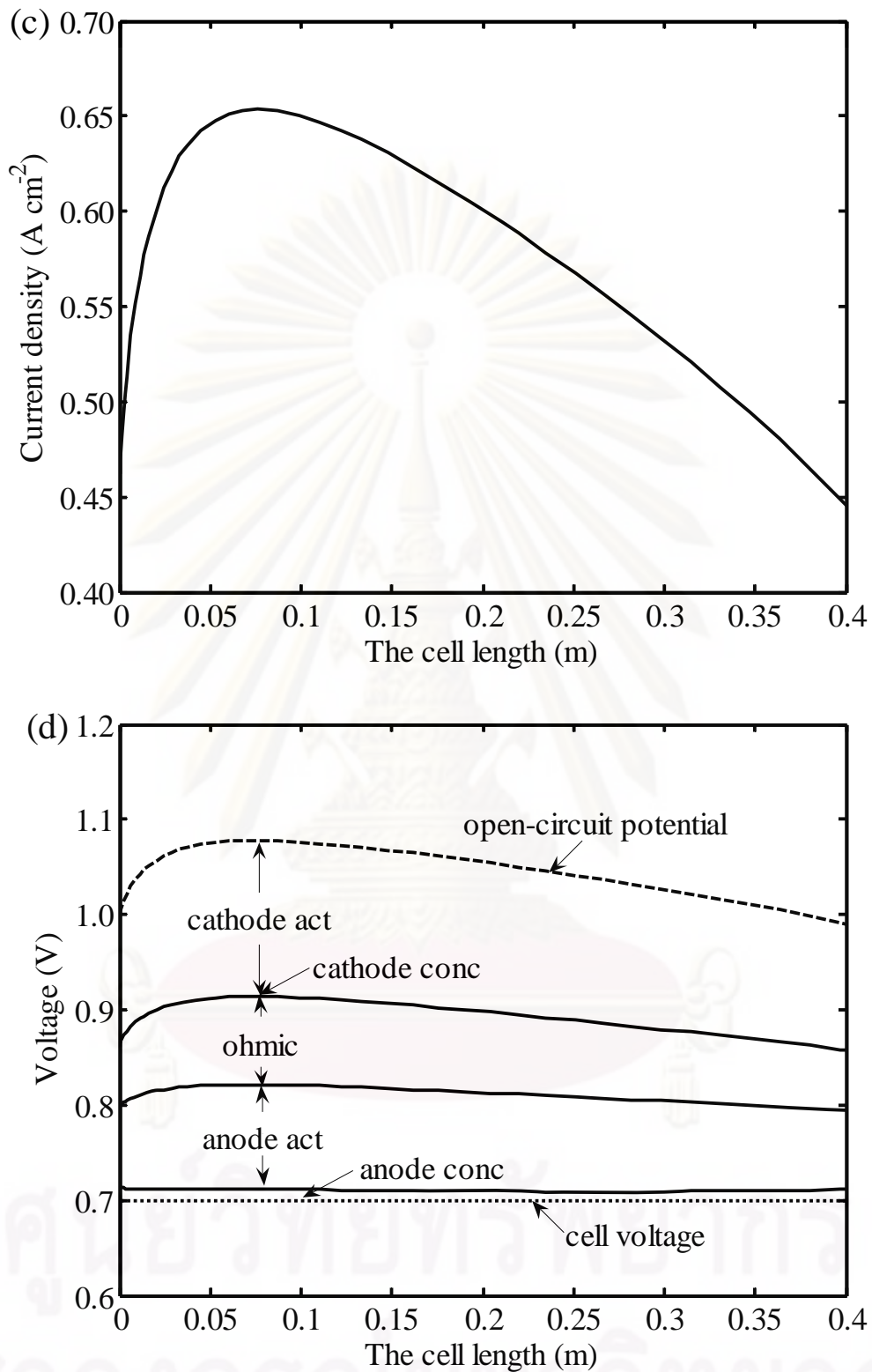


Figure 5.8 (a) Mole fraction profiles of gas compositions at fuel channel, (b) Mole fraction profiles of gas compositions at air channel, (c) distribution of current density, and (d) distribution of individual voltage losses.

5.3.1.1 Effect of operating temperature

Figure 5.9a shows the fuel cell efficiency and the power density of an anode-supported SOFC at intermediate temperatures varying from 873 K to 1023 K. An increase in operating temperatures can improve the cell performance. This is due to the fact that increasing cell temperatures pronounces more electrochemical reaction and the consumption of fuel, the current density is more generated and thus, the power density and fuel cell efficiency are enhanced. The operating temperature is also strongly affected the individual contribution of all voltage losses, as demonstrated in Figure 5.9b. The activation overpotential decreases significantly whereas the anode concentration overpotential slightly increases with temperatures. It is noted that although the area specific resistance (R_{ohm}) decreases at high-temperature operation, the ohmic loss is increased. This is because the ohmic loss is a linear function of current density; therefore, its value highly increases when current density is more generated at a higher operating temperature.

5.3.1.2 Effect of operating pressure

Figure 5.10a shows the fuel cell efficiency and the power density as a function of operating pressures. The simulation result demonstrates that that an increase in pressure from 0.5 to 2 atm can improve both the fuel cell efficiency and the power density. This is because at high operating pressure, the partial pressure of H_2 in the fuel channel and O_2 in the air channel increases; higher open-circuit voltage and current density can be achieved. In addition, under high pressure operation, H_2 and O_2 can easily diffuse into the reaction site at the electrode|electrolyte interface, in turn the decreased concentration overpotential (Figure 5.10b). It should be noted that although a higher fuel cell efficiency is obtained when operating at elevated pressure, an operating cost for the operation at high pressure will be increased. In addition, increasing the operating pressure may affect the lifetime of the fuel cell.

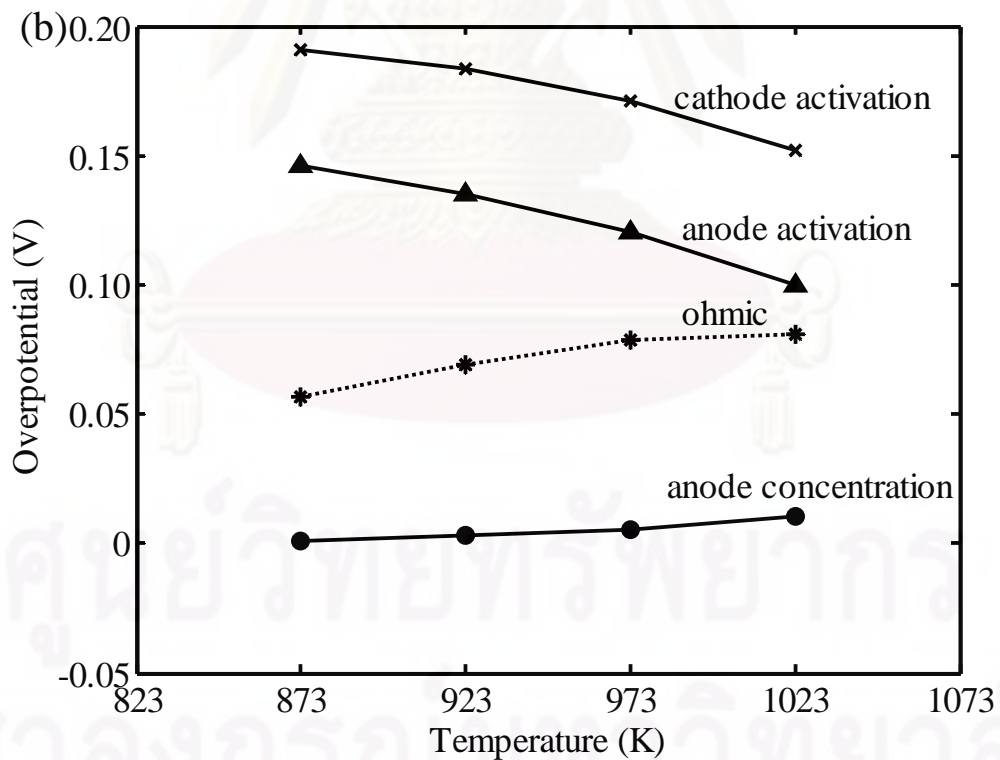
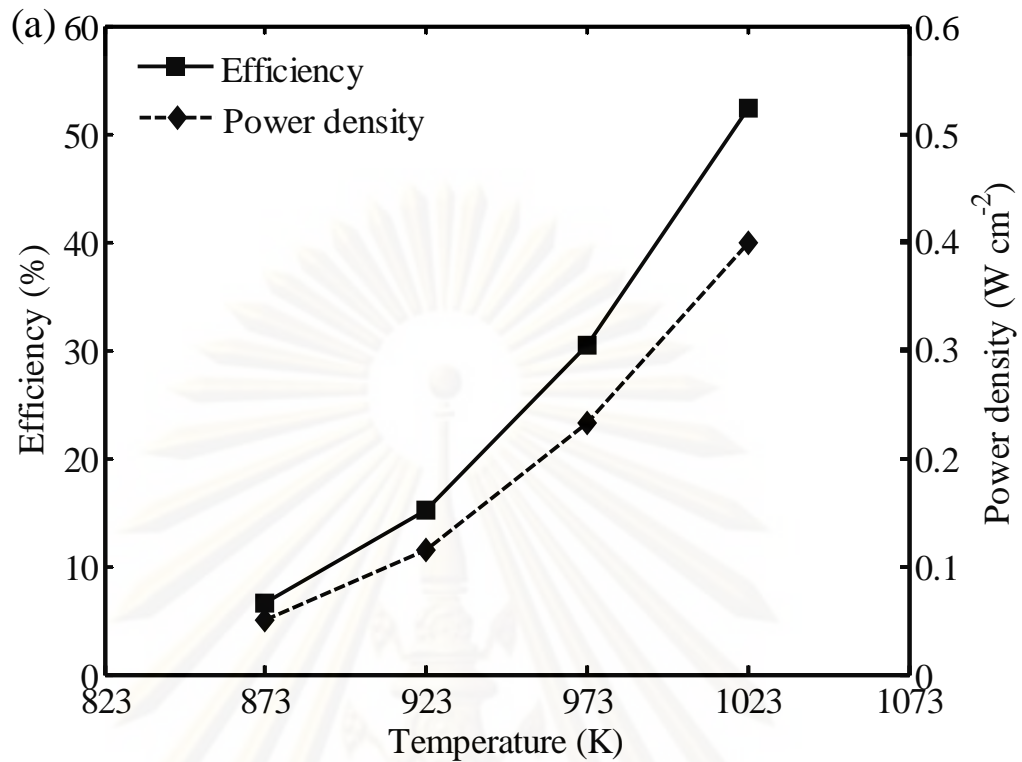


Figure 5.9 Effect of operating temperature on: (a) fuel cell efficiency and power density and (b) cathode and anode activation, ohmic and anode concentration overpotentials.

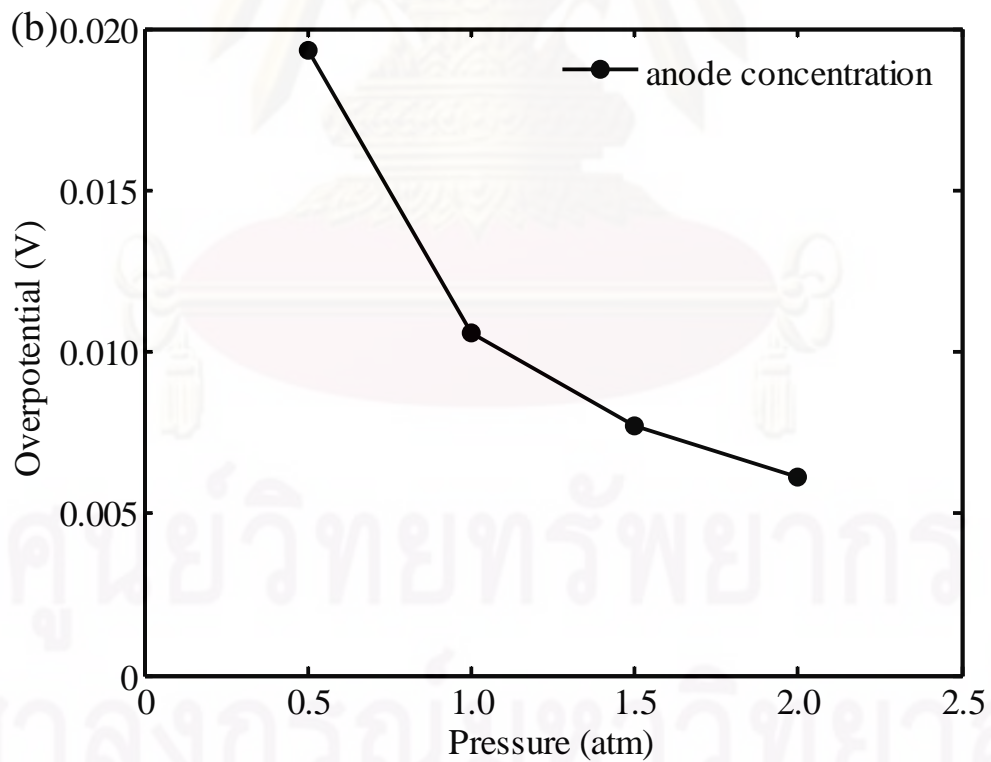
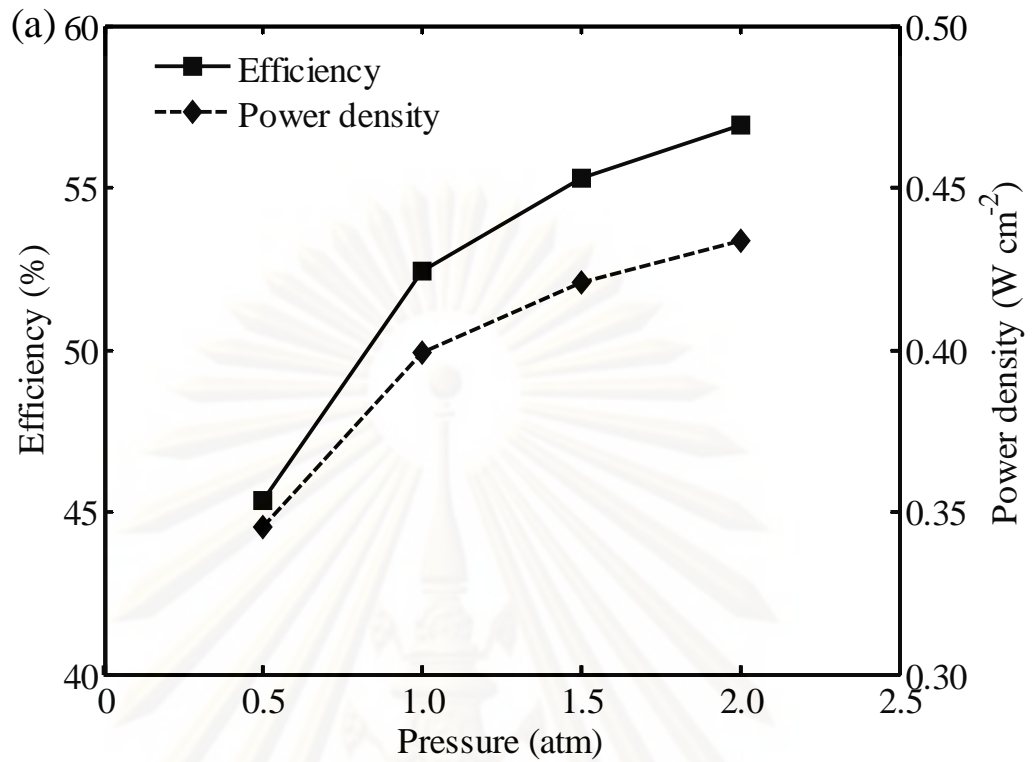


Figure 5.10 Effect of operating pressure on: (a) fuel cell efficiency and power density and (b) anode concentration overpotentials.

5.3.1.3 Effect of degree of pre-reforming of methane

As mentioned earlier, an external pre-reformer should be applied in the SOFC system to avoid some problems related to a complete internal reforming, and thus the effect of the degree of pre-reforming of methane on SOFC performance is studied in this section. It is noted that a higher degree of pre-reforming results in an increase in the H_2 concentration in the fuel stream. In general, high hydrogen fuel increases the open-circuit voltage and current density and thus, higher power density is expected. However, the simulation results as shown in Figure 5.11a presents the opposite trend. This is because as the fuel is more consumed (fuel utilization $> 90\%$), the concentration overpotentials (Figure 5.11b) become more significant and the current density that can be locally drawn drops considerably to maintain a constant voltage. As a consequence, the power density decreases with increasing methane pre-reforming level. However, the fuel cell efficiency is enhanced because of a decrease in inlet fuel molar flow rate according to more fuel utilization, which provides lower total chemical energy in the inlet fuel.

5.3.1.4 Effect of steam to carbon ratio

Figure 5.12 shows the current density, fuel cell efficiency and power density of an anode-supported SOFC against the steam to carbon ratio. Within the range of the steam to carbon ratio, the current density decreases with increasing steam to carbon ratio (Figure 5.12a). This is because increasing steam to carbon ratio leads to less fraction of H_2 in fuel stream, resulting in the decreased rate of the electrochemical. The power density is also reduced with the reduction of the current density (Figure 5.12b). However, the inlet total flow rate of fuel (methane + carbon monoxide + hydrogen) used to produce current in the fuel cell decreases when the steam to carbon ratio increases. Since a decrease in the inlet fuel flow rate has more effect than a decrease in the current density, the fuel cell efficiency is enhanced as shown in Figure 5.12b.

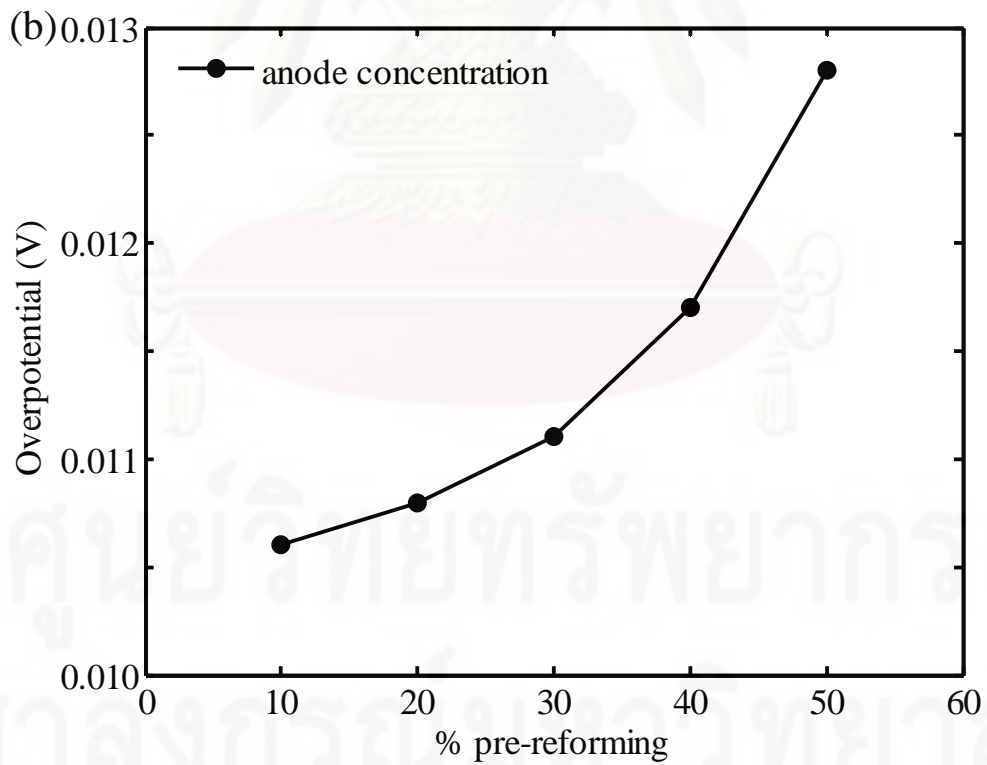
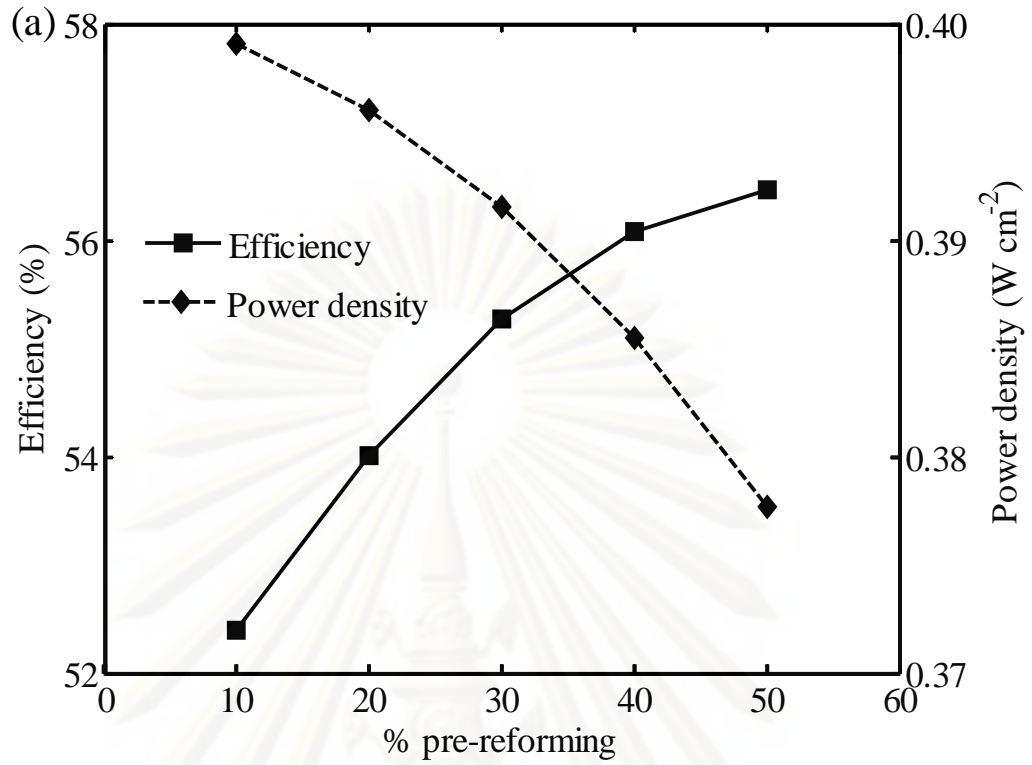


Figure 5.11 Effect of degree of pre-reforming on: (a) fuel cell efficiency and power density and (b) anode concentration overpotentials.

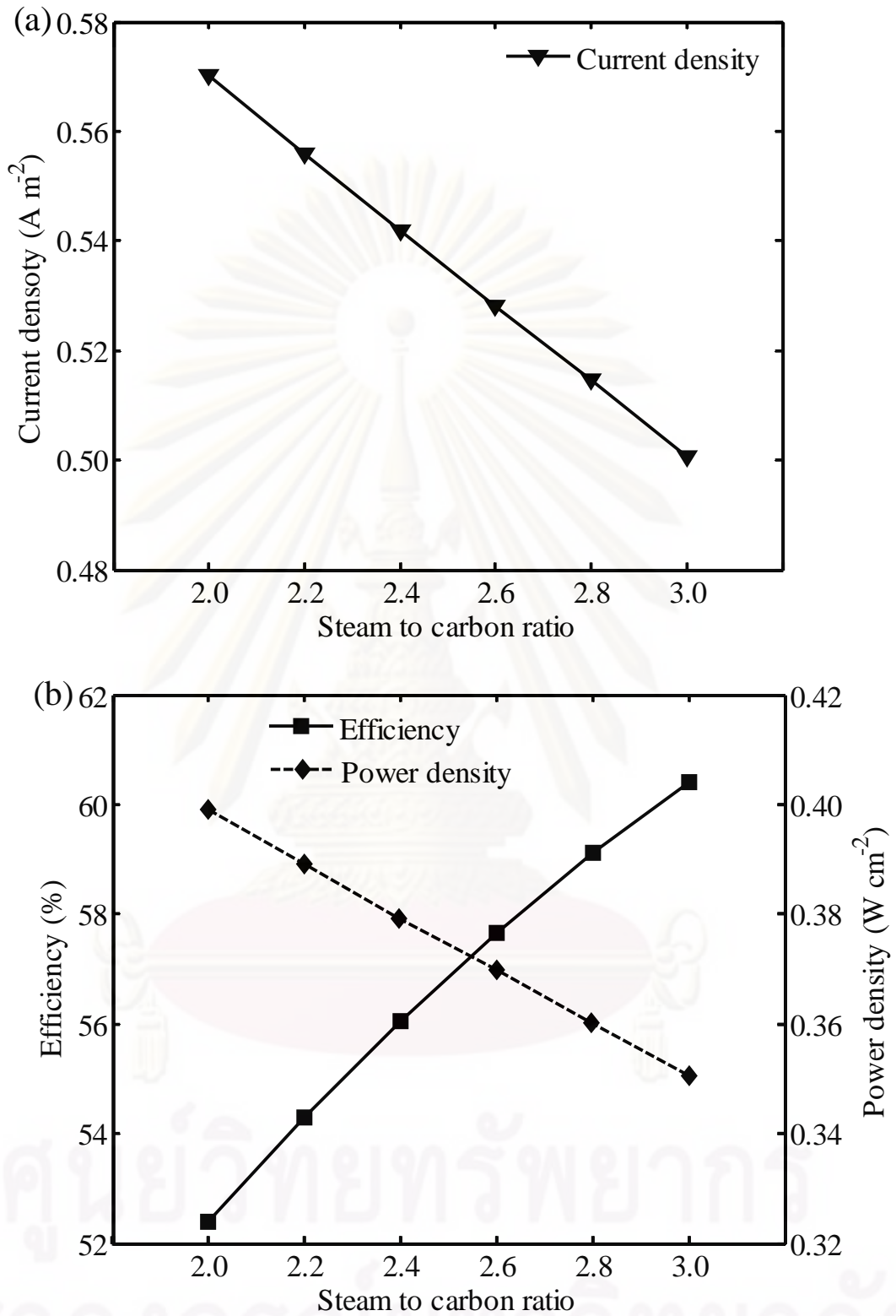


Figure 5.12 Effect of steam to carbon ratio on: (a) current density and (b) fuel cell efficiency and power density.

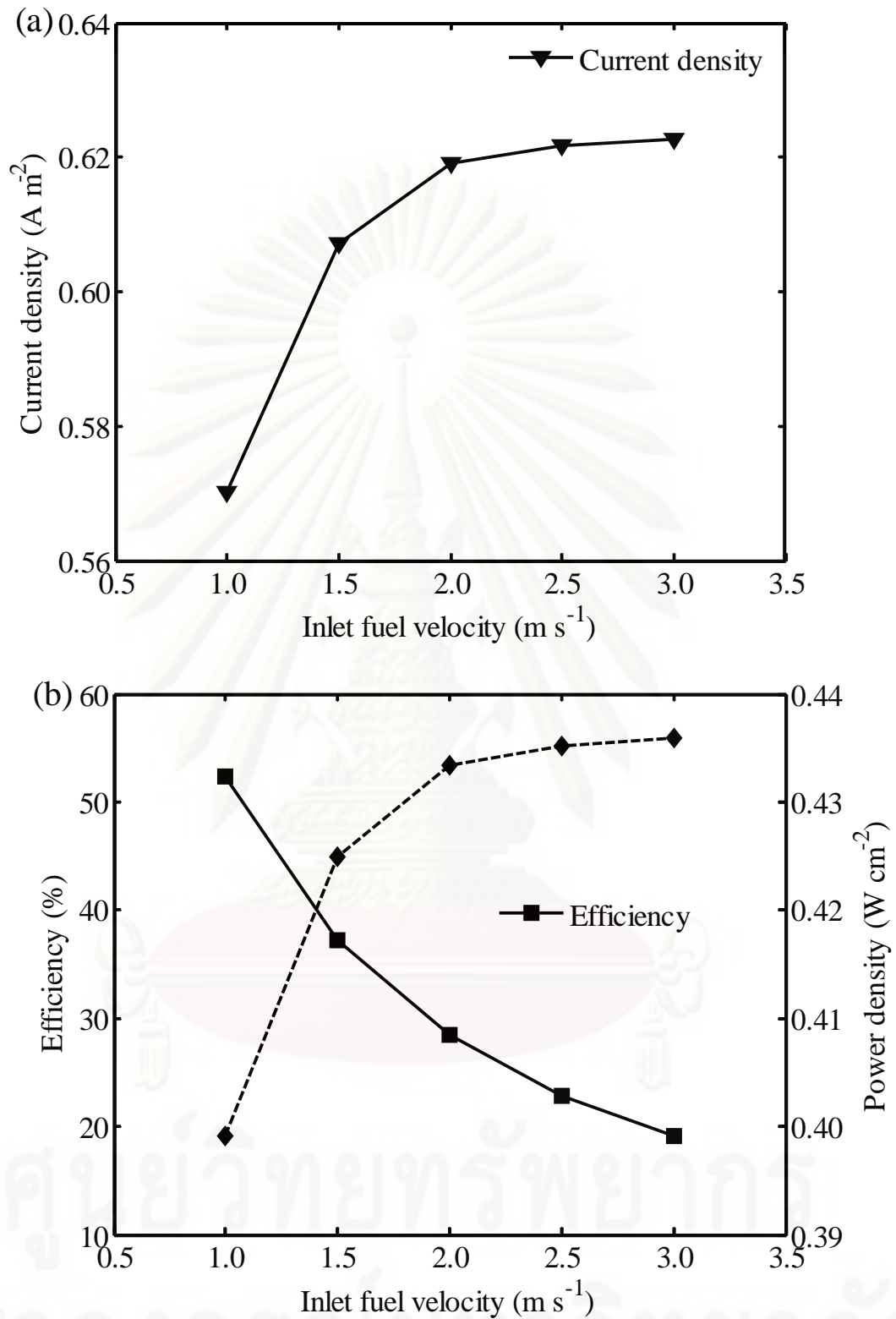


Figure 5.13 Effect of inlet fuel velocity on: (a) current density and (b) fuel cell efficiency and power density.

5.3.1.5 Effect of inlet fuel velocity

The effect of inlet fuel velocity (1 to 3 m/s) on the current density, the fuel cell efficiency and the power density is investigated. It is found that even though an increase in the fuel velocity results in more electric current generated (Figure 5.13a), it causes a decrease in the fuel cell efficiency (Figure 5.13b). This implies that the conversion of chemical energy in fuel to electrical energy reduces as a result of the fuels having less residence time within the fuel cell for a complete electrochemical reaction. Although, the improvement of fuel cell efficiency can be done by decreasing inlet fuel velocity; the amount of the electric current produced is also decreased. Therefore, the inlet fuel flow rate should be carefully determined.

5.3.2 Conclusions

In this study, a numerical study of an anode-supported planar SOFC operated under an intermediate temperature and direct internal reforming of methane was presented. A one-dimensional steady-state fuel cell model and a detailed electrochemical model taking into account all various voltage losses (i.e., activation, ohmic and concentration losses) was employed to determine the steady-state performance of the anode-supported SOFC with respect to changes in temperature, pressure, degree of pre-reforming of methane, steam to carbon ratio, and inlet fuel velocity. It was found that the operating temperature, the steam to ethanol ratio, and the inlet fuel velocity have significant effects on the electrical efficiency of fuel cell and the generation of current density.

ศูนย์วิจัยทรัพยากร

จุฬาลงกรณ์มหาวิทยาลัย

CHAPTER VI

SOLID OXIDE FUEL CELL BASED ON A PROTON-CONDUCTING ELECTROLYTE

This chapter aims to present the electrochemical performance of solid oxide fuel cell with a proton-conducting electrolyte (SOFC-H⁺) in terms of cell voltage and power density by considering the role of support structure (anode-, cathode- and electrolyte-supported SOFC) and the effect of design parameters (i.e., cell component thickness, porosity and pore size). The optimal SOFC-H⁺ design is further used to investigate the steady-state performance of SOFC-H⁺. The effect of key cell operating parameters, i.e., steam to carbon ratio, temperature, pressure, and water content in oxidant, on the performance of SOFC-H⁺ is also presented in this chapter.

6.1 Introduction

In general, there are two types of electrolyte (i.e., oxygen-ion and proton-conducting electrolytes) possible for SOFC. Currently, many studies have been focused on SOFC technology using oxygen-ion conducting electrolytes (SOFC-O²⁻) because the chemical stability and low electrical resistance of oxygen ion conductors, i.e., stabilized zirconia and doped ceria. However, a great effort is still required to handle some problems, which include materials incompatibility (Ranran et al., 2006) and incomplete hydrogen utilization due to water vapor produced at the anode (Coors, 2003). As solid oxides with proton conduction have been discovered and developed (Zhu and Mellander, 1994; Iwahara, 1996; Coors, 2003; Iwahara et al., 2004; Meng et al., 2007), a number of the researches related to the use of such a proton-conducting solid oxides for SOFC (SOFC-H⁺) have been reported (Iwahara, 1988; Demin and Tsiakaras, 2001; Taherparvar et al., 2003; Potter and Baker, 2006; Ranran et al., 2006; Epifanio et al., 2008; Jamsak et al., 2006; Ni et al., 2008; Zamfirescu and Dincer, 2009). When a proton conducting electrolyte is used, water vapor is produced at the

cathode side. Higher hydrogen partial pressure at the anode side can improve the efficiency of the SOFC as higher utilization of hydrogen can be reached (Epifanio et al., 2008). More complete hydrogen utilization of SOFC-H⁺ makes further the SOFC system possible to be simple and compact by eliminating the need of the afterburner (Zamfirescu and Dincer, 2009). In addition, the SOFC-H⁺ exhibits high proton conductivity at intermediate temperature operations (300-700°C) which can achieve an acceptable start-up time and may be possible to use in vehicular application (Epifanio et al., 2008; Zamfirescu and Dincer, 2009).

In the past years, many researchers concentrated on the synthesis and characterization of proton-conducting materials for SOFC-H⁺ (Coors, 2003; Taherparvar et al., 2003; Iwahara et al., 2004; Potter and Baker, 2006; Ranran et al., 2006; Meng et al., 2007; Epifanio et al., 2008). However, there are currently limited works concentrating on modeling and analysis of the SOFC-H⁺ (Demin and Tsiakaras, 2001; Jamsak et al., 2006; Ni et al., 2008; Zamfirescu and Dincer, 2009). Further, most studies investigated the theoretical performance of the SOFC-H⁺ without considering the presence of actual losses in a real operation of fuel cells (Demin and Tsiakaras, 2001; Jamsak et al., 2006; Zamfirescu and Dincer, 2009). An electrochemical model to predict accurately the characteristic performance of SOFC-H⁺ is particularly required for analysis, design, and improvement of SOFC-H⁺ (Chan et al., 2001; Hernandez-Pacheco et al., 2004). Recently, Ni et al. (2008) analyzed the theoretical performance of CH₄-fed SOFC-H⁺ by considering detailed voltage losses. However, in their work, the gas transport inside porous electrodes was developed based on the dusty gas model, which is more complicated and involves various physical and diffusion parameters. Besides the dusty gas model, Fick's model that the explicit analytical expression to determine the gaseous component at the electrode/electrolyte interface can be easily derived with acceptable accuracy is widely used (Suwanwarangkul et al., 2003; Hernandez-Pacheco et al., 2004). This reduces the complexity of the model to describe mass transfer within the electrodes, leading to less computational time.

In this study, the electrochemical performance of a planar SOFC-H⁺ fueled on H₂ was investigated using a detailed electrochemical model which takes into account the voltage losses, i.e., ohmic, activation and concentration losses. The impact of the

design parameters in terms of the role of support structure (anode-, cathode- and electrolyte-supported SOFC) and cell component thickness, porosity and pore size was considered to determine account to find an optimal structure of the SOFC-H⁺. Further, the steady-state performance of SOFC-H⁺ with direct internal reforming operation (DIR) fueled by methane is evaluated based on a one-dimensional steady-state fuel cell model and detailed electrochemical. The steady-state performance analysis was presented with respect to the effect of operating condition, i.e., steam to carbon ratio, temperature, pressure, and water content in oxidant, on the performance of SOFC-H⁺.

6.2. Electrochemical Study

This section deals with the performance analysis of a planar SOFC-H⁺ using a detailed electrochemical model, which takes into account all cell voltage losses, i.e., ohmic, activation, and concentration losses. The Fick's model was used to explain gas diffusion in porous electrodes. The effects of cell design (i.e., anode, cathode, and electrolyte supports) and design parameters (i.e., thickness of cell component and electrode microstructure) on the electrical characteristics of SOFC-H⁺ were examined.

As mentioned earlier in Chapter III, a single planar SOFC-H⁺ consists of anode, electrolyte and cathode made from Pt, SrCe_{0.95}Yb_{0.05}O_{3- α} (SCYb), Pt, respectively. The governing equations describing the relationship between the operating voltage and all related losses via an electrochemical model of SOFC-H⁺ developed in Chapter IV are summarized in Table 6.1.

6.2.1 Results and discussion

Since planar SOFCs can generally be designed with different configurations, i.e., electrolyte and electrode supported structures, the impact of the design parameter is taken into account to find an optimal structure of the SOFC-H⁺. Table 6.2 shows the standard values of the operating conditions, cell geometry and material properties of SOFC-H⁺ used in the present study. Humidified hydrogen (~3% H₂O) and dry air (< 0.1% H₂O) are used as fuel and oxidant for fuel cell.

Table 6.1 Electrochemical model of SOFC-H⁺

Open-circuit voltage (E^{OCV}):

$$E^{\text{OCV}} = E^0 + \frac{\mathfrak{R}T}{2F} \ln \left(\frac{p_{\text{H}_2(\text{an})} p_{\text{O}_2(\text{ca})}^{0.5}}{p_{\text{H}_2\text{O}(\text{ca})}} \right) \quad (6.1)$$

Operating voltage (V):

$$V = E^{\text{OCV}} - \eta_{\text{ohm}} - \eta_{\text{act}} - \eta_{\text{conc}} \quad (6.2)$$

Ohmic loss (η_{ohm}):

$$\eta_{\text{Ohm}} = iR_{\text{Ohm}} \quad \text{where } R_{\text{ohm}} = \tau_{\text{electrolyte}} / \sigma_{\text{electrolyte}} \quad (6.3)$$

Activation overpotential (η_{act}):

$$i = i_{0,\text{electrode}} \left[\exp \left(\frac{\alpha n F}{\mathfrak{R}T} \eta_{\text{act,electrode}} \right) - \exp \left(- \frac{(1-\alpha) n F}{\mathfrak{R}T} \eta_{\text{act,electrode}} \right) \right] \quad (6.4)$$

Concentration overpotential (η_{conc}):

$$\eta_{\text{conc}} = \frac{\mathfrak{R}T}{2F} \ln \left(\frac{p_{\text{H}_2(\text{an})}}{p_{\text{H}_2(\text{an})}^{\text{I}}} \right) + \frac{\mathfrak{R}T}{2F} \ln \left(\left(\frac{p_{\text{O}_2(\text{ca})}}{p_{\text{O}_2(\text{ca})}^{\text{I}}} \right)^{0.5} \frac{p_{\text{H}_2\text{O}(\text{ca})}^{\text{I}}}{p_{\text{H}_2\text{O}(\text{ca})}} \right) \quad (6.5)$$

$$\text{where } p_{\text{H}_2(\text{an})}^{\text{I}} = P - (P - p_{\text{H}_2(\text{an})}) \exp \left(\frac{\mathfrak{R}T \tau_{\text{an}}}{2FD_{\text{an,eff}} P} i \right) \quad (6.6)$$

$$p_{\text{O}_2(\text{ca})}^{\text{I}} = p_{\text{O}_2(\text{ca})} - \frac{\mathfrak{R}T \tau_{\text{ca}}}{2FD_{\text{ca,eff}}} i \quad (6.7)$$

$$p_{\text{H}_2\text{O}(\text{ca})}^{\text{I}} = p_{\text{H}_2\text{O}(\text{ca})} + \frac{\mathfrak{R}T \tau_{\text{ca}}}{4FD_{\text{ca,eff}}} i \quad (6.8)$$

Table 6.2 Values of input parameters used in the present study.

Parameters	Value
Operating temperature, T (K)	1073
Operating pressure, P (atm)	1.0
Electrode porosity, ε	0.4
Electrode pore radius, r (μm)	0.5
Electrode tortuosity, ξ	5.0
Electrolyte conductivity, $\sigma_{\text{electrolyte}}$ ($\Omega^{-1}\text{m}^{-1}$)	$225.92 \exp(-6.3 \times 10^3/T)$
Electrode exchange current density, $i_{0,\text{electrode}}$ (A m^{-2})	800
Electrolyte supported: ES-SOFC- H^+	
Thickness of anode, τ_{anode} (μm)	50
Thickness of electrolyte, $\tau_{\text{electrolyte}}$ (μm)	500
Thickness of cathode, τ_{cathode} (μm)	50
Anode supported: AS-SOFC- H^+	
Thickness of anode, τ_{anode} (μm)	500
Thickness of electrolyte, $\tau_{\text{electrolyte}}$ (μm)	50
Thickness of cathode, τ_{cathode} (μm)	50
Cathode supported: CS-SOFC- H^+	
Thickness of anode, τ_{anode} (μm)	50
Thickness of electrolyte, $\tau_{\text{electrolyte}}$ (μm)	50
Thickness of cathode, τ_{cathode} (μm)	500

6.2.1.1 Role of support structures

The electrical characteristics of an anode-supported SOFC-H⁺ are shown in Figure 6.1. The cell voltage decreases with an increase in operating current density. This is due to the increased voltage losses from the irreversible SOFC-H⁺ cell resistance. As seen in Figure 6.1a, the power density reaches a maximum value as 0.26 W cm⁻² at the current density of 0.48 A cm⁻². When the fuel cell is operated at the current density of 1.00 A cm⁻², cell the voltage and power density drop to zero and the fuel efficiency at this condition is 51%. From the simulation results, the ohmic loss represents a major loss in the cell, followed by the cathode and anode activation overpotentials (Figure 6.1b) and thus, the development of electrolyte with higher ionic conductivity could improve the performance of the SOFC-H⁺. It is noted that at the current density of 1.00 A cm⁻², the cell performance is not controlled by the concentration loss as a rapid voltage drop is not observed. Since both the anode and the cathode are made from the porous platinum, the exchange current densities of both electrodes are equivalent and thus, resulting in the same activation overpotential on the anode and cathode sides. The results show that although the anode-supported SOFC is considered, the concentration overpotential at the anode is negligible because H₂ gas can be transported quickly through the anode. Unlike the cathode side, higher molecular weights of O₂ and H₂O result in low effective diffusion that causes high concentration overpotential at the cathode side.

Figure 6.2a presents the performance of SOFC-H⁺ with different support structures (i.e., anode, cathode and electrolyte supports). It clearly indicates that the electrode-supported SOFC-H⁺ provides a higher performance compared with the electrolyte-supported SOFC-H⁺. Individual ohmic and concentration overpotentials of SOFC-H⁺ are given in Figures 6.2b and 6.2c, respectively. It is noted that the plot of the activation overpotential is not given as it is independent on the electrode thickness. As shown in Figure 6.2b, the ohmic loss dominates the electrolyte-supported SOFC-H⁺ performance due to higher electrolyte thickness and a low ionic conductivity of the proton-conducting electrolyte. To reduce an ohmic loss in the electrolyte-supported SOFC-H⁺, operating cell at higher temperature and/or adopting an alternative electrolyte material with higher ionic conductivity are required.

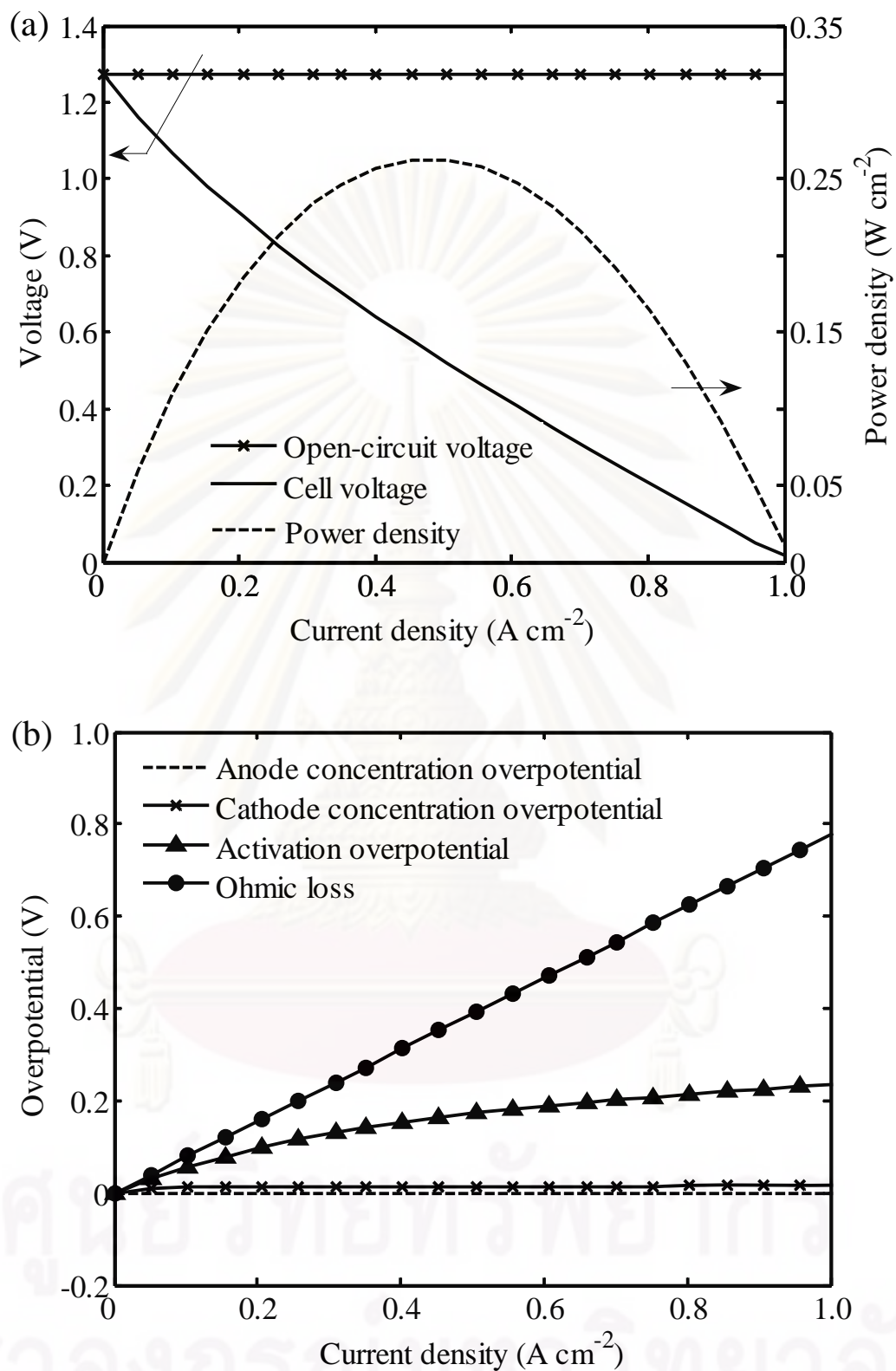
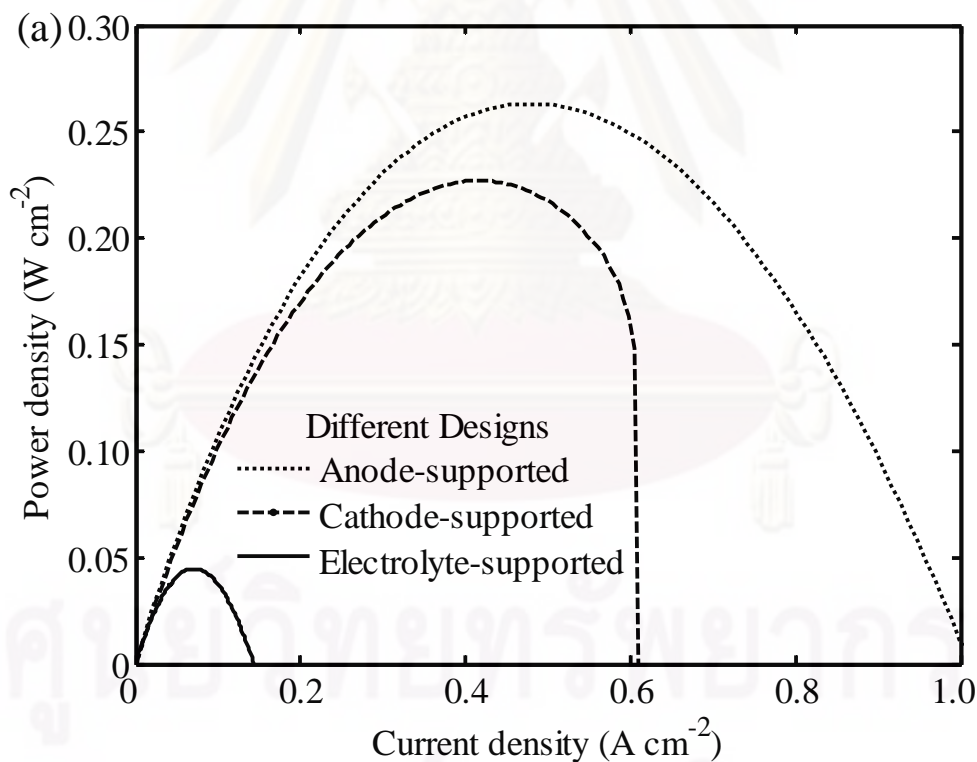


Figure 6.1 The electrical characteristics of anode-supported SOFC-H⁺ at different current densities under isothermal condition: (a) open-circuit voltage, cell voltage and power density and (b) individual overpotentials.

Figure 6.2c shows the difference of cathode concentration overpotential in the anode- and cathode-supported SOFC-H⁺. Since the transport of H₂ as a single component in the porous anode is quick, the anode concentration overpotential in both the anode- and cathode-supported SOFC-H⁺ is relatively small. From Figure 6.2c, it can be seen that the cathode concentration overpotential in the cathode-supported SOFC-H⁺ is higher than that in the anode-supported SOFC-H⁺. The use of thicker cathode can hinder the transport of O₂ and H₂O, resulting in higher concentration overpotential at the cathode side. Due to the difference in concentration overpotential, the anode-supported SOFC-H⁺ shows better performance than the cathode-supported SOFC-H⁺; the anode-supported SOFC-H⁺ can be operated at higher current densities and power densities. Therefore, the anode-supported SOFC-H⁺ is selected as the standard design to investigate the effects of structural and operational parameters on the SOFC-H⁺ performance in the next section.



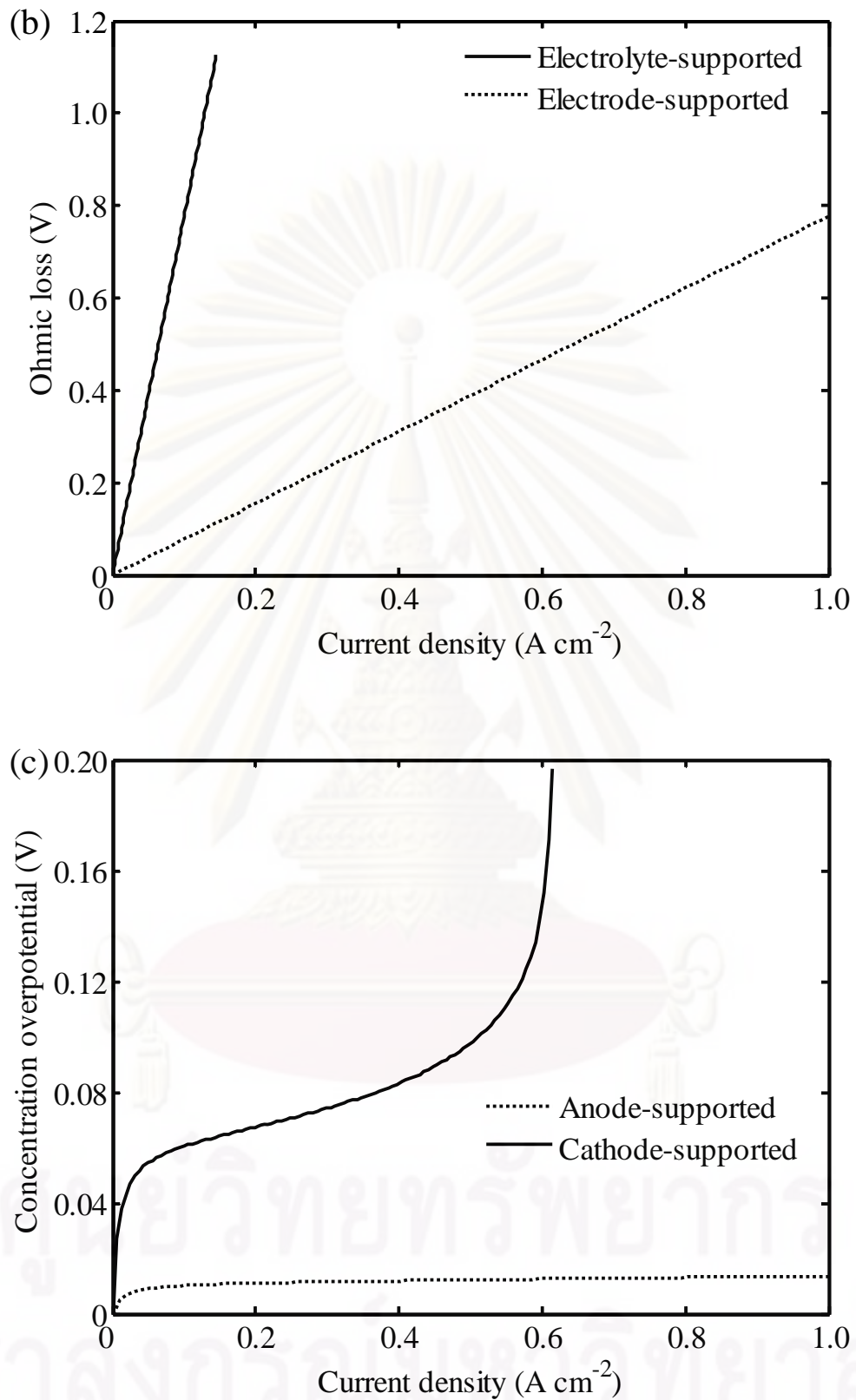


Figure 6.2 Comparison of SOFC-H⁺ with different support structures: (a) power density, (b) ohmic loss, and (c) concentration overpotential.

6.2.1.2 Effect of electrolyte thickness

In order to improve the performance of anode-supported SOFC-H⁺, the effect of operating current densities on cell power density at different electrolyte thicknesses is analyzed, as shown in Figure 6.3a. Considering the present technology of fabricating a thinner electrolyte in an SOFC, it shows that in order to avoid an increase risk of breakage causing a gas leak, the minimum of the electrolyte thickness is about 10 μm (Iwahara, 1996; Kosacki and Anderson; 1997; Hamakawa et al., 2002; Mather et al., 2003; Ito et al., 2005; Essoumhi et al., 2008; Matsumoto et al., 2008). Therefore, the effect of the electrolyte thickness varying in the range of 10-40 μm on the SOFC-H⁺ performance is studied. It is noted that the anode and cathode thickness is fixed at 500 and 50 μm , respectively. At each value of electrolyte thickness, there is an optimum current density to achieve the maximum power density. As expected, the cell performance increases dramatically when the electrolyte thickness decreases. This is because the decrease of the electrolyte thickness causes a significant decrease in the ohmic loss as shown in Figure 6.3b.

6.2.1.3 Effect of cathode thickness

Figure 6.4a presents the characterization curve of the anode-supported SOFC-H⁺ at different cathode thicknesses (25, 50, 100 and 150 μm). It is noted that the electrolyte and anode thicknesses are fixed at 10 and 500 μm , respectively. The simulation results show that the cell performance slightly decreases when the cathode thickness increases. As expected, the increased cathode thickness hinders the transport of O₂ from the surface to the cathode/electrolyte interface and the transport of H₂O from the porous cathode to the air channel is less facilitated. These results lead to an increase in the concentration overpotential, as demonstrated in Figure 6.4b. Considering the durability of an anode-supported SOFC-H⁺, it should be fabricated with the cathode thickness of 50 μm (Ni *et al.*, 2008). It is noted that the anode, electrolyte and cathode thickness of 500, 10 and 50 μm are set as the standard cell geometry for a performance analysis of the SOFC-H⁺ in subsequent sections.

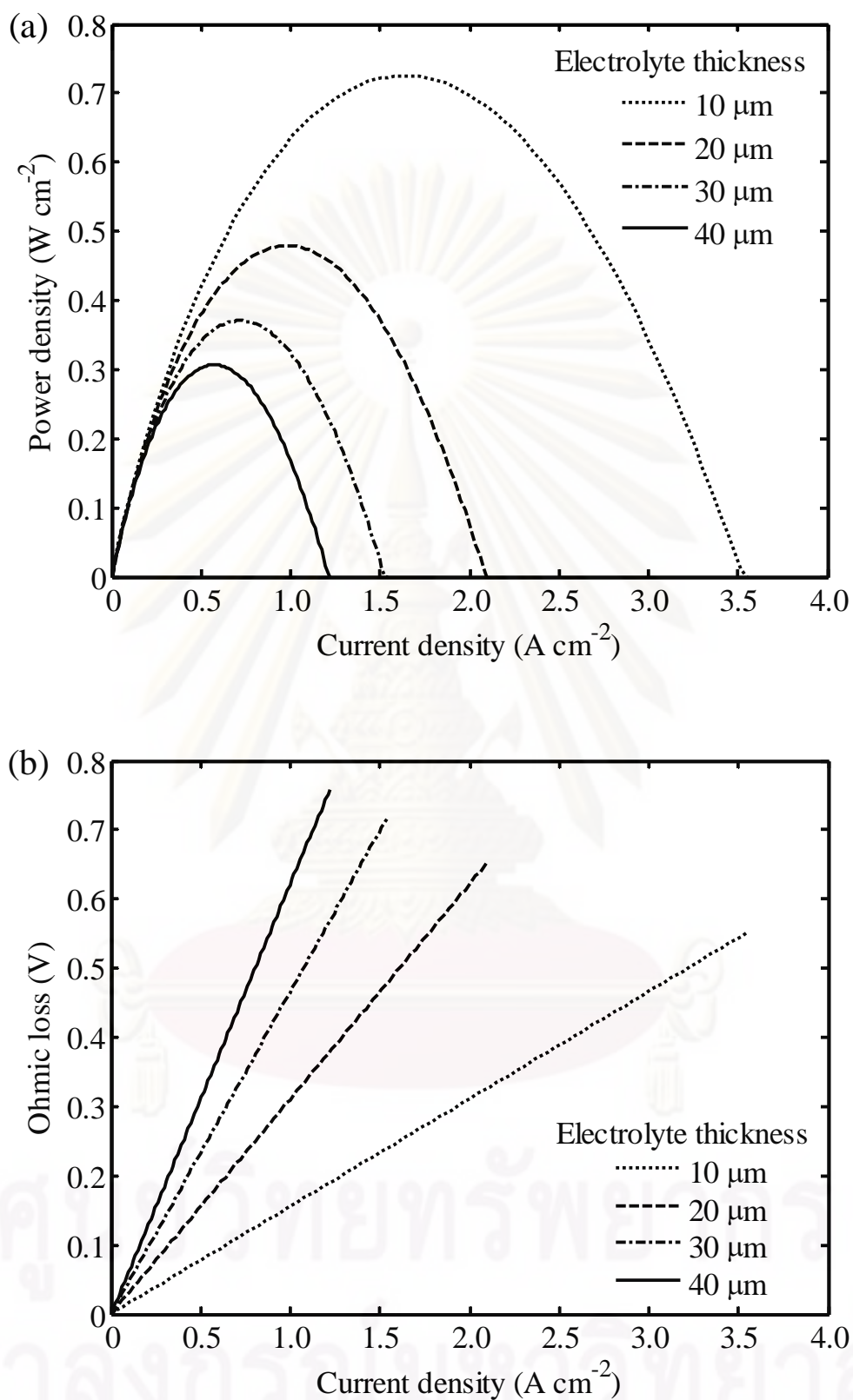


Figure 6.3 Effect of electrolyte thickness at different current densities on: (a) power density, and (b) ohmic loss.

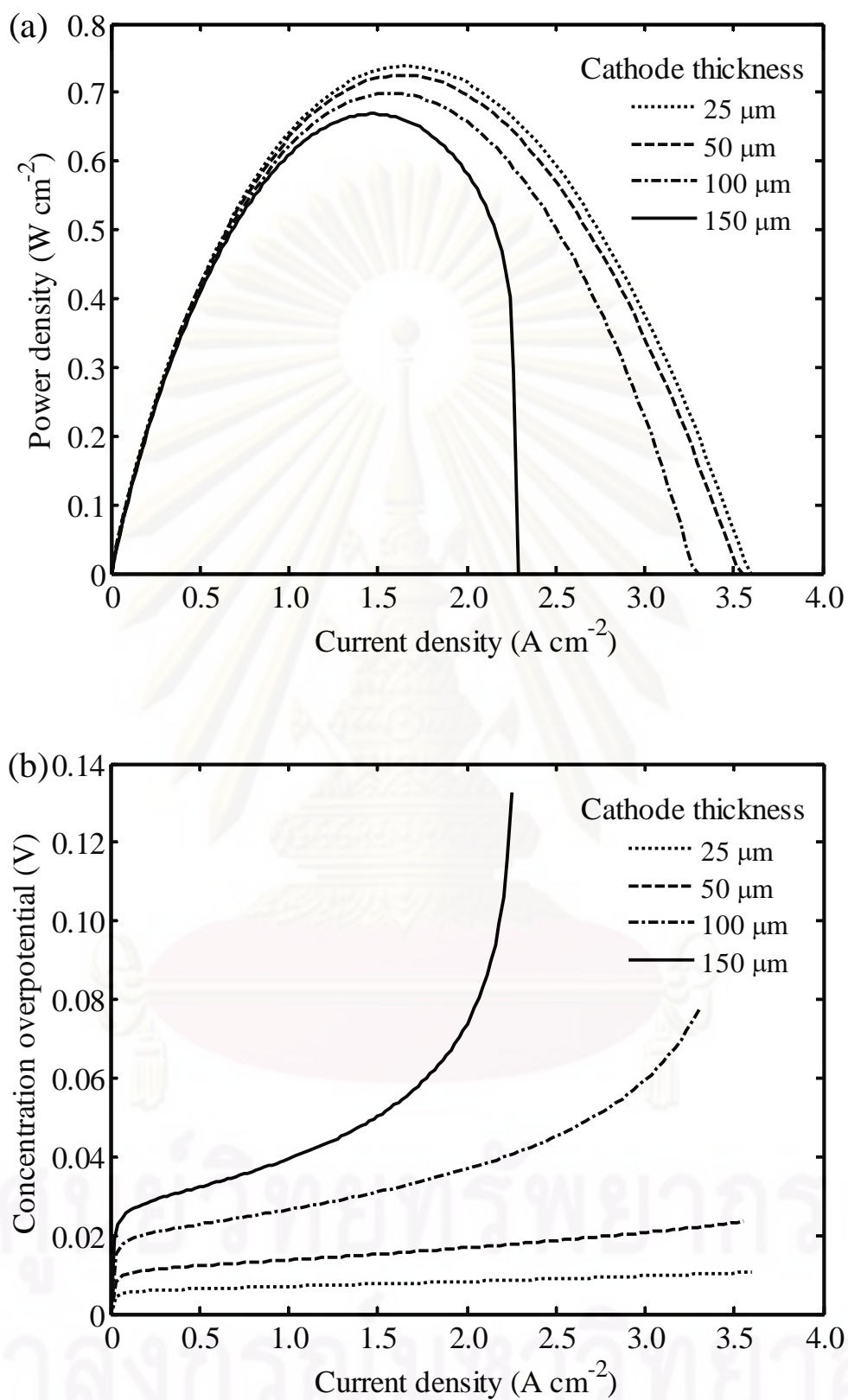


Figure 6.4 Effect of cathode thickness at different current densities on (a) power density, and (b) concentration overpotential.

6.2.1.4 Effect of electrode pore size

It is noticed that the transport of gas species in porous electrode is based on the diffusion process which also depends on the microstructure of porous electrodes, such as pore size and porosity. Therefore, the effect of electrode microstructure on the performance of SOFC-H⁺ is analyzed. Figures 6.5a-b show the effect of electrode pore size on the power density and concentration overpotential of the anode-supported SOFC-H⁺. The simulation results show that the cell performance increases with an increase in electrode pore size. When the electrode pore size increase, the gas transport process in the porous electrode based on the Knudsen diffusion is more facilitated, resulting in a significant decreased concentration overpotential. In addition, it is observed that the cell performance tends to be less sensitive when the electrode pore size is larger than 0.5 μm . This is because the ordinary diffusion is dominant over the Knudsen diffusion and thus, the concentration overpotential became less sensitive at an electrode pore size higher than 0.5 μm .

6.2.1.5 Effect of electrode porosity

The effect of electrode porosity on the cell performance and concentration overpotential of the anode-supported SOFC-H⁺ are shown in Figures 6.6a and 6.6b, respectively. Similar to the effect of electrode pore size, increasing electrode porosity can improve the cell performance of SOFC-H⁺. The concentration overpotential decreases significantly with increasing electrode porosity since more space is available for gas transport, and in turn enhances overall diffusion coefficient.

ศูนย์วิทยทรัพยากร

จุฬาลงกรณ์มหาวิทยาลัย

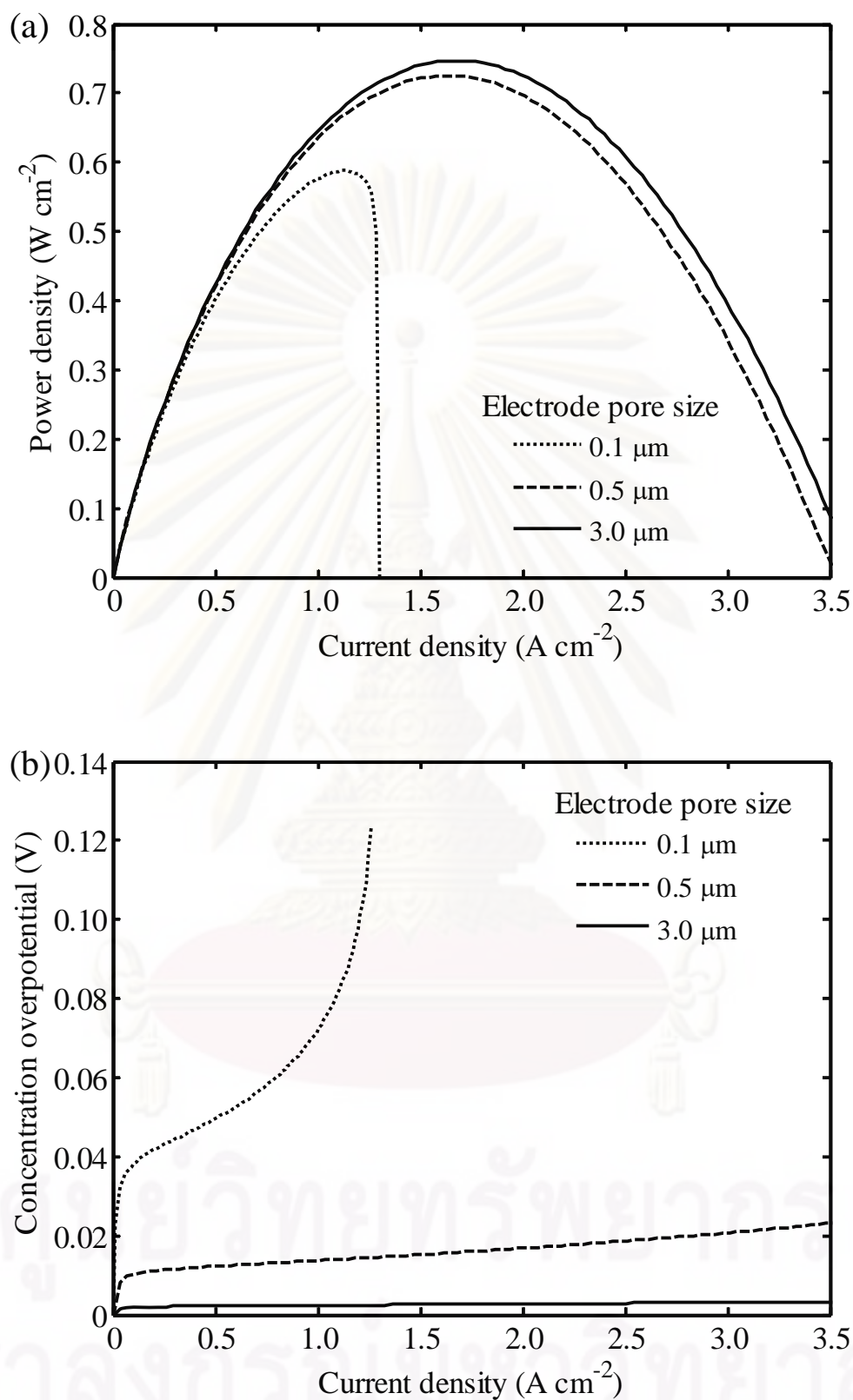


Figure 6.5 Effect of electrode pore size at different current densities on: (a) power density, and (b) concentration overpotential.

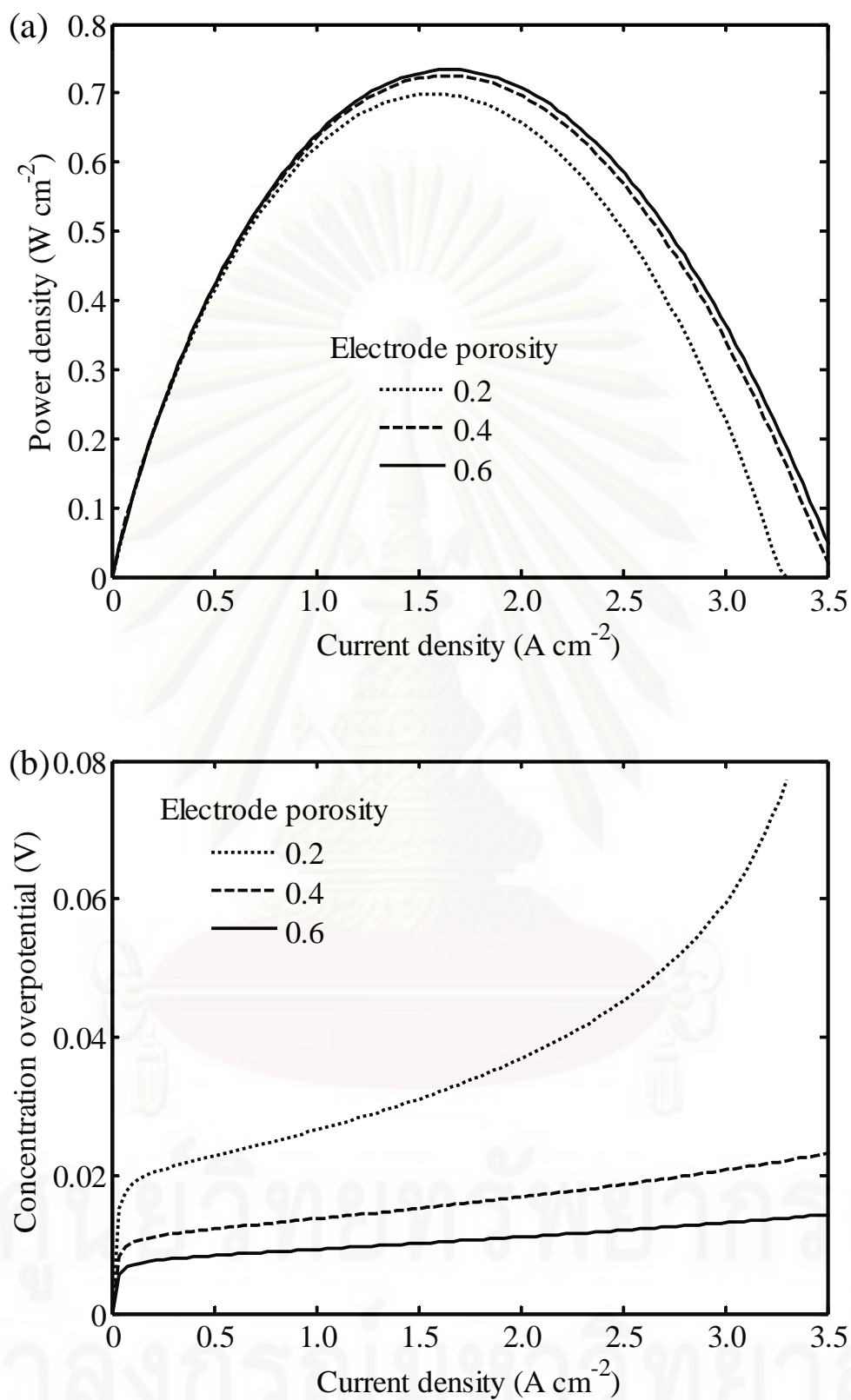


Figure 6.6 Effect of electrode porosity at different current densities on: (a) power density, and (b) concentration overpotential.

6.2.2 Conclusions

In this section, the electrochemical performance of a planar SOFC-H⁺ was analyzed with respect to different design and structural parameters. Under the standard operating conditions ($T = 1073$ K and $P = 1$ atm), it was found that an anode-supported SOFC-H⁺ provides the best electrical performance in terms of an achievable power density and a wider range of operating current density. This is because an ohmic loss in the anode-supported SOFC-H⁺ is lower than the electrolyte-supported SOFC-H⁺. Concentration overpotential becomes more significant for a cathode-supported cell. Considering the anode-supported SOFC-H⁺, the ohmic loss is still a major voltage loss due to the low protonic conductivity of electrolyte. The performance analysis of the anode-supported SOFC-H⁺ shows that a decrease in electrolyte thickness can significantly reduce the ohmic loss. Further, it is found that the anode-supported SOFC-H⁺ performance can be improved by decreasing cathode thickness and increasing the electrode pore size and porosity.

6.3 Anode-supported SOFC-H⁺ performance

This section presents a performance analysis of an anode-supported SOFC-H⁺ with planar design. The SOFC-H⁺ is fueled by methane and operated under direct internal reforming and isothermal conditions. A one-dimensional steady-state model coupled with a detailed electrochemical model is employed to investigate the distribution of gas composition along the fuel and air channels, and all the electrochemical-related variables (i.e., open-circuit voltage, activation, ohmic, and concentration overpotential, and current density) as well as fuel cell efficiency and power output.

As explained in Chapter IV, the differential equations describing the change of component concentrations in fuel and air channels along the axial direction can be written as follows:

$$\frac{dC_{i,k}}{dx} = \frac{1}{u_k} \sum_j v_{ij} R_j \frac{1}{h_k} \quad (6.9)$$

It is noted that for the fuel channel ($k = f$), i denotes CH_4 , H_2O , CO , H_2 , and CO_2 , and j represents steam reforming, water gas shift and electrochemical reactions whereas for the air channel ($k = a$), i denotes O_2 and H_2O and j represents only a electrochemical reaction. In addition, the velocities of fuel and air are assumed to be constant along the channels (Aguiar et al., 2004).

As an operating cell voltage (V) in the electrochemical model is pre-specified, an average current density (i_{ave}) can be calculated from the distribution of current density along the cell length which is obtained from the solution of the fuel cell model. It should be noted that fuel and air compositions vary along the cell channel under a real operation due to fuel and oxygen utilizations by electrochemical reactions. The cell voltage and average current density obtained are used to calculate the power density (P_{SOFC}), fuel cell efficiency ($\varepsilon_{\text{SOFC}}$) and fuel utilization (U_{fuel}) of fuel cell as shown in the following expressions:

$$P_{\text{SOFC}} = i_{\text{ave}} V \quad (6.10)$$

$$\varepsilon_{\text{SOFC}} = \frac{i_{\text{ave}} VLW}{(y_{\text{CH}_4}^{\text{in}} LHV_{\text{CH}_4} + y_{\text{H}_2}^{\text{in}} LHV_{\text{H}_2} + y_{\text{CO}}^{\text{in}} LHV_{\text{CO}}) F_{\text{fuel}}} \times 100\% \quad (6.11)$$

$$U_{\text{fuel}} = \frac{i_{\text{ave}} LW}{2F(4y_{\text{CH}_4}^{\text{in}} + y_{\text{H}_2}^{\text{in}} + y_{\text{CO}}^{\text{in}}) F_{\text{fuel}}} \quad (6.12)$$

It is noted that the definitions of fuel cell efficiency and fuel utilization (Equations (6.11)-(6.12)) are based on the fuel derived from the pre-reforming of methane. However, if the primary methane fed to the whole system consisting of the external reformer and the SOFC is considered as the basis for fuel cell efficiency, the calculated value would be higher than the one based on Equation (6.11) as the primary methane has lower heating value than that of the pre-reformed gas.

จุฬาลงกรณ์มหาวิทยาลัย

6.3.1 Results and discussion

Table 6.3 shows the values of operating condition, cell geometry and material property for simulating an SOFC-H⁺ with DIR at a nominal condition. The inlet fuel composition given in Table 6.3 is based on the synthesis gas obtained from a gas mixture of steam and methane at a ratio of 2 after 10% pre-reforming whereas dry air consisting of approximately 20.9% O₂, 79% N₂, and 0.1% H₂O is used as an oxidant.

Prior to performing an analysis of a planar SOFC-H⁺ with DIR, its current-voltage characteristic is investigated to find a suitable condition for cell operation. Figure 6.7 presents the performance characteristics of the SOFC-H⁺ with DIR under isothermal operation ($T = 1073$ K). For the SOFC-H⁺ operated at cell voltage in the range of 0.6 to 1.2 V, it can be seen that both the average current density and the power density obtained decreases with an increase in cell voltage. This is due to the increased voltage losses from the irreversible cell resistance. As shown in this figure, the maximum power density of 0.36 W cm^{-2} can be achieved when the operating cell voltage is 0.6 V. However, at this condition, high fuel utilization (90 %) is observed; the reactants are rapidly consumed to generate current and the concentration overpotential dominates the cell performance. In the present study, the operation of SOFC-H⁺ at 0.7 V is considered as it shows a good compromise on power density and fuel utilization.

In this study, the fuel gas velocity was assumed to be constant for modeling the SOFC-H⁺. However, due to the variation in the total molar flow rate of fuel caused by chemical and electrochemical reactions, the velocity of fuel gas in the fuel channel is changed. Thus, the impact of fuel velocity on the performance of SOFC-H⁺ should be investigated. Figure 6.7 shows the electrical characteristics of the SOFC-H⁺ at different fuel velocities varying from 0.75 to 1.5 m s^{-1} . The results indicate that the maximum deviation of both the current density and the power density from the nominal condition at which the fuel velocity is 1 m s^{-1} is 10.09% at the operating cell voltage of 0.6 V. It is noted that although simulations with the isochoric assumption cause the error in the prediction of the fuel cell performance, it is in the acceptable range. Further, the certain benefit of assuming the constant velocity is to shorten the computational time.

Table 6.3 Model parameters used in the performance analysis of SOFC-H⁺

Parameters	Value
<i>Operating conditions</i>	
Operating temperature, T	1073 K
Operating pressure at anode, P_{an}	1.0 atm
Operating pressure at cathode, P_{ca}	1.0 atm
Inlet fuel velocity, u_f	1 m s ⁻¹
Inlet air velocity, u_a	18 m s ⁻¹
Air composition	0.1% H ₂ O, 20.9% O ₂ , 79% N ₂
Fuel composition ^a	28.1% CH ₄ , 56.7% H ₂ O, 0.5% CO, 12% H ₂ , and 2.7% CO ₂
<i>Dimensions of cell element</i>	
Cell length, L	0.4 m
Cell width, W	0.1 m
Fuel channel height, h_f	1 mm
Air channel height, h_a	1 mm
Anode thickness, τ_{an}	500 μ m
Cathode thickness, τ_{ca}	50 μ m
Electrolyte thickness, τ_{ele}	20 μ m

^a The fuel composition is based on a steam and methane mixture with S/C = 2 after 10% pre-reforming.

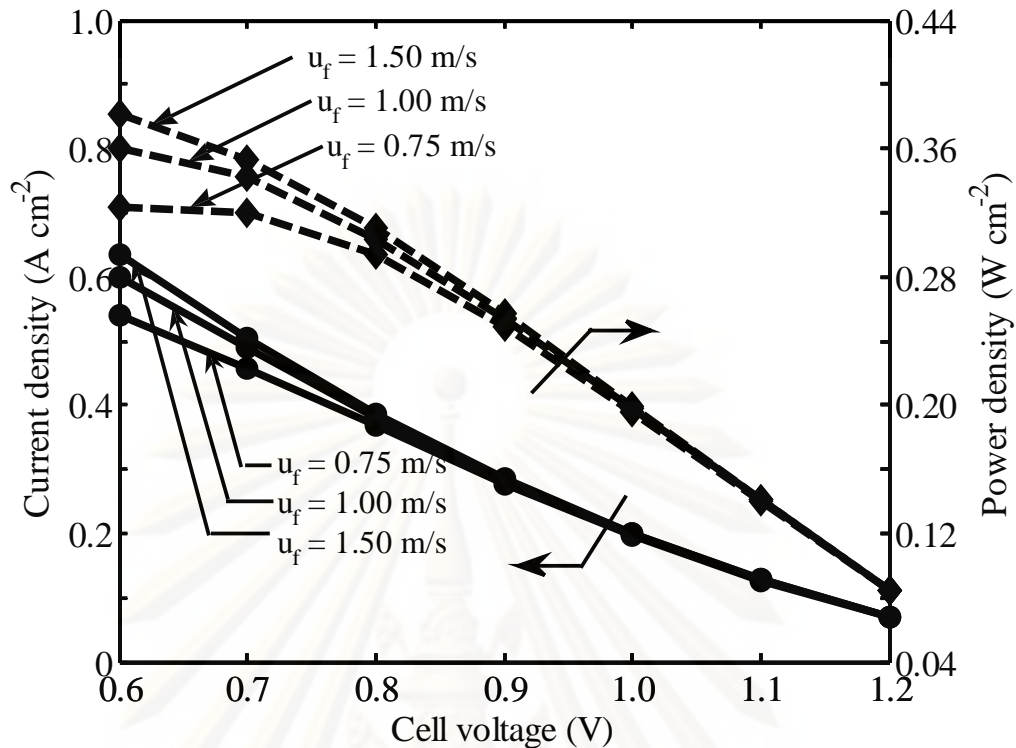


Figure 6.7 Performance characteristics of an SOFC-H⁺ at different cell voltages and fuel velocities.

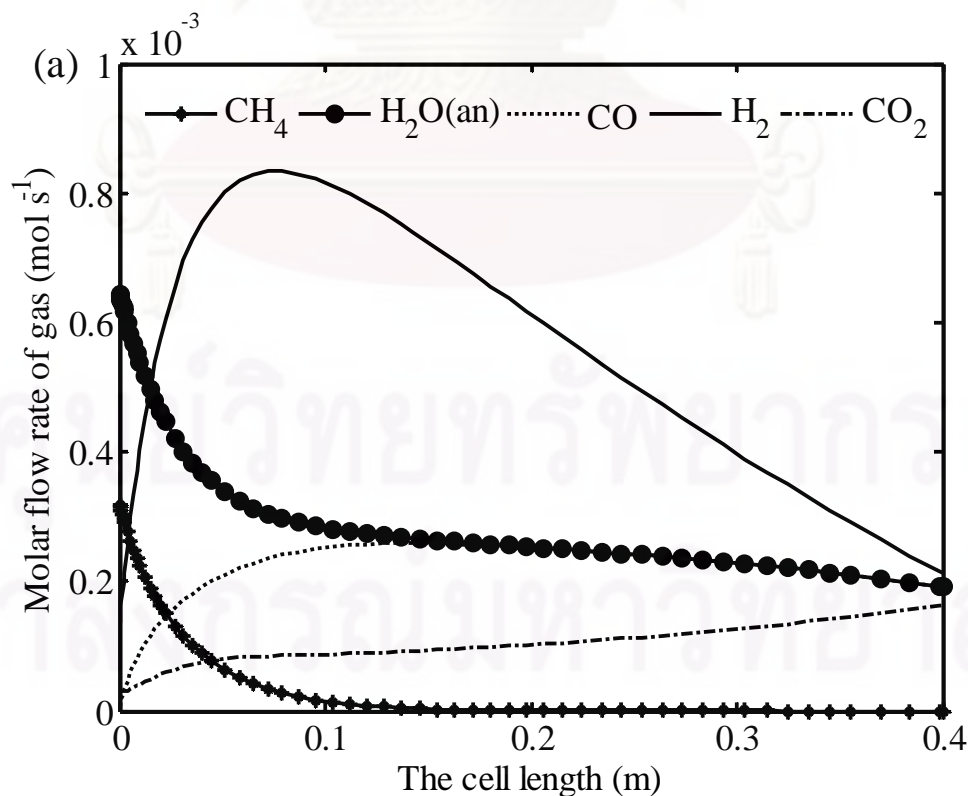
Analysis of gas compositions in fuel and air channels and all the electrochemical-related variables (i.e., current density, open-circuit voltage, and activation, ohmic, and concentration overpotentials) is shown in Figure 6.8. It can be seen from Figure 6.8a that at the entrance of fuel channel, CH₄ and H₂O are rapidly consumed via steam reforming reaction resulting in an increase in H₂ and CO. At the same time, more CO₂ is generated by the water gas shift reaction. Due to the use of a proton-conducting electrolyte in SOFC, the generation of H₂O at the air channel is observed as shown in Figure 6.8b. At the exit of the fuel channel, the fuel consists of 25% H₂O, 25% CO, 28% H₂ and 22% CO₂ whereas the oxidant consists of 5% H₂O, 18% O₂ and 77% N₂. It is noted that the presence of CO in the fuel channel may deteriorate the SOFC-H⁺ performance. This is due to the formation of carbon over the anode surface (Equation (6.13)) leading to the reduced catalyst activity:

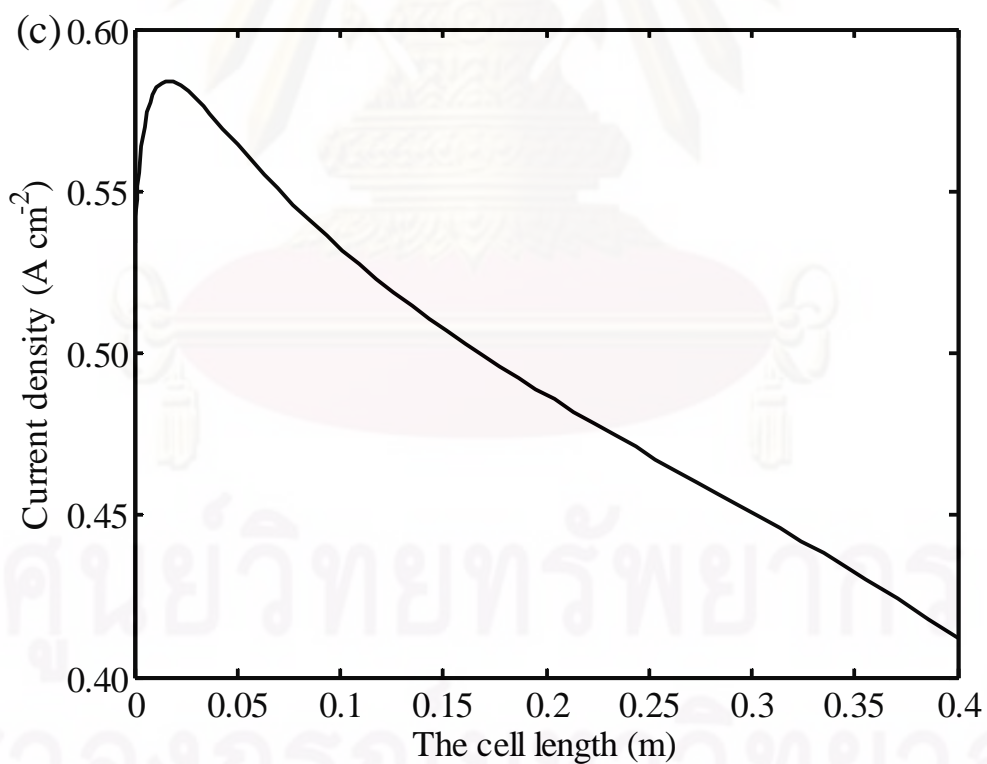
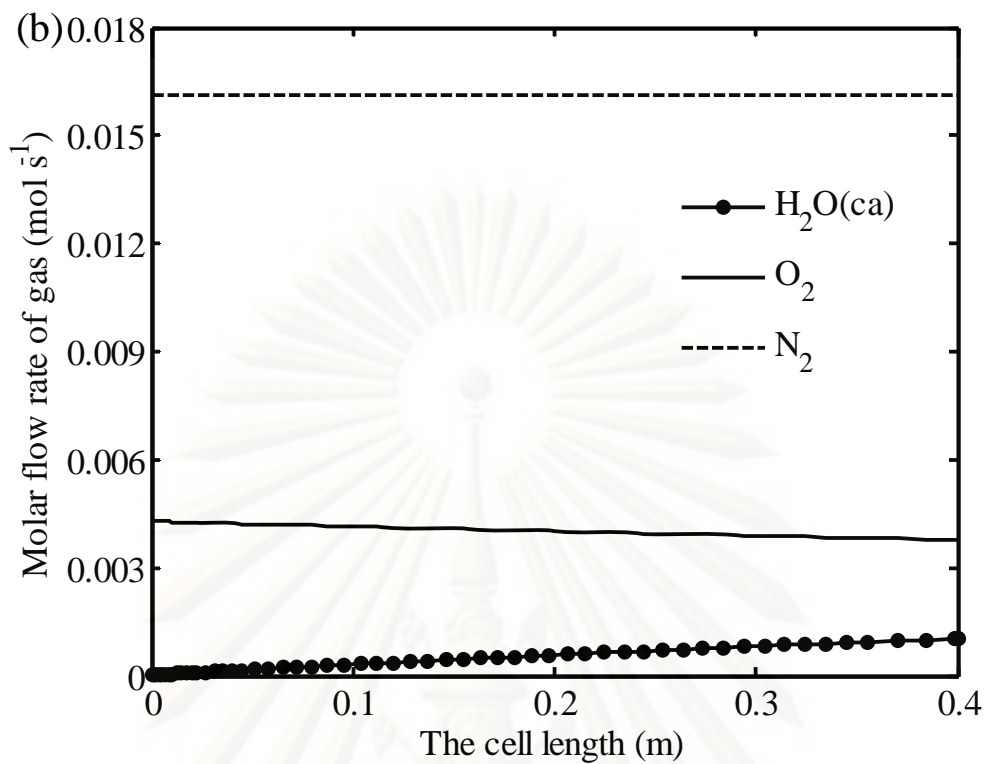


As a result, the CO content in fuel stream should be considered in analyzing the SOFC-H⁺ performances.

Since the local amount of H₂ and O₂ consumed and H₂O produced through electrochemical reactions is related to the local electric current density produced in the cell, under the isothermal condition, the key parameter affecting the electrochemical reaction rate is the local H₂ concentration in the fuel channel and the local O₂ and H₂O in the air channel. Figure 6.8c shows the current density profile along the fuel cell. It is found that the current density slightly increases at the inlet and continuously decreases toward the fuel cell outlet. This is mainly due to the depletion of H₂ in the fuel channel (Figure 6.8a).

Considering the individual contribution of cell overpotentials, it can be seen from Figure 6.8d that the activation overpotential represents a major loss, followed by the ohmic overpotential. The cathode activation overpotential is equal to the anode activation overpotential because in this study, the exchange current density of the anode and cathode has the same value (see Section 4.6.2 in Chapter IV). It is further observed that the anode and cathode concentration overpotentials can be negligible compared with other voltage losses.





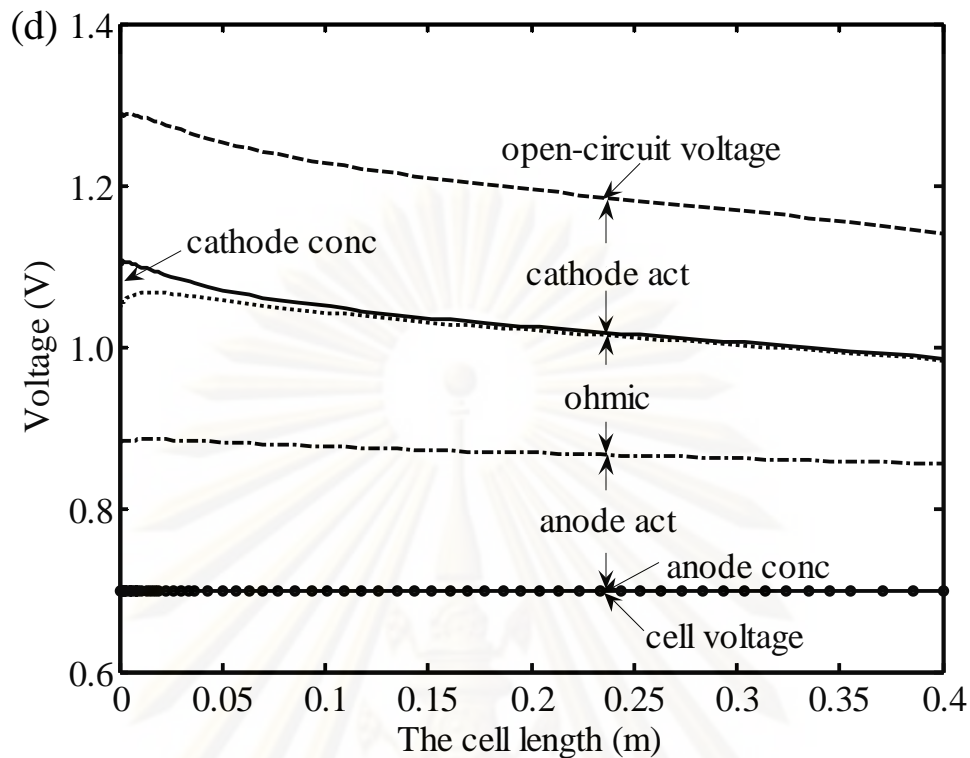


Figure 6.8 (a) Profiles of gas compositions at fuel channel, (b) Profiles of gas compositions at air channel, (c) distribution of current density, and (d) distribution of individual voltage losses.

6.3.1.1 Effect of steam/carbon (S/C) ratio

In order to study the impact of S/C ratio on the SOFC- H^+ performance, the fuel compositions given in Table 6.3 are varied by increasing the S/C ratio from 2.0 to 3.0 while the pre-reforming of methane is still 10% and the other parameters in Table 6.3 are kept constant. Figure 6.9 shows the effect of S/C ratio on SOFC- H^+ performance in terms of fuel utilization, power density, fuel cell efficiency and the CO molar flow rate at the fuel channel outlet. As can be seen in Figure 6.9a, the CO molar flow rate at the outlet is sharply reduced with increasing the S/C ratio. This is caused by the fact that increasing S/C ratio increases H_2O content in the fuel stream and thus, the CO conversion is more pronounced. However, an increase in S/C ratio dilutes the concentration of H_2 in the fuel channel, resulting in the reduction of the average current density due to a decrease in open-circuit voltage. This leads to a decrease in the power density as illustrated in Figure 6.9b. When the S/C ratio is increased, it is also found that the molar flow rates of CH_4 , CO and H_2 at the inlet of SOFC are

decreased. A lower decrease in the fuel rate compared to the generated current causes increases in the fuel utilization and fuel cell efficiency. As a result, a choice of S/C ratio has to be carefully selected to optimize the cell performance as well as the possibility of carbon formation.

6.3.1.2 Effect of operating temperature

In this section, the effect of operating temperature on the performance of SOFC-H⁺ is studied. Figure 6.10a shows that the content of CO at the fuel channel outlet increases when an operating temperature increases. This is the results of the increased rate of steam reforming reaction, leading to more generation of CO, and the exothermic nature of the water gas shift reaction. Moreover, an increase in operating temperatures increases the rate of electrochemical reaction; more hydrogen is consumed and thus the current density is more generated. Considering cell voltage losses, it is also found that the increased operating temperature causes a large reduction in ohmic overpotentials. Therefore, the power density, fuel cell efficiency and fuel utilization are increased as shown in Figures 6.10a and 6.10b.

6.3.1.3 Effect of operating pressure

Figures 6.11a and 6.11b show cell performances and the content of CO at the fuel channel outlet as a function of operating pressures; the absolute pressure at the anode and cathode channels is changed by the same value. It is found that the operation of SOFC-H⁺ at higher pressure can slightly reduce the CO content. At a high pressure operation of SOFC-H⁺, the partial pressure of H₂ in the fuel channel and O₂ in the air channel increases, resulting in an improvement of fuel cell performances; higher open-circuit voltage and current density can be achieved. This brings to an increase in power density and fuel cell efficiency.

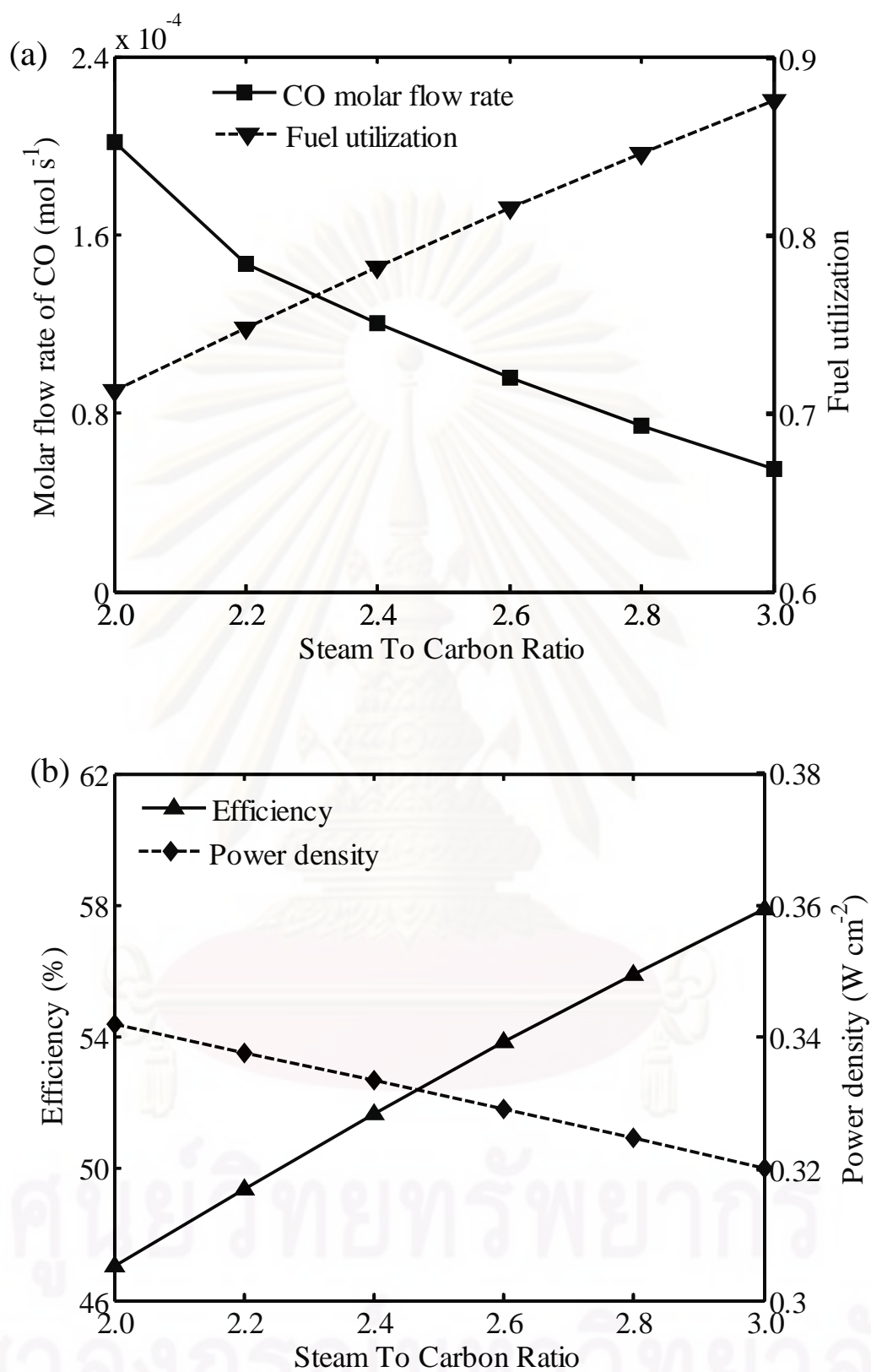


Figure 6.9 Effect of steam/carbon ratio on: (a) molar flow rate of CO and fuel utilization, and (b) cell efficiency and power density.

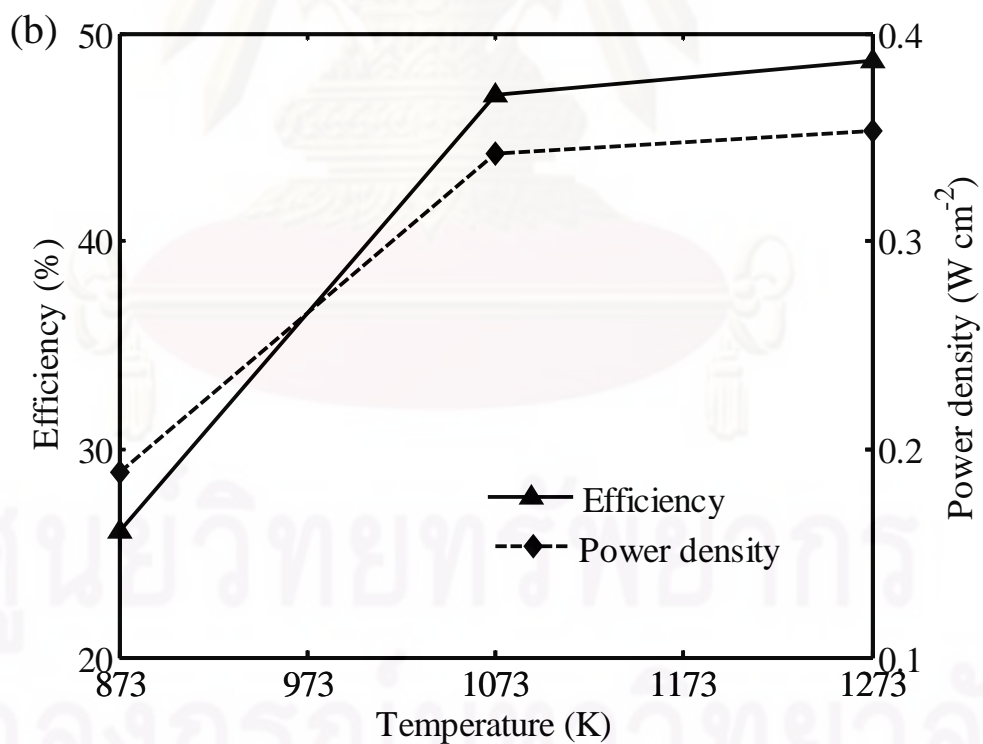
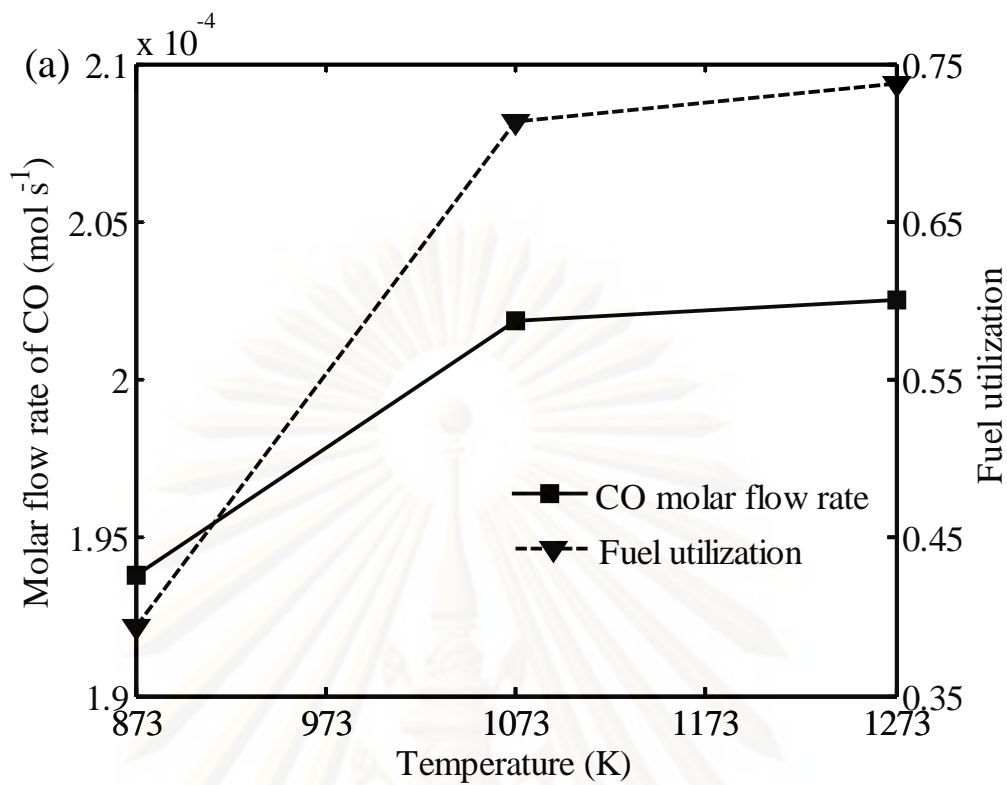


Figure 6.10 Effect of operating temperature on: (a) molar flow rate of CO and fuel utilization and (b) cell efficiency and power density.

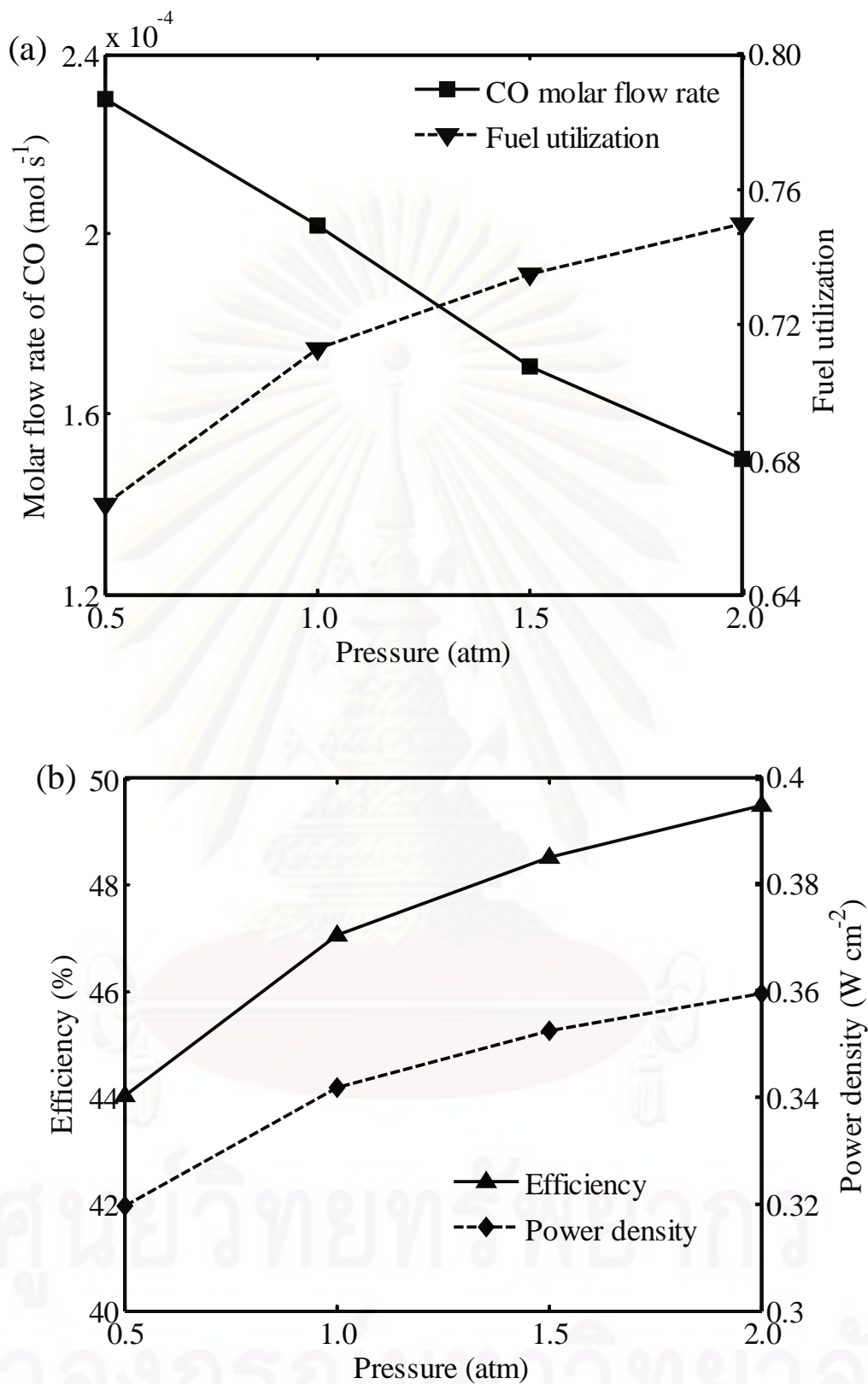


Figure 6.11 Effect of operating pressure on: (a) molar flow rate of CO and fuel utilization and (b) cell efficiency and power density.

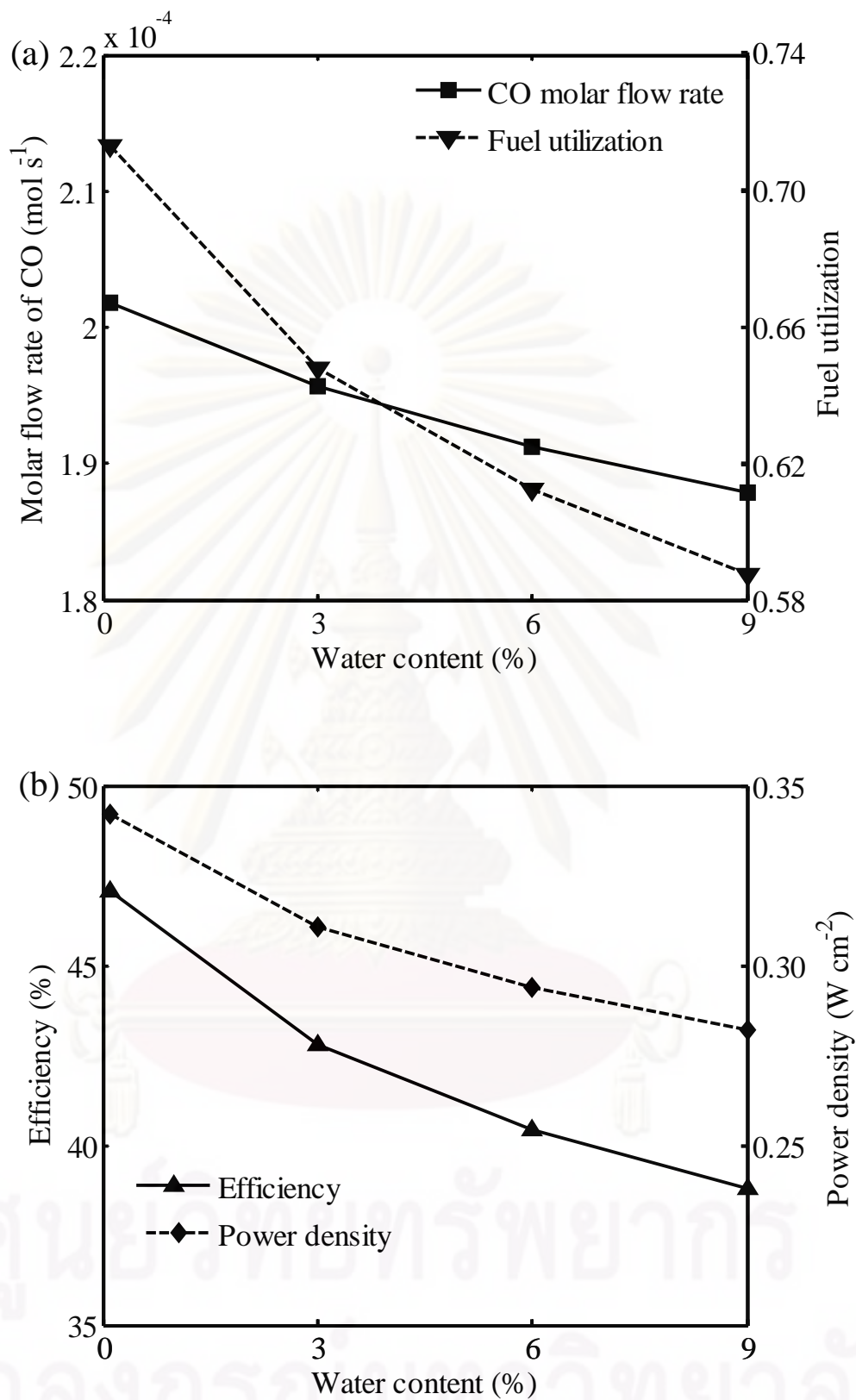


Figure 6.12 Effect of water content on: (a) molar flow rate of CO and fuel utilization and (b) cell efficiency and power density.

6.3.1.4 Effect of water content in oxidant

For an SOFC- H^+ system, the water content in oxidant feed is a further key operating parameter to be considered due to the generation of water vapor at the cathode side. In this section, the impact of water content on the cell performances and the CO molar flow rate at the fuel cell outlet are investigated. Figures 6.12a and 6.12b demonstrate that the oxidant with higher water content degrades the fuel cell performance. As the amount of O_2 required for the electrochemical reaction decreases when the water content increases, the current density is less produced, resulting in a lower fuel utilization, power density and fuel cell efficiency. In addition, the reduction of current density leads to a decrease in the electrochemical reaction rate which is related to the less consumption of H_2 , and thus the CO flow rate at the fuel outlet stream is also decreased as illustrated in Figure 6.12a.

6.3.2 Conclusions

In this study, a performance analysis of a planar SOFC with proton-conducting electrolyte (SOFC- H^+) operated under direct internal reforming of methane was performed. A one-dimensional steady state model coupled with a detailed electrochemical model was employed to predict the distribution of gas composition within fuel and air channels and all the electrochemical-related variables. From cell electrochemical characteristics, it is found that the operation of the SOFC- H^+ at the cell voltage of 0.7 V shows a good compromise on power density and fuel utilization. At this condition, the power density of 0.34 W cm^{-2} , average current density of 0.49 A cm^{-2} , fuel cell efficiency of 47%, and fuel utilization of 0.70 are predicted. However, high CO content in the fuel channel is observed at this condition and this may deteriorate the SOFC- H^+ performance by reducing catalyst activity. The performance analyses of a planar SOFC- H^+ have been performed. The results demonstrate that increasing S/C ratio decreases cell power density but increases fuel utilization and fuel cell efficiency. The content of CO at the fuel channel outlet is reduced with the increased S/C ratio. The influence of operating parameters, i.e., temperature, pressure, and the amount of water in oxidant are also investigated. The results show that increases in operating temperatures and pressures enhance the efficiency of the

SOFC-H⁺ whereas the effect of the increased water content in oxidant shows an opposite trend.



ศูนย์วิจัยทรัพยากร
จุฬาลงกรณ์มหาวิทยาลัย

CHAPTER VII

A HYBRID SYSTEM OF SOLID OXIDE FUEL CELLS WITH DIFFERENT ELECTROLYTES

This chapter presents the performance evaluation of a hybrid system of solid oxide fuel cells with different electrolytes, i.e., an oxygen ion-conducting electrolyte (SOFC-O²⁻) and a proton-conducting electrolyte (SOFC-H⁺). Due to an internal reforming operation, SOFC-O²⁻ can produce electrical power as well as high-temperature exhaust gas containing remaining fuel, i.e., H₂ and CO that can be used for SOFC-H⁺ operation. The remaining CO can further react with H₂O via water gas shift reaction to produce more H₂ within SOFC-H⁺ and thus, the possibility of carbon formation in SOFC-H⁺ can be eliminated and overall system efficiency can be improved. The SOFC hybrid system performance is investigated with respect to important operating conditions, such as temperature, pressure, degree of pre-reforming, inlet fuel velocity, and cell voltage.

7.1 Introduction

From the electrochemical study of SOFC-H⁺ as reported in Chapter VI, it was shown that SOFC-H⁺ provides a higher theoretical performance than SOFC-O²⁻. However its actual performance is much lower. In addition, the performance analysis of the SOFC-H⁺ operating with direct internal reforming (DIR) of methane revealed that the presence of high CO content in the fuel channel would cause a carbon formation and this may hinder the SOFC-H⁺ performance by reducing catalyst activity. To overcome this problem, an external reformer should be included in the SOFC-H⁺ system to fully reform CH₄ to a H₂-rich gas. However, extra CH₄ have to be supplied to the reformer due to a high endothermicity of steam reforming reaction and this results in the reduced overall system efficiency. Alternatively, SOFC-O²⁻ with internal reforming operation of methane can be applied to replace the external

reformer as it produces high-temperature exhaust gas containing unused CO and H₂ together with electrical power (Vollmar et al., 2000).

In general, the exhaust gas obtained from the SOFC is often used in cogeneration applications and bottoming cycles to improve the power generation efficiency, particularly the hybrid system combining an SOFC and a gas turbine (SOFC-GT system) can provide high electrical efficiency reach to 70% (Palsson et al., 2000; Möller et al., 2004; Calise et al., 2006; Haseli et al., 2008). However, since the efficiency of fuel cell that its energy conversion efficiency remains almost constant even as the system output decreases, is generally higher than that of gas turbine, a number of researches have been concentrated on the integration of an SOFC and other fuel cells (Dicks et al., 2000; Yokoo and Take, 2004; Araki et al., 2006; Musa and Paepe, 2008). Yokoo and Take (2004) reported that the system combining an SOFC and a polymer electrolyte fuel cell (SOFC-PEFC) provides the efficiency of 59%. Araki et al. (2006) presented the performance analyses of two-staged SOFCs with serial connection of low and high temperature SOFCs and found that the system efficiency is 50.3%. Musa and Paepe (2008) showed that a combined cycle of two-staged intermediate temperature-SOFCs (IT-SOFCs) can reach the system efficiency of 65.5%.

Although the integration of two fuel cells to improve electrical efficiency was studied by several researchers as mentioned above, the study on a combined SOFC system with different electrolytes (SOFC-O²⁻ and SOFC-H⁺) as proposed in this study (Figure 7.1) has not been reported. The proposed fuel cell system presents some interesting features. Firstly, the SOFC-H⁺ can efficiently use the remaining fuel (H₂ and CO) in the high-temperature exhaust gas of SOFC-O²⁻. Moreover, pretreatment units of CO such as a shift reactor and a selective oxidizer, can be removed from the system because the water gas shift reaction to convert CO to more H₂ can be carried out within SOFC-H⁺. Secondly, more complete fuel utilization of SOFC-H⁺ makes this system possible to be simple and compact by eliminating the need of the afterburner (Zamfirescu and Dincer, 2009).

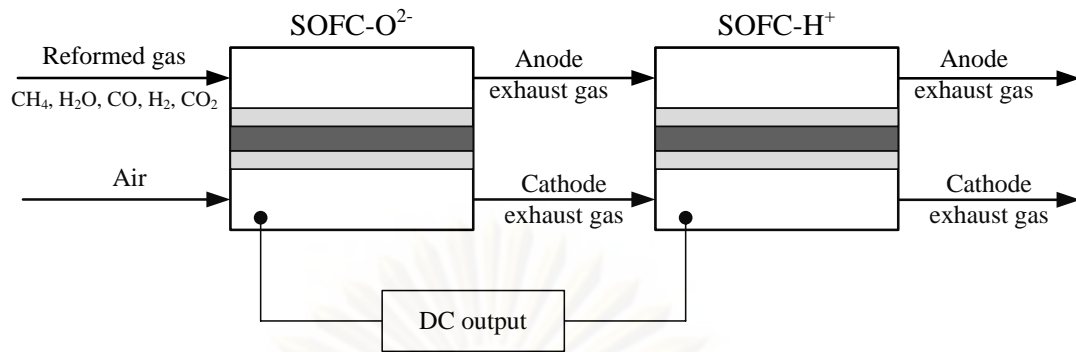


Figure 7.1 Schematic of the SOFC-O²⁻-SOFC-H⁺ system.

In a methane-fed SOFC hybrid system integrating SOFC-O²⁻ and SOFC-H⁺ as shown in Figure 7.1, the SOFC-O²⁻ produces both electrical power and exhaust gas containing useful fuel and other gaseous substances. When the exhaust gas stream is directly supplied to the SOFC-H⁺, the remaining CO can further react with H₂O via water gas shift reaction to produce more H₂, and then H₂ undergoes the electrochemical reaction. As a result, the electrical power of the SOFC hybrid system can be more produced. Due to the lack clarity in the performance of the SOFC-O²⁻-SOFC-H⁺ system, this study aims to investigate the possibility of combining two SOFC stacks, SOFC-O²⁻ and SOFC-H⁺. The performance of the SOFC hybrid system at different operating conditions is primarily evaluated by using SOFC model based on the conservation of mass and a detailed electrochemical model. The analyses of the SOFC system are performed under isothermal condition and negligible energy losses. It should be noted that if all energy losses are taken into account by an exergy analysis (Dincer, 2002; Bavarsad, 2007; Fryda et al., 2008), the real efficiency of SOFC hybrid system will be lower than the predicted one.

7.2 Single SOFC-O²⁻ and SOFC-H⁺ model

7.2.1 SOFC configuration

The basic configuration of a single SOFC-O²⁻ and SOFC-H⁺ has three main parts: a fuel channel, an air channel, and the solid part consisting of a ceramic electrolyte, anode and cathode, as shown in Figure 4.1 in Chapter IV. Both the SOFCs are configured as planar with the same stack sizes. The SOFC composed of Ni-

YSZ|YSZ|YSZ-LSM and Pt|SCYb|Pt are considered for the SOFC-O²⁻ and SOFC-H⁺, respectively.

7.2.2 SOFC operation

In this study, the synthesis gas derived from a gas mixture of CH₄ and H₂O at a ratio of 2 after 30% pre-reforming in an external reformer are considered as fuel whereas air is used as an oxidant for both SOFC-O²⁻ and SOFC-H⁺. The partial reforming of fuel helps to avoid the possibility of a carbon formation on the anode material of SOFC-O²⁻ which is caused by a complete internal reforming (Meusinger et al., 1998). Considering the SOFC with direct internal reforming (DIR), when the partially reformed gas containing of mainly CH₄ and H₂O are fed into the fuel channel, CH₄ is directly reformed within SOFC by a steam reforming reaction (Equation (7.1)) to produce H₂ and CO. CO is further reacted with residual water via a water gas shift reaction (Equation (7.2)) to produce CO₂ and H₂. Hydrogen produced from the above two reactions at the anode undergoes an oxidation reaction and releases electrons to the external circuit (Equation (7.3)). Oxygen (in air) at the cathode side accepts electrons from the external circuit, and undergoes a reduction reaction (Equation (7.4)). The electron flow in the external circuit from the anode to the cathode produces direct-current electricity. Table 1 presents all reactions which are considered in the SOFC-O²⁻ and SOFC-H⁺ models.

7.2.3 SOFC model

Both SOFCs models are based on mass balance and the electrochemical model that relates the fuel and air gas streams composition with the voltage, current density, and other cell variables. The SOFC model previously presented in Chapter IV is summarized in Table 7.2 and Table 7.3. A mathematical model of SOFC is based on the following assumptions: steady state operation, uniform operating temperature and pressure over the fuel cell geometry, and constant cell voltage operation.

Table 7.1 Reactions considered in the SOFC-O²⁻ and SOFC-H⁺ model

Steam reforming reaction	$\text{CH}_4 + \text{H}_2\text{O}$	$\rightarrow 3\text{H}_2 + \text{CO}$	(7.1)
Water gas shift reaction	$\text{CO} + \text{H}_2\text{O}$	$\leftrightarrow \text{H}_2 + \text{CO}_2$	(7.2)
Oxidation reaction	$\text{H}_2 + \text{O}^{2-}$	$\rightarrow \text{H}_2\text{O (anode)} + 2\text{e}^-$	(7.3a)
	H_2	$\rightarrow 2\text{H}^+ + 2\text{e}^-$	(7.3b)
Reduction reaction	$0.5\text{O}_2 + 2\text{e}^-$	$\rightarrow \text{O}^{2-}$	(7.4a)
	$0.5\text{O}_2 + 2\text{H}^+ + 2\text{e}^-$	$\rightarrow \text{H}_2\text{O (cathode)}$	(7.4b)
Overall Electrochemical reaction	$\text{H}_2 + 1/2\text{O}_2$	$\rightarrow \text{H}_2\text{O (anode)}$	(7.5a)
	$\text{H}_2 + 1/2\text{O}_2$	$\rightarrow \text{H}_2\text{O (cathode)}$	(7.5b)

Table 7.2 Steady-state solid oxide fuel cell model: Mass balance***Mass balance in fuel channel***

$$\frac{dC_{i,f}}{dx} = \frac{1}{u_f} \sum_j (v_{i,j} R_j) \frac{1}{h_f} \quad (7.6)$$

$i = \text{CH}_4, \text{H}_2\text{O}$ (at anode side), CO, H_2 , and CO_2

$j =$ steam reforming, water gas shift, and electrochemical reactions

Mass balance in air channel

$$\frac{dC_{i,a}}{dx} = \frac{1}{u_a} \sum_j (v_{i,j} R_j) \frac{1}{h_a} \quad (7.7)$$

$i = \text{O}_2$ for SOFC-O²⁻ and O_2 and H_2O (at cathode side) for SOFC-H⁺

$j =$ electrochemical reaction

Table 7.3 Electrochemical model in SOFC-O²⁻ and SOFC-H⁺***Electrochemical model***

Operating voltage (V):

$$V = E^{\text{OCV}} - \eta_{\text{ohm}} - \eta_{\text{act}} - \eta_{\text{conc}} \quad (7.8)$$

Open-circuit voltage (E^{OCV}):

$$\text{SOFC-O}^{2-}: \quad E_{\text{SOFC-O}}^{\text{OCV}} = E^0 - \frac{\mathfrak{R}T}{2F} \ln \left(\frac{p_{\text{H}_2\text{O}(\text{an})}}{p_{\text{H}_2(\text{an})} p_{\text{O}_2(\text{ca})}^{0.5}} \right) \quad (7.9)$$

$$\text{SOFC-H}^+: \quad E_{\text{SOFC-H}}^{\text{OCV}} = E^0 - \frac{\mathfrak{R}T}{2F} \ln \left(\frac{p_{\text{H}_2\text{O}(\text{ca})}}{p_{\text{H}_2(\text{an})} p_{\text{O}_2(\text{ca})}^{0.5}} \right) \quad (7.10)$$

Ohmic loss (η_{ohm}):

$$\eta_{\text{ohm}} = i(\tau_{\text{ele}} / \sigma_{\text{ele}}) \quad (7.11)$$

where $\sigma_{\text{ele,SOFC-O}} = 33.4 \times 10^3 \exp(-10300/T)$

$$\sigma_{\text{ele,SOFC-H}} = 225.92 \exp(-6300/T)$$

Activation overpotential (η_{act}):

$$i = i_{0,\text{electrode}} \left[\exp \left(\frac{\alpha n F}{\mathfrak{R}T} \eta_{\text{act,electrode}} \right) - \exp \left(- \frac{(1-\alpha) n F}{\mathfrak{R}T} \eta_{\text{act,electrode}} \right) \right] \quad (7.12)$$

Concentration overpotential (η_{conc}):

$$\text{SOFC-O}^{2-}: \quad \eta_{\text{conc,SOFC-O}} = \frac{\mathfrak{R}T}{2F} \ln \left(\frac{p_{\text{H}_2\text{O}(\text{an})}^{\text{I}} p_{\text{H}_2(\text{an})}}{p_{\text{H}_2\text{O}(\text{an})} p_{\text{H}_2(\text{an})}^{\text{I}}} \right) + \frac{\mathfrak{R}T}{4F} \ln \left(\frac{p_{\text{O}_2(\text{ca})}}{p_{\text{O}_2(\text{ca})}^{\text{I}}} \right) \quad (7.13)$$

$$\text{SOFC-H}^+: \quad \eta_{\text{conc,SOFC-H}} = \frac{\mathfrak{R}T}{2F} \ln \left(\frac{p_{\text{H}_2(\text{an})}}{p_{\text{H}_2(\text{an})}^{\text{I}}} \right) + \frac{\mathfrak{R}T}{2F} \ln \left(\left(\frac{p_{\text{O}_2(\text{ca})}}{p_{\text{O}_2(\text{ca})}^{\text{I}}} \right)^{0.5} \frac{p_{\text{H}_2\text{O}(\text{ca})}^{\text{I}}}{p_{\text{H}_2\text{O}(\text{ca})}} \right) \quad (7.14)$$

Table 7.4 The values of electrode exchange current densities ($i_{0,\text{electrode}}$) for computing the activation overpotential

SOFC Type	$i_{0,\text{anode}} \text{ (A m}^{-2}\text{)}$	$i_{0,\text{cathode}} \text{ (A m}^{-2}\text{)}$
SOFC-O ²⁻	$6.54 \times 10^{11} \times \frac{\mathfrak{R}T}{2F} \exp\left(-\frac{1.40 \times 10^5}{\mathfrak{R}T}\right)$	$2.35 \times 10^{11} \times \frac{\mathfrak{R}T}{2F} \exp\left(-\frac{1.37 \times 10^5}{\mathfrak{R}T}\right)$
SOFC-H ⁺	800	800

For the SOFC-O²⁻, it is noted that the approximate expression proposed by Aguiar et al. (2004) was used to determine the value of the exchange-current density, which depends only on the operating temperature. In case of the SOFC-H⁺, the concentration dependency of the exchange-current density is neglected since the rate expression is not available. In addition, the equal exchange-current density on the anode and cathode is assumed. Table 7.4 summarizes the values of the exchange-current density for computing the activation overpotential.

The partial pressures of hydrogen ($p_{\text{H}_2}^I$), water vapor ($p_{\text{H}_2\text{O}}^I$) and oxygen ($p_{\text{O}_2}^I$) at the electrode|electrolyte interfaces can be derived from Fick's model: the electrochemical reaction occurs at the electrode|electrolyte interfaces; the diffusion rate of reactants to the interfaces is equal to the rate of electrochemical reaction:

$$\text{SOFC-O}^{2-}: \quad p_{\text{H}_2(\text{an})}^I = p_{\text{H}_2(\text{an})} - \frac{\mathfrak{R}T\tau_{\text{an}}}{2FD_{\text{an,eff}}} i \quad (7.15)$$

$$p_{\text{H}_2\text{O}(\text{an})}^I = p_{\text{H}_2\text{O}(\text{an})} + \frac{\mathfrak{R}T\tau_{\text{an}}}{2FD_{\text{an,eff}}} i \quad (7.16)$$

$$p_{\text{O}_2(\text{ca})}^I = P - (P - p_{\text{O}_2(\text{ca})}) \exp\left(\frac{\mathfrak{R}T\tau_{\text{ca}}}{4FD_{\text{ca,eff}}P} i\right) \quad (7.17)$$

$$\text{SOFC-H}^+: \quad p_{\text{H}_2(\text{an})}^{\text{I}} = P - (P - p_{\text{H}_2(\text{an})}) \exp\left(\frac{\mathfrak{R}T\tau_{\text{an}}}{2FD_{\text{an,eff}}P}i\right) \quad (7.18)$$

$$p_{\text{O}_2(\text{ca})}^{\text{I}} = p_{\text{O}_2(\text{ca})} - \frac{\mathfrak{R}T\tau_{\text{ca}}}{2FD_{\text{ca,eff}}}i \quad (7.19)$$

$$p_{\text{H}_2\text{O}(\text{ca})}^{\text{I}} = p_{\text{H}_2\text{O}(\text{ca})} + \frac{\mathfrak{R}T\tau_{\text{ca}}}{4FD_{\text{ca,eff}}}i \quad (7.20)$$

The model equations of SOFC consisting of mass balances and electrochemical model are solved to predict the performance of SOFC in terms of average current density (i_{ave}), power density (P_{SOFC}) and the efficiency ($\varepsilon_{\text{SOFC}}$) of fuel cell. When an operating cell voltage (V) is pre-specified, an average current density is calculated from the distribution of current density along the cell length. The operating cell voltage and average current density obtained are used to calculate the power density and the efficiency as shown in the following expressions:

$$P_{\text{SOFC-O}} = i_{\text{ave,SOFC-O}}V \quad (7.21)$$

$$P_{\text{SOFC-H}} = i_{\text{ave,SOFC-H}}V \quad (7.22)$$

$$\varepsilon_{\text{SOFC-O}} = \frac{i_{\text{aveSOFC-O}}VLW}{(y_{\text{CH}_4}^{\text{in}}LHV_{\text{CH}_4} + y_{\text{H}_2}^{\text{in}}LHV_{\text{H}_2} + y_{\text{CO}}^{\text{in}}LHV_{\text{CO}})F_{\text{fuel,SOFC-O}}^{\text{in}}} \quad (7.23)$$

$$\varepsilon_{\text{SOFC-H}} = \frac{i_{\text{aveSOFC-H}}VLW}{y_{\text{H}_2}^{\text{in}}LHV_{\text{H}_2}F_{\text{fuel,SOFC-H}}^{\text{in}}} \quad (7.24)$$

7.3 SOFC-O²⁻-SOFC-H⁺ system model

As shown in Figure 7.1, the synthesis gas partially reformed in an external reformer is supplied to the SOFC-O²⁻ at the fuel channel where steam reforming and water gas shift reactions occur. At the same time, the electrochemical reaction is carried out when oxygen is simultaneously supplied at the air channel. The SOFC-O²⁻ can produce both electrical power and high-temperature exhaust gas containing H₂O, CO, H₂ and CO₂. The anode exhaust gas from SOFC-O²⁻ is continuously delivered to

the SOFC-H⁺ without the requirement of external reformers and shift reactors. This is because the amount of H₂ contained in the anode exhaust gas is sufficient to carry out the electrochemical reaction and the low amount of CO (less than 10%) can further reacted with H₂O via water gas shift reaction to produce more H₂ in the SOFC-H⁺. After the anode exhaust gas from SOFC-O²⁻ is fed into the SOFC-H⁺, H₂ contained in the anode exhaust gas and produced from the water gas shift reaction reacts with O₂ from the cathode exhaust gas of the SOFC-O²⁻ to produce additional electrical power. The power density of the SOFC-O²⁻-SOFC-H⁺ system, P_{system} , and the overall efficiency, $\varepsilon_{\text{system}}$, can be calculated by

$$P_{\text{System}} = P_{\text{SOFC-O}} + P_{\text{SOFC-H}} \quad (7.19)$$

$$\varepsilon_{\text{System}} = \frac{P_{\text{System}} LW}{(y_{\text{CH}_4}^{\text{in}} LHV_{\text{CH}_4} + y_{\text{H}_2}^{\text{in}} LHV_{\text{H}_2} + y_{\text{CO}}^{\text{in}} LHV_{\text{CO}}) F_{\text{fuel,SOFC-O}}^{\text{in}}} \quad (7.20)$$

7.4 Results and discussion

Table 7.5 shows the values of operating conditions and cell geometry used in the performance analysis of SOFC-O²⁻-SOFC-H⁺ system at the standard condition, which are derived from the data available in literatures (Aguiar et al., 2004).

7.4.1 Performance of a single SOFC-O²⁻ and SOFC-H⁺

Considering the changing of gas composition along the cell length of the SOFC-O²⁻ and SOFC-H⁺, it can be found that the production of H₂O at the fuel channel of SOFC-O²⁻ can be beneficially used in converting CO through the water gas shift reaction. At the exit of the fuel channel, the fuel consists of 55% H₂O, 7.3% CO, 25.2% H₂ and 12.5% CO₂ whereas the oxidant consists of 18.1% O₂ and 81.9% N₂. Although the generation of H₂O at the air channel of SOFC-H⁺ can improve the open-circuit voltage, less H₂O at the fuel channel is insufficient to convert CO into H₂ and thus, the high content of CO is observed. At the exit of the fuel channel of the SOFC-H⁺, the fuel consists of 20.2% H₂O, 20.2% CO, 49.6% H₂ and 10% CO₂ whereas the oxidant consists of 5.2% H₂O, 17.9% O₂ and 76.9% N₂.

Table 7.5 Operation conditions used in the performance analysis of SOFC-O²⁻-SOFC-H⁺ system

Parameters	Value
<i>Operating conditions</i>	
Operating temperature, T	750°C
Operating pressure, P	1.0 atm
Fuel feed to SOFC-O ²⁻	Steam/Carbon = 2, 30% pre-reforming
Air feed to SOFC-O ²⁻	21 % O ₂ , 79% N ₂
Air feed to SOFC-H ⁺	0.1% H ₂ O, 20.9% O ₂ , 79% N ₂
Cell voltage	0.65 V
Inlet fuel velocity	2 m/s
Inlet air velocity	18 m/s
<i>Dimensions of cell element</i>	
Cell length, L	0.4 m
Cell width, W	0.1 m
Fuel channel height, h_f	1 mm
Air channel height, h_a	1 mm
Anode thickness, τ_{an}	500 μm
Cathode thickness, τ_{ca}	50 μm
Electrolyte thickness, τ_{ele}	20 μm

Figures 7.2(a)-(b) show the distributions of all individual voltage losses along the cell length in the SOFC-O²⁻ and SOFC-H⁺, respectively. As expected, the open-circuit voltage of the SOFC-H⁺ is considerably higher than the SOFC-O²⁻. Due to the higher internal losses presented in the SOFC-H⁺, the SOFC-H⁺ provides lower actual performance than the SOFC-O²⁻ under the same operating conditions. In order to explain the influence of the electrolyte types on the cell performance, the relative magnitude of all individual voltage losses in each type of SOFC is given in Figure 7.3. Considering the ohmic loss, it can be seen that the ohmic loss of the SOFC-H⁺ is much higher than the SOFC-O²⁻ due to lower conductivity of the proton-conducting electrolyte. For the concentration overpotential, the SOFC-O²⁻ has higher anode concentration overpotential compared with the SOFC-H⁺. This is because H₂O generated in the anode side for the SOFC-O²⁻ inhibits the diffusion of H₂ from the anode site to the interface. While H₂ is only presented in the anode side for the SOFC-H⁺, the faster transport of H₂ leads to lower concentration overpotential. Unlike anode concentration overpotential, the cathode concentration overpotential of SOFC-H⁺ is much higher than that of SOFC-O²⁻. Due to the transport of the reactant O₂ and the product H₂O in the cathode side of the SOFC-H⁺, the H₂O molecules hinder the transport of O₂, resulting in high concentration overpotential.

From the above results, it can be concluded that the current density obtained from SOFC-O²⁻ is higher than the SOFC-H⁺ under specified operating conditions. As a result, the power density and the efficiency of the SOFC-O²⁻ are higher than those of SOFC-H⁺ as shown in Table 7.6. It is noted that for the SOFC-O²⁻-SOFC-H⁺ system, a low degree of fuel utilization of SOFC-O²⁻ should be maintained in order to provide the exhaust gas with higher useful fuel for the SOFC-H⁺ and thus, the low efficiency of SOFC-O²⁻ and high unused H₂ obtained in this work is reasonable for applying to the SOFC-O²⁻-SOFC-H⁺ system.

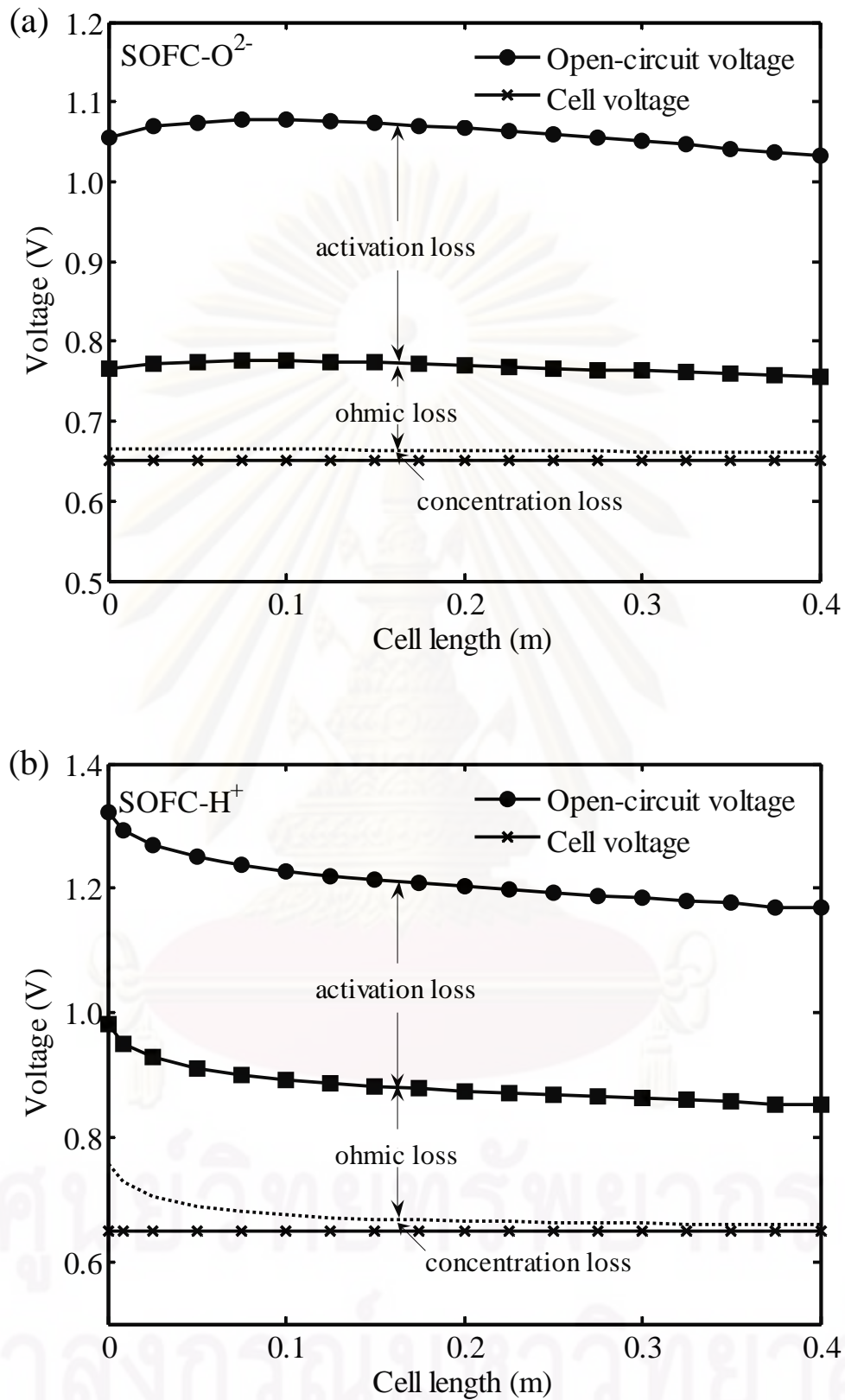


Figure 7.2 Distributions of all voltage losses in: (a) SOFC-O²⁻, and (b) SOFC-H⁺.

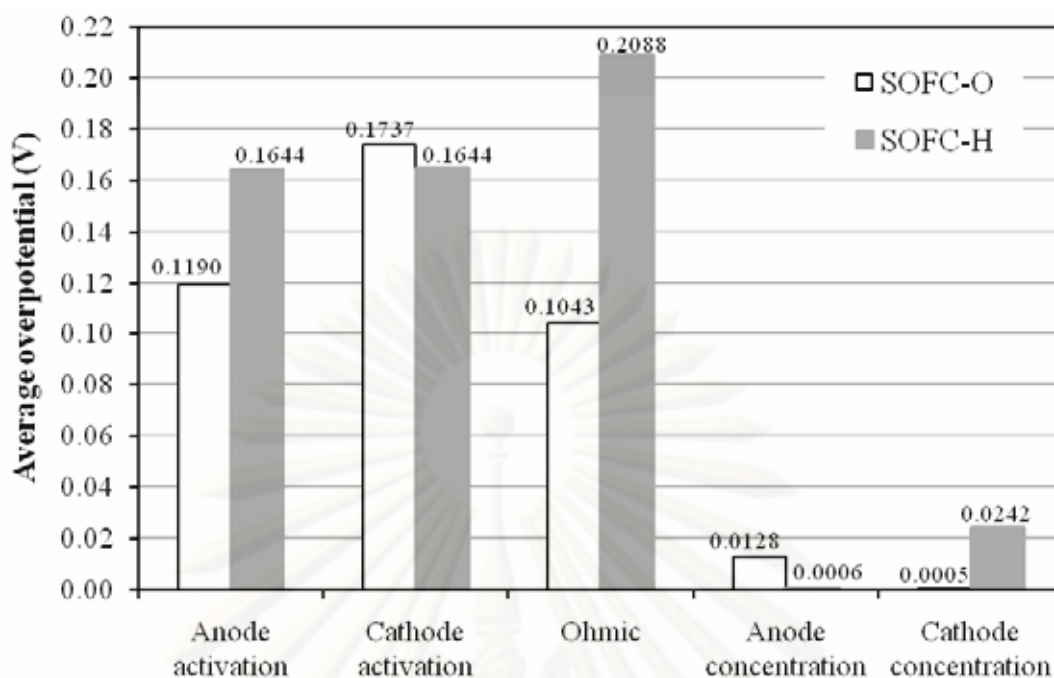


Figure 7.3 Comparison the results of all voltage losses in SOFC-O²⁻ and SOFC-H⁺.

Table 7.6 Performance results of single-SOFC-O²⁻ and SOFC-H⁺ and SOFC hybrid system

Results	SOFC-O ²⁻	SOFC-H ⁺	SOFC hybrid
			system
Average current density (A cm ⁻²)	0.74	0.52	1.18
Power density (W cm ⁻²)	0.48	0.33	0.77
Efficiency (%)	33.84	23.45	54.11

7.4.2 Performance of a SOFC-O²⁻-SOFC-H⁺ system

For the SOFC-O²⁻-SOFC-H⁺ system (denoted as SOFC hybrid system), the exhaust gas from the SOFC-O²⁻ is used as the inlet fuel for the SOFC-H⁺. The gas composition at the outlet of the SOFC-O²⁻ consists of 55% H₂O, 7.3% CO, 25.2% H₂ and 12.5% CO₂. It can be seen that CH₄ is fully reformed within the SOFC-O²⁻ and thus, the remaining CO and H₂ is considered to continue the water gas shift and electrochemical reactions in the fuel channel of the SOFC-H⁺, respectively. Under the standard operating conditions, it is found that the SOFC-O²⁻-SOFC-H⁺ system have a higher efficiency compared to the use of a single SOFC as shown in Table 7.6. The total power density and overall efficiency of SOFC hybrid system are 0.77 W cm⁻² and 54.11%, respectively. In comparison with the efficiency of the single SOFC-H⁺ ($\epsilon_{\text{SOFC-H}} = 23.45\%$), it can be seen that the overall system efficiency is improved by 57.66%.

7.4.2.1 Effect of operating temperature

In this section, the effect of operating temperatures on the efficiencies of the SOFC-O²⁻, SOFC-H⁺ and SOFC hybrid system are studied as shown in Figure 7.4. Since a decrease in operating temperatures decreases the rate of electrochemical reaction; the consumption of hydrogen is lower and thus, the current density also decreases. Considering cell voltage losses, it is also found that the decreased operating temperature causes an increase in voltage losses, particularly in ohmic and activation losses. Therefore, the efficiencies of all the SOFC systems are decreased with decreasing temperature. It can be observed that the efficiency of the SOFC-H⁺ is superior to that of SOFC-O²⁻ when the operating temperature is lower (650-710°C), implying the proton conducting electrolyte can be enhanced at lower temperatures.

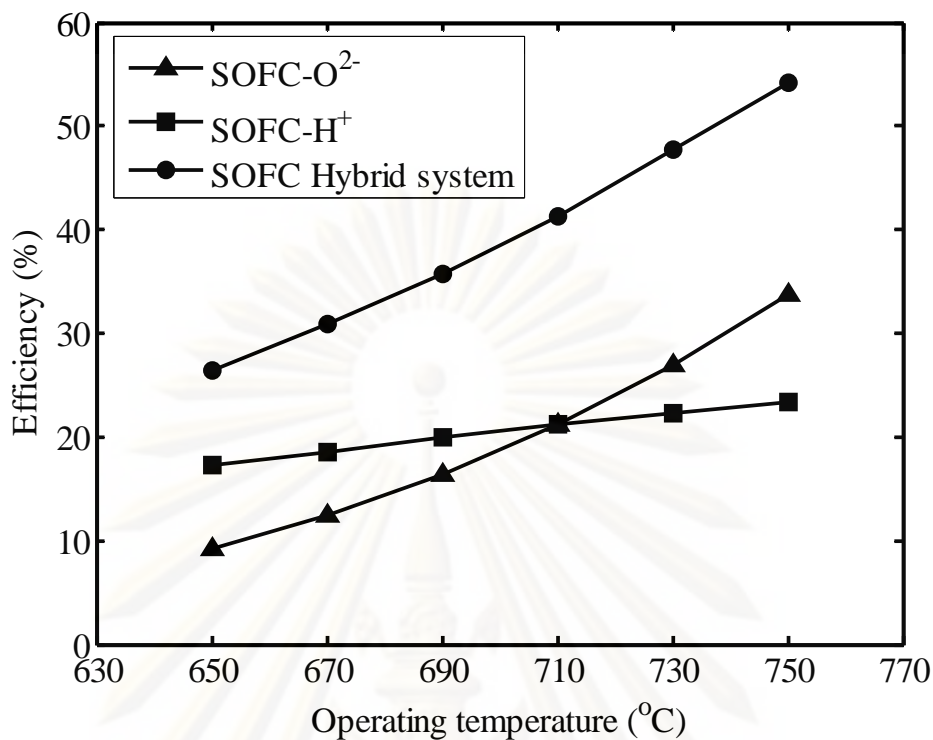


Figure 7.4 Effect of operating temperature on the efficiency of the SOFC-O²⁻, SOFC-H⁺, and SOFC hybrid system.

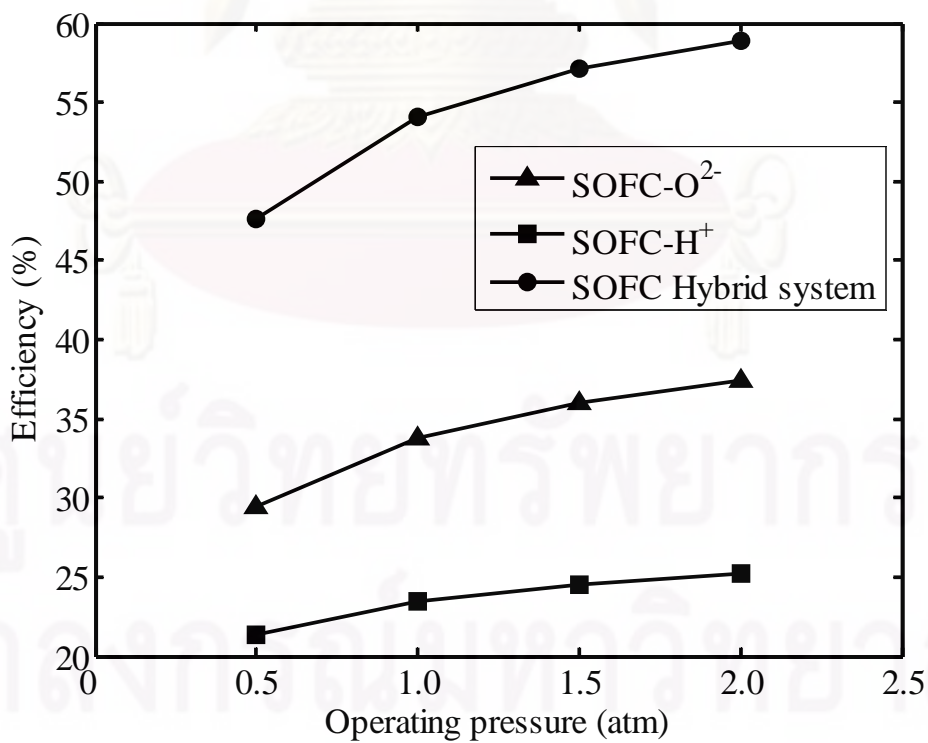


Figure 7.5 Effect of operating pressure on the efficiency of the SOFC-O²⁻, SOFC-H⁺, and SOFC hybrid system.

7.4.2.2 Effect of operating pressure

Figure 7.5 illustrates the efficiencies of the SOFC-O²⁻, SOFC-H⁺ and SOFC hybrid system as a function of operating pressures. It is found that the efficiency of SOFC can be improved by increasing operating pressure. Higher pressure operation increases the partial pressure of gas in the system and thus, higher open-circuit voltage and current density can be achieved. In addition, the transports of gas to the interface are higher and this results in the lower concentration overpotential.

7.4.2.3 Effect of degree of pre-reforming

In this section, the effect of the degree of pre-reforming of CH₄ on the efficiencies of the SOFC-O²⁻, SOFC-H⁺ and SOFC hybrid system is investigated. According to Figure 7.6, the efficiency of SOFC increases with increasing degree of pre-reforming. This is because higher degree of pre-reforming results in an increase in the H₂ concentration in the fuel composition, leading to larger open-circuit voltage and thus, current density is more produced. In addition, higher H₂ easily diffuse to the interface, thereby decreasing anode concentration overpotential.

7.4.2.4 Effect of inlet fuel velocity

Generally, an increase in the inlet fuel velocity decreases the consumption of fuel, resulting in a higher H₂ concentration. This causes an increase in open-circuit voltage and current density. However, since the molar flow rate of fuel is also much higher when inlet fuel velocity increases and thus, the cell efficiencies of the SOFC-O²⁻, SOFC-H⁺ and SOFC hybrid system are considerably decreased, as shown in Figure 7.7.

ศูนย์วิทยทรัพยากร
จุฬาลงกรณ์มหาวิทยาลัย

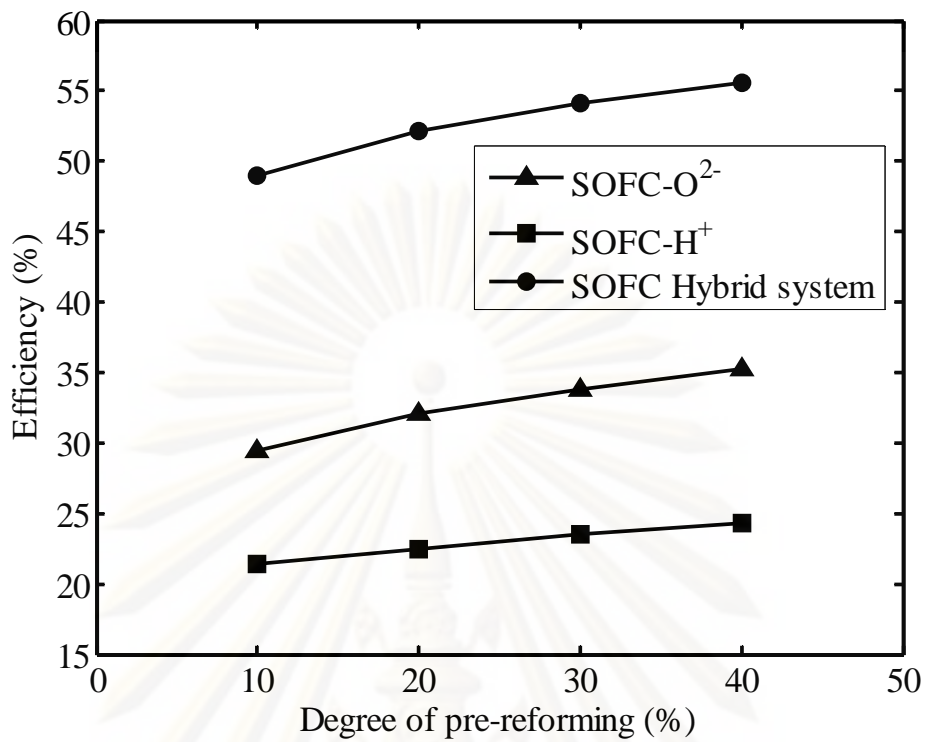


Figure 7.6 Effect of degree of pre-reforming on the efficiency of the SOFC-O²⁻, SOFC-H⁺, and SOFC hybrid system.

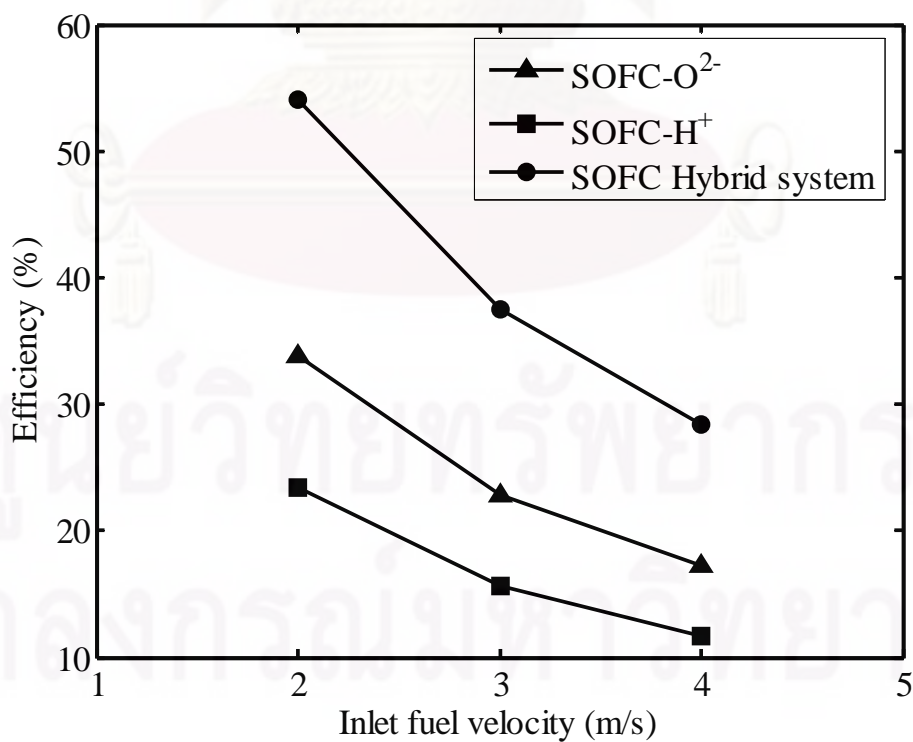


Figure 7.7. Effect of inlet fuel velocity on the efficiency of the SOFC-O²⁻, SOFC-H⁺, and SOFC hybrid system.

7.4.2.5 Effect of cell voltage

Due to the SOFC operated with a constant cell voltage, the change of cell voltage in the SOFC hybrid system is studied. The operating cell voltage of SOFC-O²⁻ or SOFC-H⁺ in the SOFC hybrid system is varied from 0.65 to 0.75 V. The results show that the average current density and the power density decrease with an increase in cell voltage, due to the increased voltage losses. This results in the reduced efficiency of SOFC hybrid system when the cell voltage of the SOFC-O²⁻, SOFC-H⁺, or both the SOFCs in the SOFC hybrid system increases, as shown in Figure 7.8. Increasing cell voltage in the SOFC-O²⁻ lowers the efficiency of the SOFC hybrid system compared to that in the SOFC-H⁺. This is because the efficiencies of both the SOFC-O²⁻ and SOFC-H⁺ are reduced with increasing cell voltage of the SOFC-O²⁻ whereas only efficiency of SOFC-H⁺ is decreased when the cell voltage of the SOFC-H⁺ increases. It is noted that the efficiency of the SOFC-O²⁻ is an important factor which has an effect on the overall efficient of the SOFC hybrid system.

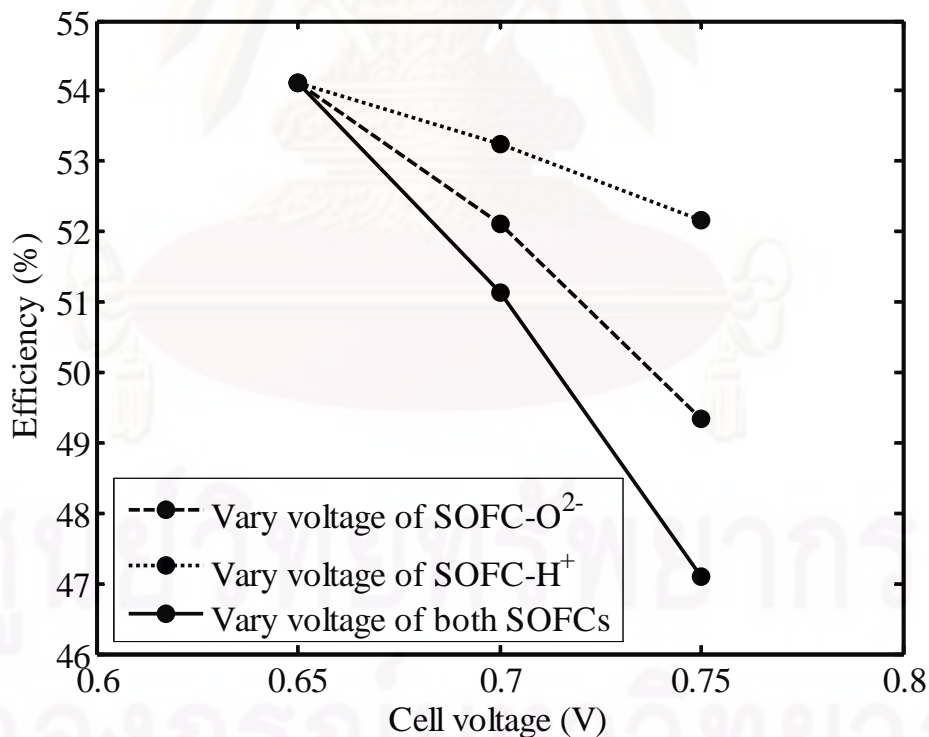


Figure 7.8 Effect of changing the cell voltage in the SOFC-O²⁻, SOFC-H⁺, and SOFC hybrid system on the efficiency of the SOFC hybrid system.

7.5 Conclusion

The performance analysis of a methane-fed SOFC hybrid system combining SOFC-O²⁻ and SOFC-H⁺ is presented in this study. In the SOFC hybrid system, the exhaust gas from SOFC-O²⁻ is directly fed into SOFC-H⁺. The simulation result shows that the SOFC hybrid system provides the electrical efficiency of 54.11% whereas a single SOFC-O²⁻ and SOFC-H⁺ has the efficiency of 33.84% and 22.45%, respectively. The performance of the SOFC hybrid system at different temperature, pressure, degree of pre-reforming, inlet fuel velocity and cell voltage is also presented. It is found that increasing the operating temperature, pressure, degree of pre-reforming as well as decreasing inlet fuel velocity, cell voltage can improve the efficiency of the SOFC system. Interestingly, it is shown that the efficiency of SOFC-O²⁻ is an important factor having an effect on the overall efficient of the SOFC hybrid system. Design of SOFC-O²⁻ for producing both electrical power and exhaust gas for SOFC-H⁺ should be significantly considered in the SOFC hybrid system.

CHAPTER VIII

CONCLUSION AND RECOMMENDATION

8.1 Conclusion

The objective of this research aims to analyze the performance of a planar solid oxide fuel cell fed by methane with direct internal reforming under an intermediate temperature operation. The electrolyte material used in SOFC was focused on an oxygen ion-conducting and a proton-conducting electrolyte (denoted as SOFC-O²⁻ and SOFC-H⁺, respectively). A detailed electrochemical model of both the SOFC-O²⁻ and SOFC-H⁺ which takes into account all voltage losses (i.e., ohmic, activation and concentration losses) was employed to analyze the characteristics performance of SOFC in terms of operating voltage, power density and efficiency. The influence of the role of support structure (anode-, cathode- and electrolyte-supported SOFC) and design parameters (i.e., cell component thickness, electrode porosity and electrode pore size) was also investigated.

When the optimal design of SOFC-O²⁻ and SOFC-H⁺ was determined, the performance of SOFC-O²⁻ and SOFC-H⁺ fed by methane under a direct internal reforming operation and isothermal condition was analyzed based on a one-dimensional steady-state fuel cell model coupled with a detailed electrochemical model taking into account all various voltage losses. The model was employed to analyze the cell performance (operating voltage, power density and efficiency) as well as its behavior (gas composition and current density profiles) over a wider range of operating conditions (i.e., operating temperature, operating pressure, gas composition and gas velocity).

In addition, this work studied the performance of a combined SOFC system with different electrolytes (SOFC-O²⁻ and SOFC-H⁺). The effect of operating conditions, such as temperature, pressure, degree of pre-reforming, inlet fuel velocity, and cell voltage on SOFC hybrid system was also investigated.

The main issues studied in this research are summarized as in the following subsections.

8.1.1 Solid oxide fuel cell based on oxygen ion-conducting electrolyte

A numerical study of the performance of a SOFC based on oxygen ion-conducting electrolyte with different support structures was presented in this work. The simulation results showed that an anode-supported SOFC provides the best characteristics performance compared with a cathode- and electrolyte-supported SOFC. Further, it was found that the performance of an anode-supported SOFC could be improved by decreasing the electrolyte and anode thickness as well as increasing electrode porosity and pore size. However, it should be noted that although the anode-supported SOFC, which has thinner electrolyte and is suitable for low temperature operation, is used with the aim to decrease an ohmic loss, it is still relatively major loss in the fuel cell. In order to improve SOFC performance, an electrolyte with high ionic conductivity is required.

For the performance analysis of an anode-supported SOFC fed by methane with direct internal reforming, the results showed that when SOFC is operated at the standard conditions ($V = 0.70$ V, $T = 1023$ K, and $P = 1$ atm), the power density of 0.40 W cm⁻² and fuel efficiency of 52% were obtained. The fuel cell efficiency of the anode-supported SOFC could be improved by either increasing temperature, pressure, degree of pre-reforming and steam to carbon ratio or decreasing inlet flow velocity. However, a choice of degree of pre-reforming, steam to carbon ratio and inlet flow velocity has to be carefully selected to optimize fuel cell efficiency as well as power density.

8.1.2 Solid oxide fuel cell based on proton-conducting electrolyte

In case of SOFC based on proton-conducting electrolyte (SOFC-H⁺), the simulation results showed that an anode-supported SOFC-H⁺ provides the best electrical performance in terms of an achievable power density and a wider range of operating current density. Considering the anode-supported SOFC-H⁺, the ohmic loss is still a major voltage loss due to the low protonic conductivity of electrolyte. As

expected, decreasing electrolyte and cathode thickness and increasing the electrode pore size and porosity can improve the performance of SOFC-H⁺.

Next, a performance analysis of an anode-supported SOFC-H⁺ with proton-conducting electrolyte (SOFC-H⁺) operated under direct internal reforming of methane was performed. Under the standard condition ($V = 0.70$ V, $T = 1073$ K, and $P = 1$ atm), the power density of 0.34 W cm⁻², average current density of 0.49 A cm⁻², fuel cell efficiency of 47%, and fuel utilization of 0.70 were predicted. However, high CO content in the fuel channel was observed and this may deteriorate the SOFC-H⁺ performance by reducing catalyst activity. From the simulation results, it was found that the content of CO at the fuel channel outlet can be reduced with the increased S/C ratio. Moreover, the results showed that increases in operating temperature and pressure enhance the electrical efficiency of the SOFC-H⁺ whereas the effect of the increased water content in oxidant shows an opposite trend.

8.1.3 Performance comparisons between SOFC-O²⁻ and SOFC-H⁺

Since this work was focused on both the SOFC-O²⁻ and SOFC-H⁺, their performance should be summarized. Under same operating conditions ($T = 1073$ K, and $P = 1$ atm), it was found that the theoretical performance of SOFC-H⁺ is superior to that of SOFC-O²⁻. However, the actual performance of SOFC-H⁺ is much lower than SOFC-O²⁻. This is mainly caused by that the ohmic loss of the SOFC-H⁺ is much higher than the SOFC-O²⁻ due to a lower conductivity of the proton-conducting electrolyte. In addition, the activation overpotential of the SOFC-H⁺ is more dominant due to the lower exchange current density. Considering the concentration overpotential, although the SOFC-H⁺ has lower anode concentration overpotential compared with the SOFC-O²⁻, the cathode concentration overpotential of SOFC-H⁺ is much higher than that of SOFC-O²⁻ due to the presence of H₂O in the cathode side. To enhance the performance of SOFC-H⁺, the ohmic and other voltage losses need to be reduced simultaneously.

For the performance of SOFC-O²⁻ and SOFC-H⁺ under direct internal reforming of methane, it was found that the production of H₂O at the fuel channel of SOFC-O²⁻ can be beneficially used in converting CO through the water gas shift reaction. Conversely, the generation of H₂O at the air channel of SOFC-H⁺ results in

less H₂O at the fuel channel; it is insufficient to convert CO into H₂ and thus, the high content of CO is observed. It was noted that the SOFC-H⁺ with DIR operation was risk to the carbon formation over the anode surface leading to the reduced catalyst activity and thus, the SOFC-H⁺ performance may be deteriorated, particularly, the carbon poisons on platinum electrode.

8.1.4 A hybrid system of solid oxide fuel cells with different electrolytes

Due to some problems associated with low actual performance and the presence of high CO content at the fuel channel of SOFC-H⁺, the integration between SOFC-O²⁻ and SOFC-H⁺ was proposed in this work. SOFC-O²⁻ with direct internal reforming of methane can produce electrical power as well as high-temperature exhaust gas containing remaining fuel, i.e., H₂ and CO. This exhaust gas can be directly fed into SOFC-H⁺. This because the remaining CO can further react with H₂O via water gas-shift reaction to produce more H₂ within SOFC-H⁺ and thus, the possibility of carbon formation in SOFC-H⁺ can be eliminated. From the performance analysis of a methane-fed SOFC hybrid system combining SOFC-O²⁻ and SOFC-H⁺, it was found that the SOFC hybrid system provides higher electrical efficiency of 54.11% compared with a single SOFC-O²⁻ and SOFC-H⁺ (33.84% and 22.45%, respectively). The performance of the SOFC hybrid system at different temperature, pressure, degree of pre-reforming, inlet fuel velocity and cell voltage was also investigated. It was found that increasing operating temperature, operating pressure, degree of pre-reforming as well as decreasing inlet fuel velocity and cell voltage can improve the efficiency of the SOFC system. Interestingly, it was shown that the efficiency of SOFC-O²⁻ is an important factor having an effect on the overall efficient of the SOFC hybrid system. Design of SOFC-O²⁻ for producing both electrical power and exhaust gas for SOFC-H⁺ should be significantly considered in the SOFC hybrid system.

8.2 Recommendations

(1) Although an anode-supported structure of SOFC-O²⁻ and SOFC-H⁺ provides the best fuel cell performance, the use of thicker anode leads to an increase in concentration loss. The optimization of anode thickness is useful for determining the maximum performance under specific conditions.

(2) In this work, the performance analysis of a planar SOFC is based on isothermal operation. However, it is well known that the cell temperature has an effect on its performance. The future work should concentrate on the analysis of SOFC under non-isothermal condition.

(2) The performance evaluation of the SOFC hybrid system presented in this work is based on the conservation of mass and a detailed electrochemical model. It should be noted that if all energy losses are taken into account for an exergy analysis, the real efficiency of SOFC hybrid system would be lower than the predicted one. In the future work, exergy analysis should be included to clarify the advantages of a combining SOFC-O²⁻ and SOFC-H⁺.

REFERENCES

- Achenbach, E., Three-dimensional and time-dependent simulation of a planar solid oxide fuel cell stack. Journal of Power Sources 49 (1994) : 333–348.
- Achenbach, E., and Riensche, E., Methane/steam reforming kinetics for solid oxide fuel cells. Journal of Power Sources 52 (1994) : 283–288.
- Aguiar, P., Chadwick, D., and Kershenbaum, L., Modelling of an indirect internal reforming solid oxide fuel cell. Chemical Engineering Science 57 (2002) : 1665–1677.
- Aguiar, P., Adjiman, C.S., and Brandon, N.P., Anode-supported intermediate-temperature direct internal reforming solid oxide fuel cell. I : Model-based steady-state performance. Journal of Power Sources 138 (2004) : 120-136.
- Araki, T., Ohbaa, T., Takezawa, S., Ondaa, K., Sakaki, Y., Cycle analysis of planar SOFC power generation with serial connection of low and high temperature SOFCs. Journal of Power Sources 158 (2006) : 52–59.
- Assabumrungrat, S., Pavarajarn, V., Charojrochkul, S., and Laosiripojana, N., Thermodynamic analysis for a solid oxide fuel cell with direct internal reforming fueled by ethanol. Chemical Engineering Science 59 (2004) : 6015-6020.
- Assabumrungrat, S., Laosiripojanam N., Pavarajarn, V., Sangtongkitcharoen, W., Tangjitmatee, A., and Prasertthdam, P., Thermodynamic analysis of carbon formation in a solid oxide fuel cell with a direct internal reformer fuelled by methanol. Journal of Power Sources 139 (2005) : 55–60.
- Bavarsad, P.G., Energy and exergy analysis of internal reforming solid oxide fuel cell-gas turbine hybrid system. International Journal of Hydrogen Energy 32 (2007) : 4591-4599.
- Bird, R.B., Stewart, W.E., and Lightfoot, E.N., Transport Phenomena, Wiley : 2nd Ed., 2006.

- Burt, A.C., Celik, I.B., Gemmen, R.S., and Smirnov, A.V., A numerical study of cell-to-cell variations in a sofc stack. Journal of Power Sources 126 (2004) : 76–87.
- Calise, F., Palombo, A., and Vanoli, L., Design and partial load exergy analysis of hybrid SOFC–GT power plant. Journal of Power Sources 158 (2006) : 225–244.
- Campanari, S., and Iora, P., Definition and sensitivity analysis of a finite volume SOFC model for a tubular cell geometry. Journal of Power Sources 132 : (2004) 113–126.
- Chan, S.H., Khor, K.A., and Xia, Z.T., A complete polarization model of a solid oxide fuel cell and its sensitivity to the change of cell component thickness. Journal of Power Sources 93 (2001) : 130–140.
- Chen, X.J., Liu, Q.L., Chan, S.H., Brandon, N.P., and Khor, K.A., High performance cathode-supported SOFC with perovskite anode operating in weakly humidified hydrogen and methane. Electrochemistry Communications 9 (2007) : 767-772.
- Clarke, S.H., Dicks, A.L., Pointon K., Smith T.A., and Swann A., Catalytic aspects of the steam reforming of hydrocarbons in internal reforming fuel cells. Catalysis Today 38 (1997) : 411–423.
- Costamagna, P., Selimovic, A., Borghi, M.D., and Agnew, G., Electrochemical model of the integrated planar solid oxide fuel cell (IP-SOFC). Chemical Engineering Journal 102 (2004) : 61–69.
- Coors, W.G., Protonic ceramic fuel cells for high-efficiency operation with methane. Journal of Power Sources 118 (2003) : 150–156.
- Demin, A., and Tsiakaras, P., Thermodynamic analysis of a hydrogen fed solid oxide fuel cell based on a proton conductor. International Journal of Hydrogen Energy 26 (2001) : 1103–1108.
- Demin, A., Tsiakaras, P., Sobyenin, V., and Hramova, S., Thermodynamic analysis of a methane fed SOFC system based on a protonic conductor. Solid State Ionics 152– 153 (2002) : 555– 560.

- Dicks, A.L., Fellows, R.G., Mescal, C.M., and Seymour, C., A study of SOFC–PEM hybrid systems. Journal of Power Sources 86 (2000) : 501-506.
- Dicks, A.L., Pointon, K.D., and Siddle, A., Intrinsic reaction kinetics of methane on Ni/YSZ-based anode. Journal of Power Sources 86 (2000) : 523-530.
- Dincer, I., Technical, environmental and exergetic aspects of hydrogen energy systems. International Journal of Hydrogen Energy 27 (2002) : 265–285.
- Dokiya, M., SOFC system and technology. Solid State Ionics 152– 153 (2002) : 383-392.
- Epifanio, A., Fabbri, E., Bartolomeo, E.D., Licocchia, S., and Traversa, E., Design of BaZr_{0.8}Y_{0.2}O_{3-α} Protonic Conductor to Improve Electrochemical Performance in Intermediate Temperature Solid Oxide Fuel Cells (IT-SOFCs). Fuel Cells 1 (2008) : 69-76.
- Essoumhi, A., Taillades, G., Taillades-Jacquín, M., Jones, D.J., and Rozière, J., Synthesis and characterization of Ni-cermet/proton conducting thin film electrolyte symmetrical assemblies. Solid State Ionics 179 (2008) : 2155–2159.
- Fellows, R., A novel configuration for direct internal reforming stacks. Journal of Power Sources 71 (1998) : 281-287.
- Feng, Y., Luo, J., and Chuang, K.T., Conversion of propane to propylene in a proton-conducting solid oxide fuel cell. Fuel 86 (2007) : 123–128.
- Ferguson, J.R., Fiard, J.M., and Herbin, R., Three-dimensional numerical simulation for various geometries of solid oxide fuel cells. Journal of Power Sources 58 (1996) : 109–122.
- Fryda, L., Panopoulos, K.D., Karl, J., and Kakaras, E., Exergetic analysis of solid oxide fuel cell and biomass gasification integration with heat pipes. Energy 33 (2008) : 292-299.
- Gorte, R.J., and Vohs, J.M., Novel SOFC anodes for the direct electrochemical oxidation of hydrocarbons. Journal of Catalysis 216 (2003) : 477–486.

- Hamakawa, S., Li, L., Li, A., and Iglesia, E., Synthesis and hydrogen permeation properties of membranes based on dense $\text{SrCe}_{0.95}\text{Yb}_{0.05}\text{O}_{3-\alpha}$ a thin films. Solid State Ionics 48 (2002) : 71– 81.
- Haberman, B.A., and Young, J.B., Three-dimensional simulation of chemically reacting gas flows in the porous support structure of an integrated-planar solid oxide fuel cell. International Journal of Heat and Mass Transfer 47 (2004) : 3617–3629.
- Haseli, Y., Dincer, I., and Naterer, G.F., Thermodynamic modeling of a gas turbine cycle combined with a solid oxide fuel cell. International Journal of Hydrogen Energy 33 (2008) : 5811-5822.
- Haynes, C., Simulating process settings for unslaved sofc response to increases in load demand. Journal of Power Sources 109 (2000) : 365–376.
- Hayre, R.O., Cha, S.W., Colella, W., and Prinz, F.B., Fuel Cell Fundamentals, John Wiley & Sons : New York, 2006.
- Hernandez-Pacheco, E., Singh, D., Hutton, P.N., Patel, N., and Mann, M.D., A macro-level model for determining the performance characteristics of solid oxide fuel cells. Journal of Power Sources 138(1-2) (2004) : 174–86.
- Hernandez-Pacheco, E., Mann, M.D., Hutton, P.N., Singh, D., and Martin, K.E., A cell-level model for a solid oxide fuel cell operated with syngas from a gasification process. International Journal of Hydrogen Energy 30 (2005) : 1221–1233.
- Hibino, Y., Tsunekawa, H., Tanimoto, S., and Sano, M., Improvement of a Single-Chamber Solid-Oxide Fuel Cell and Evaluation of New Cell Designs. Journal of The Electrochemical Society 147 (2000) : 1338-1343.
- Hirschenhofer, J.H., Stauffer, D.B., Engleman, R.R., and Klett, M.G., Fuel Cell Handbook, U.S. Department of Energy, Federal Energy Technology Center : 4th Ed., 1998.

- Huang, K., Feng, M., and Goodenough, J.B., Electrode Performance Test on Single Ceramic Fuel Cells Using as Electrolyte Sr- and Mg-Doped LaGaO₃. Journal of The Electrochemical Society 144 (1997) : 3620-3624.
- Hussain, M.M., Li, X., and Dincer, I., Mathematical modeling of planar solid oxide fuel cells. Journal of Power Sources 161 (2006) : 1012–1022.
- Inui, Y., Urata, A., Ito, N., Nakajima, T., and Tanaka, T., Performance simulation of planar SOFC using mixed hydrogen and carbon monoxide gases as fuel. Energy Conversion and Management 47 (2006) : 1738–1747.
- Ishihara, T., Honda, M., Shibayama, T., Minami, H., Nishiguchi, H., and Takita, Y., Intermediate Temperature Solid Oxide Fuel Cells Using a New LaGaO₃ Based Oxide Ion Conductor. Journal of The Electrochemical Society 145 (1998) : 3177-3183.
- Ito, N., Iijima, M., Kimura, K., and Iguchi, S., New intermediate temperature fuel cell with ultra-thin proton conductor electrolyte. Journal of Power Sources 152 (2005) : 200–203.
- Iwahara, H., Uchida, H., and Maeda, N., High temperature fuel and steam electrolysis cells using proton conductive solid electrolysis. Journal of Power Sources 7 (1982) : 293-301.
- Iwahara, H., High temperature proton conducting oxides and their applications to solid electrolyte fuel cells and steam electrolyzer for hydrogen production. Solid State Ionics 28-30 (1988) : 573-578.
- Iwahara, H., Yajima, T., Hibino, T., Ozaki, K., and Suzuki, H., Protonic conduction in calcium, strontium and barium zirconates. Solid State Ionics 61 (1993) : 65-69.
- Iwahara, H., Proton conducting ceramics and their application. Solid State Ionics 86–88 (1996) : 9–15.
- Iwahara, H., Asakura, Y., Katahira, K. and Tanaka, M., Prospect of hydrogen technology using proton-conducting ceramics. Solid State Ionics 168 (2004) : 299-310.

- Jamsak, W., Assabumrungrat, S., Douglas, P.L., Laosiripojana, N., and Charojrochkul, S., Theoretical performance analysis of ethanol-fuelled solid oxide fuel cells with different electrolytes. Chemical Engineering Journal 119 (2006) : 11–18.
- Jamsak, W., Assabumrungrat, S., Douglas, P.L., Laosiripojana, N., Suwanwarangkul, R., Charojrochkul, S., and Croiset, E., Performance of ethanol-fuelled solid oxide fuel cells : Proton and oxygen ion conductors. Chemical Engineering Journal 133 (2007) : 187–194.
- Joo, J.H., Kim, D.Y., and Choi, G.M., Thick-Film Electrolyte-Supported SOFC Based on Lanthanum-Gallate Electrolyte Without Using Buffer Layer. Electrochemical and Solid-State Letters 12 (2009) : 65-68.
- Kakaç, S., Pramuanjaroenkij, A., Zhou, X.Y., A review of numerical modeling of solid oxide fuel cells. International Journal of Hydrogen Energy 32 (2007) : 761-786.
- Kim, S.D., Hyun, S.H., Moon, J., Kim, J.H., and Song, R.H., Fabrication and characterization of anode-supported electrolyte thin films for intermediate temperature solid oxide fuel cells, Journal of Power Sources 139 (2005) : 67–72.
- Kosacki, I., and Anderson, H.U., The structure and electrical properties of $\text{SrCe}_{0.95}\text{Yb}_{0.05}\text{O}_3$ thin film protonic conductors. Solid State Ionics 97 (1997) : 429-436.
- Larminie, J., and Dicks, A., Fuel Cell Systems Explained. New York : John Wiley & Sons, 2003.
- Leah, R.T., Brandon, N.P., and Aguiar, P., Modelling of cells, stacks and systems based around metal-supported planar IT-SOFC cells with CGO electrolytes operating at 500–600°C. Journal of Power Sources 145 (2005) : 336–352.
- Leng, Y.J., Chan, S.H., Khor, K.A., and Jiang, S.P., Performance evaluation of anode-supported solid oxide fuel cells with thin film YSZ electrolyte. International Journal of Hydrogen Energy 29 (2004) : 1025-1033.

- Li, P., and Chyu, M.K., Simulation of the chemical/electrochemical reactions and heat/mass transfer for a tubular SOFC in a stack. Journal of Power Sources 124 (2003) : 487–498.
- Lin, B., Sun, W., Xie, K. Dong, K., Dong, D., Liu, X., Gao, J., and Meng, G., A cathode-supported SOFC with thin $\text{Ce}_{0.8}\text{Sm}_{0.2}\text{O}_{1.9}$ electrolyte prepared by a suspension spray. Journal of Alloys and Compounds 465 (2008) : 285-290.
- Liu, Q.L., Khor, K.A., Chan, S.H., and Chen, X.J., Anode-supported solid oxide fuel cell with yttria-stabilized zirconia/gadolinia-doped ceria bilayer electrolyte prepared by wet ceramic co-sintering process. Journal of Power Sources 162 (2006) : 1036-1042.
- Maric, R., Ohara, S., Fukui, T., Yoshida, H., Nishimura, M., Inagaki, T., and Miura, K., Solid Oxide Fuel Cells with Doped Lanthanum Gallate Electrolyte and LaSrCoO_3 Cathode, and Ni-Samarium-Doped Ceria Cermet Anode. Journal of The Electrochemical Society 146 (1999) : 2006-2010.
- Mather, G.C., Figueiredo, F.M., Jurado, J.R., and Frade, J.R., Synthesis and characterisation of cermet anodes for SOFCs with a proton-conducting ceramic phase. Solid State Ionics 162–163 (2003) : 115–120.
- Matsumoto, H., Nomura, I., Okada, S., and Ishihara T., Intermediate-temperature solid oxide fuel cells using perovskite-type oxide based on barium cerate. Solid State Ionics 179 (2008) : 1486–1489.
- Meng, G.Y., Ma, G.L., Ma, Q.L., Peng, R.R. and Liu, X.Q., Ceramic membrane fuel cells based on solid proton electrolytes. Solid State Ionics 178 (2007) : 697–703.
- Minh, N.Q., and Takahashi, T., Science and technology of ceramic fuel cells. New York : Elsevier, 1995.
- Minh, N.Q., Solid oxide fuel cell technology-features and applications. Solid State Ionics 174 (2004) : 271–277.
- Möller, B.F., Arriagada, J., Assadi, M., and Potts, I., Optimisation of an SOFC/GT system with CO_2 -capture. Journal of Power Sources 131 (2004) : 320–326.

- Musa, A., and Paepe, M.D., Performance of combined internally reformed intermediate/high temperature SOFC cycle compared to internally reformed two-staged intermediate temperature SOFC cycle. International Journal of Hydrogen Energy 33 (2008) : 4665–4672.
- Nagata, S., Momma, A., Kato, T., and Kasuga, Y., Numerical analysis of output characteristics of tubular SOFC with internal reformer. Journal of Power Sources 101 (2001) : 60–71.
- Ni, M., Leung, M.K.H., and Leung, D.Y.C., Parametric study of solid oxide fuel cell performance. Energy conversion and Management 48 (2007) : 1525-1535.
- Ni, M., Leung, D.Y.C., and Leung, M.K.H., Modeling of methane fed solid oxide fuel cells : Comparison between proton conducting electrolyte and oxygen ion conducting electrolyte. Journal of Power Sources 183 (2008) : 133-142.
- Palsson, J., Selimovic, A., and Sjunnesson, L., Combined solid oxide fuel cell and gas turbine systems for efficient power and heat generation. Journal of Power Sources 86 (2000) : 442-448.
- Park, S., Gorte, R.J. and Vohs, J.M., Applications of heterogeneous catalysis in the direct oxidation of hydrocarbons in a solid-oxide fuel cell. Applied Catalysis A : General 200 (2000) : 55–61.
- Pekridis, G., Kalimeri, K., Kaklidis, N., Athanasiou, C., Marnellos, G., Electrode polarization measurements in the Fe|SrCe_{0.95}Yb_{0.05}O_{2.975}|Au proton conducting solid electrolyte cell. Solid State Ionics 178 (2007) : 649–656.
- Peters, R., Riensche, E. and Cremer, P., Pre-reforming of natural gas in solid oxide fuel-cell systems. Journal of Power Sources 86 (2000) : 432 - 441.
- Petruzzi, L., Cocchi, S. and Fineschi, F., A global thermo-electrochemical model for SOFC systems design and engineering. Journal of Power Sources 118 (2003) : 96–107.

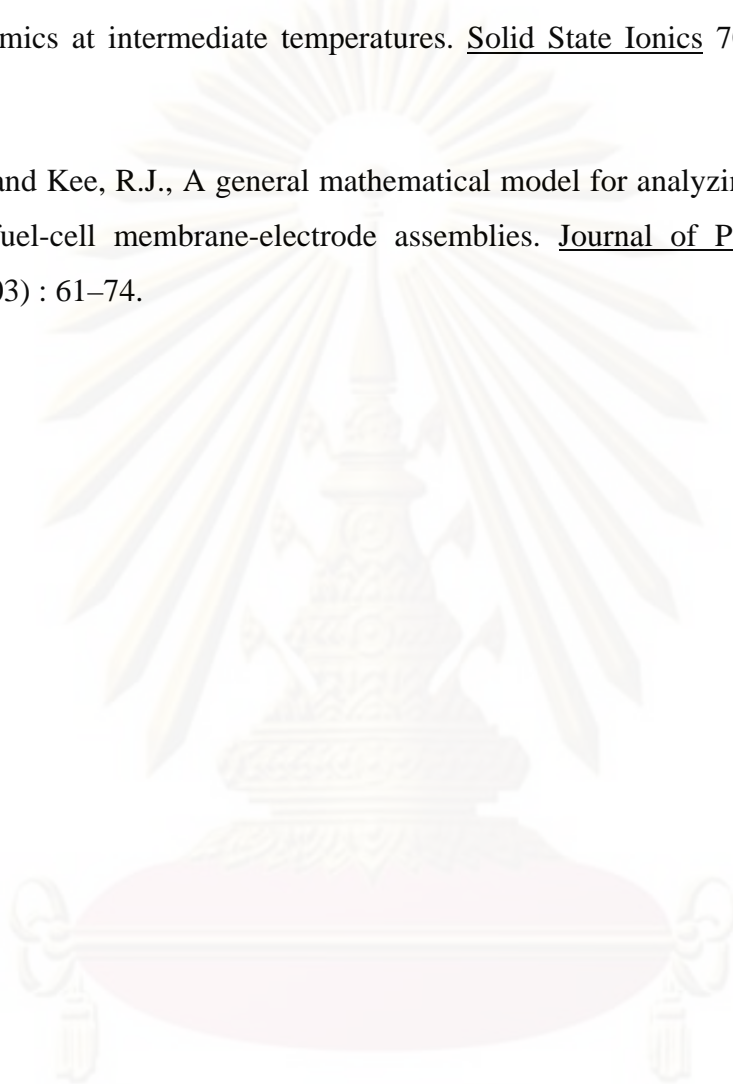
- Pfafferoth, M., Heidebrecht, P., Stelter, M., and Sundmacher, K., Model-based prediction of suitable operating range of a SOFC for an auxiliary power unit. Journal of Power Sources 149 (2005) : 53–62.
- Potter, A.R., and Baker, R.T., Impedance studies on Pt|SrCe_{0.95}Yb_{0.05}O₃|Pt under dried and humidified air, argon and hydrogen. Solid State Ionics 177 (2006) : 1917–1924.
- Ranran, P., Yan, W., Lizhai, Y. and Zongqiang M., Electrochemical properties of intermediate-temperature SOFCs based on proton conducting Sm-doped BaCeO₃ electrolyte thin film. Solid State Ionics 177 (2006) : 389-393.
- Sangtongkitcharoen, W., Assabumrungrat, S., Pavarajarn, V., Laosiripojana, N. and Praserttham, P., Comparison of carbon formation boundary in different modes of solid oxide fuel cells fueled by methane. Journal of Power Sources 142 (2005) : 75–80.
- Sasaki, K., Tamura, J., and Dokiya, M., Pt-cermet cathode for reduced temperature SOFCs. Solid State Ionics 144 (2001) : 223–232.
- Shi, Y., Cai, N., and Li, C., Numerical modeling of an anode-supported SOFC button cell considering anodic surface diffusion. Journal of Power Sources 164 (2007) : 639–648.
- Singhal, S.C., Solid oxide fuel cells for stationary, mobile, and military applications. Solid State Ionics 152–153 (2002) : 405– 410.
- Suksamai, W., and Metcalfe, I.S., Measurement of proton and oxide ion fluxes in a working Y-doped BaCeO₃ SOFC. Solid State Ionics 178 (2007) : 627–634.
- Suwanwarangkul, R., Croiset, E., Fowler, M.W., Douglas, P.L., Entchev, E., and Douglas, M.A., Performance comparison of Fick's, dusty-gas and Stefan–Maxwell models to predict the concentration overpotential of a SOFC anode. Journal of Power Sources 122 (2003) : 9–18.

- Suzuki, T., Jasinski, P., Anderson, H.U. and Dogan, F., Single Chamber Electrolyte Supported SOFC Module. Electrochemical and Solid-State Letters 7 (2004) : 391-393.
- Taherparvar, H., Kilner, J.A., Baker, R.T., and Sahibzada, M., Effect of humidification at anode and cathode in proton-conducting SOFCs. Solid State Ionics 162– 163 (2003) : 297– 303.
- Vollmar, H.E., Maier, C.U., Nölscher, C., Merklein, T., and Poppinger, M., Innovative concepts for the coproduction of electricity and syngas with solid oxide fuel cells. Journal of Power Sources 86 (2000) : 90-97.
- Virkar, A.V., Chen, J., Tanner, C.W., and Kim, J., The role of electrode microstructure on activation and concentration polarizations in solid oxide fuel cells. Solid State Ionics 131 (2000) : 189–198.
- Xin, X., Lu, Z., Huang, X., Sha, X., Zhang, Y., Su, W., Anode-supported solid oxide fuel cell based on dense electrolyte membrane fabricated by filter-coating. Journal of Power Sources 159 (2006) : 1158–1161.
- Xue, X., Tang, J., Sammes, N., and Du, Y., Dynamic modeling of single tubular SOFC combining heat/mass transfer and electrochemical reaction effects. Journal of Power Sources 142 (2005) : 211–222.
- Yakabe, H., Ogiwarw, T., Hishinuma, M., and Yasuda, I., 3-D model calculation for planar SOFC. Journal of Power Sources 102 (2001) : 144–154.
- Yamaguchi, T., Shimizu, S., Suzuki, T., Fujishiro, Y., and Awano, M., Fabrication and characterization of high performance cathode supported small-scale SOFC for intermediate temperature operation. Electrochemistry Communications 10 (2008) : 1381-1383.
- Yokoo, M., and Take, T., Simulation analysis of a system combining solid oxide and polymer electrolyte fuel cells. Journal of Power Sources 137 (2004) : 206–215.
- Zamfirescu, C., and Dincer, I., Thermodynamic performance analysis and optimization of a SOFC-H⁺ system. Thermochimica Acta 486 (2009) : 32–40.

Zhao, F., and Virkar, A.V., Dependence of polarization in anode-supported solid oxide fuel cells on various cell parameters. Journal of Power Sources 141 (2005) : 79–95.

Zhu, B. and Mellander B.E., Proton conduction in nitrate-based oxides and related ceramics at intermediate temperatures. Solid State Ionics 70/71 (1994) : 285-290.

Zhu, H., and Kee, R.J., A general mathematical model for analyzing the performance of fuel-cell membrane-electrode assemblies. Journal of Power Sources 117 (2003) : 61–74.



ศูนย์วิจัยทรัพยากร
จุฬาลงกรณ์มหาวิทยาลัย



APPENDICES

ศูนย์วิทยทรัพยากร
จุฬาลงกรณ์มหาวิทยาลัย

APPENDIX A

DIFFUSION COEFFICIENT

The diffusion coefficient plays an important role to determine the rate of gas diffusion in side SOFCs. Gas diffusion in a porous material is mainly described by two mechanisms; namely, ordinary diffusion and Knudsen diffusion. Ordinary diffusion occurs when the pore diameter of material is larger in comparison to the mean free path of the gas molecules. On the other hand, when the pore diameter is much smaller than the mean free path of the gas molecules, the Knudsen diffusion becomes an important mechanism. The Knudsen diffusion coefficient can be predicted using the kinetic theory by relating the diameter of the pore and the mean free path of the gas (Chan et al., 2001; Suwanwarangkul et al., 2003; Hernandez-Pacheco et al., 2004).

For straight and round pores (Chan et al., 2001), the diffusion coefficient of the gaseous component A becomes:

$$D_{Ak} = 97\bar{r} \sqrt{\frac{T}{M_A}} \quad (\text{A.1})$$

$$\bar{r} = \frac{2\varepsilon}{S_A \rho_B} \quad (\text{A.2})$$

where S_A is the surface area of the porous solid ($\text{m}^2 \text{kg}^{-1}$), ρ_B is the bulk density of the solid particle (kgm^{-3}), ε is the porosity material, and M is the molecular mass (kg kmol^{-1}).

In order to account for the electrode porosity and pore tortuosity, the Knudsen coefficient has to be modified in terms of an effective coefficient (Chan et al., 2001; Suwanwarangkul et al., 2003):

$$D_{Ak,\text{eff}} = D_{Ak} \left(\frac{\varepsilon}{\xi} \right) \quad (\text{A.3})$$

where ε and ξ represent the porosity and the tortuosity.

The binary ordinary diffusion coefficient in the gas phase can be determined by using the Chapman-Enskog theory (Bird et al., 2006) as follows:

$$D_{AB} = 0.0018583 \left(\frac{1}{M_A} + \frac{1}{M_B} \right)^{1/2} \frac{T^{3/2}}{p \sigma_{AB}^2 \Omega_{DAB}} \quad (\text{A.4})$$

where p is the total pressure (atm), σ_{AB} (\AA) is the characteristic length, and Ω_{DAB} is the collision integral. Using the Lennard–Jones potential model, Ω_{DAB} is given by

$$\Omega_{DAB} = \frac{A}{\tau^B} + \frac{C}{\exp(D\tau)} + \frac{E}{\exp(F\tau)} + \frac{G}{H\tau} \quad (\text{A.5})$$

where the constants appearing in the collision integral are reported in Table A.1.

$$\tau = \frac{kT}{\varepsilon_{AB}} \quad (\text{A.6})$$

where k is the Boltzmann's constant and ε_{AB} (K) is the characteristic Lennard–Jones length. σ_{AB} and ε_{AB} are given by

$$\sigma_{AB} = \frac{\sigma_A + \sigma_B}{2} \quad (\text{A.7})$$

$$\varepsilon_{AB} = (\varepsilon_A \varepsilon_B)^{1/2} \quad (\text{A.8})$$

where σ_i the diameter of the collision. The values for σ_i and ε_i are summarize in Table A.2.

Table A.1 Collision integral constants

A	B	C	D	E	F	G	H
1.06036	0.15610	0.19300	0.47635	1.03587	1.52996	1.76474	3.89411

Table A.2 Lennard–Jones potential

Gas species	Molecular weight	σ_i (Å)	ϵ_i/k
CH ₄	16.043	3.758	148.6
H ₂ O	18.015	2.641	809.1
CO ₂	44.01	3.941	195.2
CO	28.01	3.690	91.7
H ₂	2.016	2.827	59.7
N ₂	28.014	3.798	71.4
O ₂	31.999	3.467	106.7

Similar to the Knudsen diffusion, the effective diffusion coefficient for the binary diffusion has to be modified in order to account for the tortuosity of the material:

$$D_{AB,\text{eff}} = D_{AB} \left(\frac{\epsilon}{\tau} \right) \quad (\text{A.9})$$

Both ordinary diffusion and Knudsen diffusion may occur simultaneously. For self-diffusion transfer, the effective diffusion coefficient can be written as

$$\frac{1}{D_{A,\text{eff}}} = \frac{1}{D_{AB,\text{eff}}} + \frac{1}{D_{Ak,\text{eff}}} \quad (\text{A.10})$$

APPENDIX B

LIST OF PUBLICATIONS

International Publications

1. **Patcharavorachot, Y.**, Arpornwichanop, A. and Chuachuensuk, A. (2008). Electrochemical Study of a Planar Solid Oxide Fuel Cell: Role of Support Structures, *Journal of Power Source*, 177, 254-261.
2. Arpornwichanop, A., **Patcharavorachot, Y.** and Assabumrungrat, S. (2010). Analysis of a proton-conducting SOFC with direct internal reforming. *Chemical Engineering Science*, 65, 581-589.
3. **Patcharavorachot, Y.**, Paengjuntuek, W., Assabumrungrat, S. and Arpornwichanop, A. (2010). Performance evaluation of combined solid oxide fuel cells with different electrolytes, *International Journal of Hydrogen Energy*, 35, 4301-4310.
4. **Patcharavorachot, Y.**, Brandon, N. P., Paengjuntuek, W., Assabumrungrat, S. and Arpornwichanop, A. (2009). Analysis of Planar Solid Oxide Fuel Cells based on Proton-Conducting Electrolyte. *Solid State Ionics* (under revision).

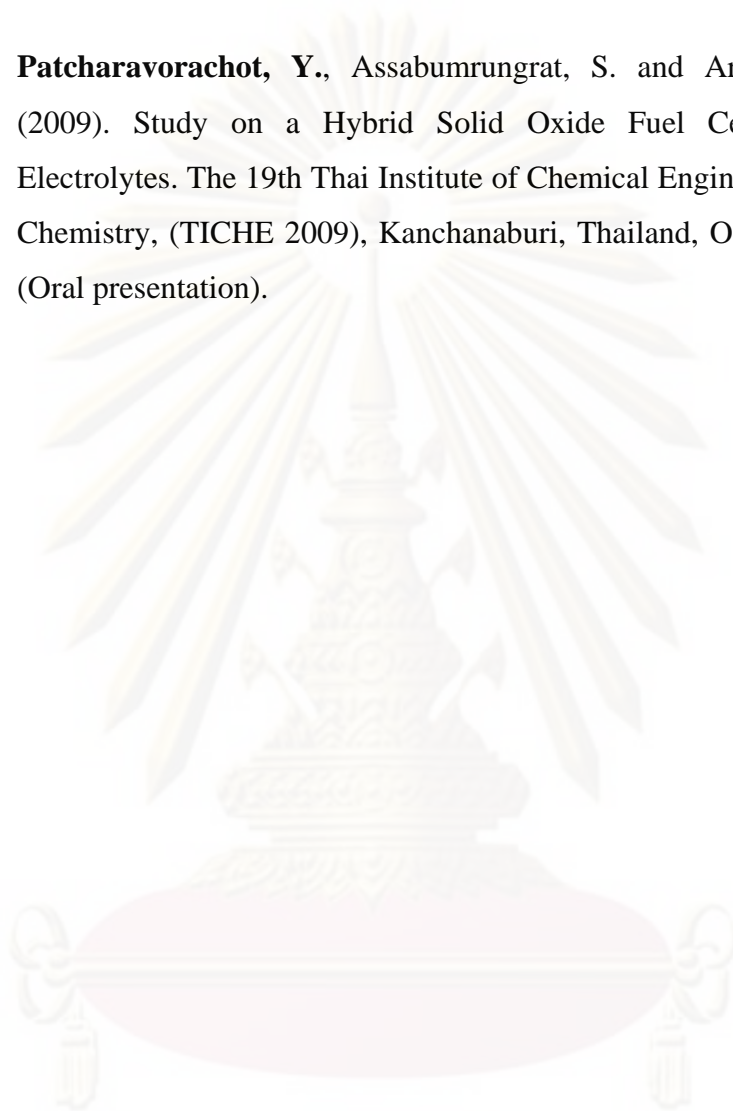
International conferences

1. **Patcharavorachot, Y.**, Saebea, D., Assabumrungrat, S. and Arpornwichanop, A. (2008). Investigation of Electrochemical Behavior of SOFCs with a Proton-Conducting Electrolyte. Mexican Congress on Chemical Reaction Engineering (MCCRE 2008), Ixtapa-Zihuatanejo, Guerrero, Mexico, June 15-19, 2008.
2. **Patcharavorachot, Y.** and Arpornwichanop, A. (2007). Simulation of a Direct Internal Reforming Solid Oxide Fuel Cell. The 4th International

Symposium on Design, Operation and Control of Chemical Processes (PSE ASIA 2007), Xi'an, China, August 15-18, 2007.

National conferences

1. **Patcharavorachot, Y.**, Assabumrungrat, S. and Arpornwichanop, A. (2009). Study on a Hybrid Solid Oxide Fuel Cell with Different Electrolytes. The 19th Thai Institute of Chemical Engineering and Applied Chemistry, (TICHE 2009), Kanchanaburi, Thailand, October 26-27, 2009 (Oral presentation).



ศูนย์วิจัยทรัพยากร
จุฬาลงกรณ์มหาวิทยาลัย

VITA

Miss Yaneeporn Patcharavorachot was born in Suratthanee, on January 25, 1983. She received the Bachelor Degree in Chemical Engineering from Srinakarinwirot University in 2005. She began her graduate studies in May 2005 when she entered the Graduate School of Chulalongkorn University and joined the Control and Systems Engineering group in the Department of Chemical Engineering.



ศูนย์วิทยทรัพยากร
จุฬาลงกรณ์มหาวิทยาลัย